Structure-function analysis of the Vesicular glutamate transporter 1 (VGLUT1) C-terminus

by Julia-Christine Jordan

2014

Supervision: Prof. Dr. Christian Rosenmund
Prof. Dr. Constance Scharff

Disputation date: 4th Mai 2015

For a `bigger picture´,
many little puzzle pieces need to be put together

(Julia-Christine Jordan, 2014)

Acknowledgement

I would like to thank Prof. Dr. Christian Rosenmund, not only for the opportunity to do exciting research in his laboratory, but more for the chance to work in a great team to find together answers of fundamental neuroscientific questions. Christian Rosenmund supported me to work independently ("learning by doing"), but always with good advice for difficult questions. I learned from him all necessary electrophysiological skills, but also to be patient especially with complicated or time consuming experiments. The investigations of structures of the vesicular glutamate transporter 1 (VGLUT1), to test their potential role in VGLUT1 function, were sometimes challenging, but altogether I really lerned a lot during all my PhD years.

I also thank Melissa Herman for her outstanding support, her technical and theoretical help, as well as her patience to answer all my questions. Alike, I thank Marcial Camacho-Pérez for teaching me how to perform whole-cell voltage clamp recordings and how to analyze the electrophysiological data. I got also great support from Johannes Zimmermann, especially with help of all kinds of computer problems.

Just as much, I would like to thank all other labmembers of the Rosenmunds group:

Thorsten Trimbuch for designing and producing all the lentiviral constructs, Tanja Rosenmund for being the contact person with mouse line questions, Frauke Ackermann for all performed EM images and all the other great colleagues for discussions together, but also for many funny moments in the daily routine and outside the laboratory life: Charanya Sympathkumar, Gülcin Vadar, Lauren Mamer, Katharina Grauel, Ranjita Dutta-Roi, Yuan-Ju Wu, Shuwen Chang, Cristina Pulida Lozano and Benjamin Rost.

In addition, I would like to emphasize the special technical and administrative support by Berit Söhl-Kielczynski, Annegret Felies, Katja Pötschke, Bettina Brokowski, Carola Schweynoch, Sabine Lenz and Heidi Pretorious.

Besides my colleagues and other employees of the CCO community, I would like to thank very, very much my partner and family: thank you Jens, mom, dad, brother and grandparents, but also all my friends, especially Annika, Christa, Mandy, Kirsten, Christine G., Christine R., Raffael, Andreas and Maik for all your love and ties of friendship. It is a great pleasure for me to count on you in every life situation!

Cover sheets

Table of contents

List of abbreviation

A	alanine
aa	amino acid
Acb	nucleus accumbens
AP	action potential
AP	adapter protein
AS	Aminosäure(n)
ATP	adenosine triphosphate
ATPase	ATP hydrolase
a.u.	arbitrary unit
AZ	active zone
BFA	brefeldin A
bs	brainstem
°C	degree Celsius
C	carboxy
Ca^{2+}	calcium ion
$CaCl_2$	calcium chloride
CaMKII	calcium/calmodulin-dependent protein kinase II
CAZ	cytoskeletal matrix at the active zone
Cb	cerebellum
Cb nu	deep cerebellar nuclei
CBS	center for biological sequence analysis
Cdk	cyclin-dependent kinase
cf.	latin "confer": compare with
CNS	central nervous system
CO_2	carbon dioxid
cp.	abbreviation „compare“
CPu	caudate putamen
C-term	C-terminus
Cx	cerebral cortex
ΔF	delta F
D	aspartic acid
D38G	amino acid substitution of D to G
DAT	dopamine transporter
dd	distilled
DDSA	dodecenyl succinic anhydride
del.	deletion
DIV	days *in vitro*
DMEM	Dulbecco's modified eagle's medium
DMP	dipropylene glycol monomethyl ether
DNA	deoxyribonucleic acid
E	glutamic acid
EAAT	excitatory amino-acid transporter
EDTA	ethylenediaminetetraacetic acid
EEA1	early endosome antigen 1
e.g.	latin "exempli gratia": for example
EGTA	ethylene glycol tetraacetic acid
Ent Cx	entorhinal cortex
EPSCs	excitatory postsynaptic currents

EtOH	ethanol
F	fluorescence
F	phenylalanine
FUDR	5-fluoro-2-deoxyuridine
FV510/511AA	amino acid substitution of FV to AA
G	glycine
GA	glutaraldehyde
GABA	gamma-aminobutyric acid
GFP	green fluorescent protein
gp	guinea pig
GTP	guanosine triphosphate
h	hour
H	histidine
H^+	proton
H_2O	water
HBSS	Hank's balanced salt solution
HCl	hydrochloride acid
HEPES	2-[4-(2-hydroxyethyl)piperazin-1-yl]ethanesulfonic acid
Hi	hippocampus
Hy	hypothalamus
Hz	Hertz
HPMA	hydroxypropyl methacrylate
I	isoleucine
IC	inferior colliculus
IPSC	inhibotory postsynaptic current
k	kilo
K	lysine
KCl	potassium chloride
KD	knockdown
KO	knockout
L	leucine
LDCV	large dense core vesicle
m	mouse
mEPSCs	miniature EPSCs
Mg^{2+}	magnesium ion
$MgCl_2$	magnesium chloride
min	minutes
mM	milimolar
MNA	methyl nadic anhydride
mOsm	milliosmol
ms	millisecond
mV	millivolts
MVB	multivesicular bodies
N°	number
NaCl	sodium chloride
NBA	neurobasal A solution
Nck	non-catalytic region of tyrosine kinase adaptor protein 1
NT	neurotransmitter
NGS	normal goat serum
NLS	nuclear localization signal

nm	nanometer
norm	normalized
NSF	N-ethylmaleimide-sensitive-factor
N-terminus	NH_2-terminus
NTP	nucleoside triphosphate
OB	olfactory bulb
P	postnatal
p (value)	percentage (%)
$^{32}P_i$	phosphorus-32
PB	phosphate buffer
PBS	phosphate buffered saline
PBST	phosphate buffered saline solution with Tween-20
pC	pico coulomb
PCR	polymerase chain reaction
PFA	paraformaldehyde
pH	power of hydrogen
pI	isoelectrical point
PKA	protein kinase A
PKC	protein kinase C
pmol	picomol
PNS	peripheral nervous system
PP	paired pulse
PPR	paired pulse ratio
PRD	polyproline-rich domain
PSC	postsynaptic current
Pvr	vesicular release probability
R	arginine
rb	rabbit
RISC	RNA-induced silencing complex
RNA	ribonucleic acid
ROI	region of interest
RRP	readily releasable pool
RT	room temperature
S	serine
S	subiculum
s	second
S504	serine at the position 504
S519	serine at the position 519
S522	serine at the position 522
S540	serine at the position 540
S504A	amino acid substitution of S to A
S519A	amino acid substitution of S to A
S522A	amino acid substitution of S to A
S540A	amino acid substitution of S to A
SC	superior collioculus
s.e.m	standard error of mean
shRNA	small hairpin RNA
SNARE	SNAP-(soluble NSF attachment protein) receptor
SOC	superior olivary complex
SLC	solute carrier

SV	synaptic vesicle, in german: synaptische Vesikel
SLMV	synaptic-like microvesicle
STh	subthalamic nucleus
SypHl	synaptophysin-pHluorin
Thal	thalamus nuclei
t-SNARE	target SNARE
U	unit
UK	United Kingdom
USA	United States of America
V	valine
VACht	vesicular acetylcholine transporter
vATPase	vacuolar ATPase
VGAT	vesicular GABA transporter
VGLUT	vesicular glutamate transporter
VMAT	vesicular monoamine transporters
v-SNARE	vesicular SNARE
WT	wildtype
µg	microgramm
µl	microliter
µm	micrometer
°	degree
±	minus or plus
=	equal to
<	around
∞	infinity
<	less-than
>	greater-than
%	percentage
Δ	delta; used in this study to illustrate the missing aa of VGLUT1 truncation versions
τ	tau
#	number

List of figures

Fig. 19 (A-D): **Electrophysiological analysis of a myc tagged VGLUT2 C-terminus truncation construct (VGLUT2Δ493-582) and a VGLUT2 full-length construct (WT rescue) in VGLUT1 KO background in comparison with endogenously expressed VGLUT1 WT**

Fig. 20 (A-G): **Electrophysiological analysis of a VGLUT1 C-terminus chimera with WT rescue and VGLUT1 KO neurons**

Fig. 21 (A-G): **Electrophysiological analysis of the VGLUT1 C-terminus chimera with additional VGLUT2 KD in comparison with WT rescue and VGLUT1 KO neurons**

Fig. 22 (A-G): **Electrophysiological analysis of a shorter C-terminus truncation VGLUT1Δ504-560 in comparison with WT rescue and VGLUT1 KO neurons**

Fig. 23 (A and B): **SV depletion and recovery of the shorter C-terminus truncation VGLUT1Δ504-560 in comparison with WT rescue and VGLUT1 KO neurons**

Fig. 24 (A-C): **Example images of WT and mutant VGLUT1-pHluorin constructs in hippocampal VGLUT1 KO neurons**

Fig. 25 (A-G): **pHluorin-based VGLUT1 cycling and electrophysiology analyses of the shorter C-terminus truncation VGLUT1Δ504-560**

Fig. 26: **Synaptophysin-pHluorin-based analysis of the shorter C-terminus truncation VGLUT1Δ504-560 to investigate the general SV cycling**

Fig. 27 (A-D): **Example EM images of the SV morphology of different VGLUT1 variants**

Fig. 28 (A-E): **Morphological quantifications of SVs from VGLUT1 C-terminal truncation constructs by EM in comparison to WT rescue and KO**

Fig. 29 (A-I): **Electrophysiological characterization of putative C-terminal VGLUT1 serine phosphorylation site mutants**

Fig. 30 (A-E): **Direct comparison of the C-terminal VGLUT1 mutants S504A and S504E with WT rescue**

Fig. 31 (A-D): **pHluorin-based SV cycling analysis of putative C-terminal VGLUT1 serine phosphorylation site mutants**

Fig. 32 (A-C): **Analysis of NT release parameters of putative VGLUT1 C-terminal serine phosphorylation site mutants during pHluorin-based imaging experiments in comparison to WT rescue and FV510/511AA mutant**

Fig. 33 (A-E): **Morphological quantification of SVs from putative VGLUT1 C-terminal serine phosphorylation sites by EM**

Fig. 34: **ICC quantification of VGLUT2 KD in hippocampal neurons**

Fig. 35: **ICC quantification of VGLUT2 KD in thalamic neurons**

Fig. 36 (A-E): **Electrophysiological quantification of VGLUT2 KD**

Fig. 37 (A-F): **ICC quantifications of different VGLUT1 constructs**

List of tables

1. Introduction

The mammalian nervous system can be divided into two parts: the central nervous system (CNS) and the peripheral nervous system (PNS) (Kandel et al., 2000). The CNS contains the brain and the spinal cord and is often named "the processing center" of the nervous system. Its main role is to send, receive and interpret information from the PNS, which connects the CNS to the extremities and organs. The transmission of information is accomplished by a complex network of millions of nerve cells also known as neurons. Neurons, electrically excitable cells, are the smallest functional units of the nervous system. The transfer of information between neurons occurs by specialized connections, the synapses (Kandel et al., 2000; Reichert, 2000).

1.1 Electrical and chemical synapses

Synapses are the conductive link between adjacent neurons and can be divided into two groups: electrical and chemical synapses (fig.1).

Electrical synapses are linked by a specialization called gap junction, a cluster of intercellular hemichannels (connexins), which connects between pre- and postsynaptic membranes.

The gap junctions permit current to flow bidirectional and passively across an intercellular small distance of about 3 nm (Larsen, 1977; fig.1). Therefore, electrical synapses can conduct nerve impulses very fast. The speed of the signal transmission of electrical synapses is about ten times faster than that of chemical synapses.

In contrast, chemical synapses, which are the most common type of synapses in the brain, send a chemical signal across the space between the pre- and postsynaptic site, the synaptic cleft (about 20 nm). This happens actively with a relatively slow speed about 2 ms (Kandel et al., 2000; fig.1). These messenger molecules are called neurotransmitters (NTs) and stored in synaptic vesicles (SVs). SVs are lipid bilayer compartments about 40-50 nm diameter and the essential organelle for NT release at the presynaptic site of a chemical synapse (Kandel et al., 2000; Südhof and Jahn, 1991).

NTs are released in a process named SV fusion, which occurs spontaneously or calcium (Ca^{2+})-dependent in response to an action potential (AP) (Kandel et al., 2000; Reichert, 2000; further described in the following paragraph 1.3). An AP is a short-lasting rise about 1 to 2 ms of the membrane potential and generated by sodium influx through voltage-gated ion channels, which open when the membrane potential increases (depolarization, Kandel et al.,

2000). At rest the membrane potential in a mammalian neuron of the CNS is about –60 to –85 mV and caused by differences in distinct ion concentrations on opposite sites of the cellular membrane

After SV fusion the NTs travel across the synaptic cleft and bind to a receptor on the surface of the postsynaptic site. Thereby ligand-gated ion channels on the postsynaptic membrane are activated and the resulting ion flux changes the membrane potential of the postsynaptic neuron. Dependent on the type of ions the postsynaptic membrane potential rises or declines and thereby the probability that the target neuron will fire a new AP increases or decreases.

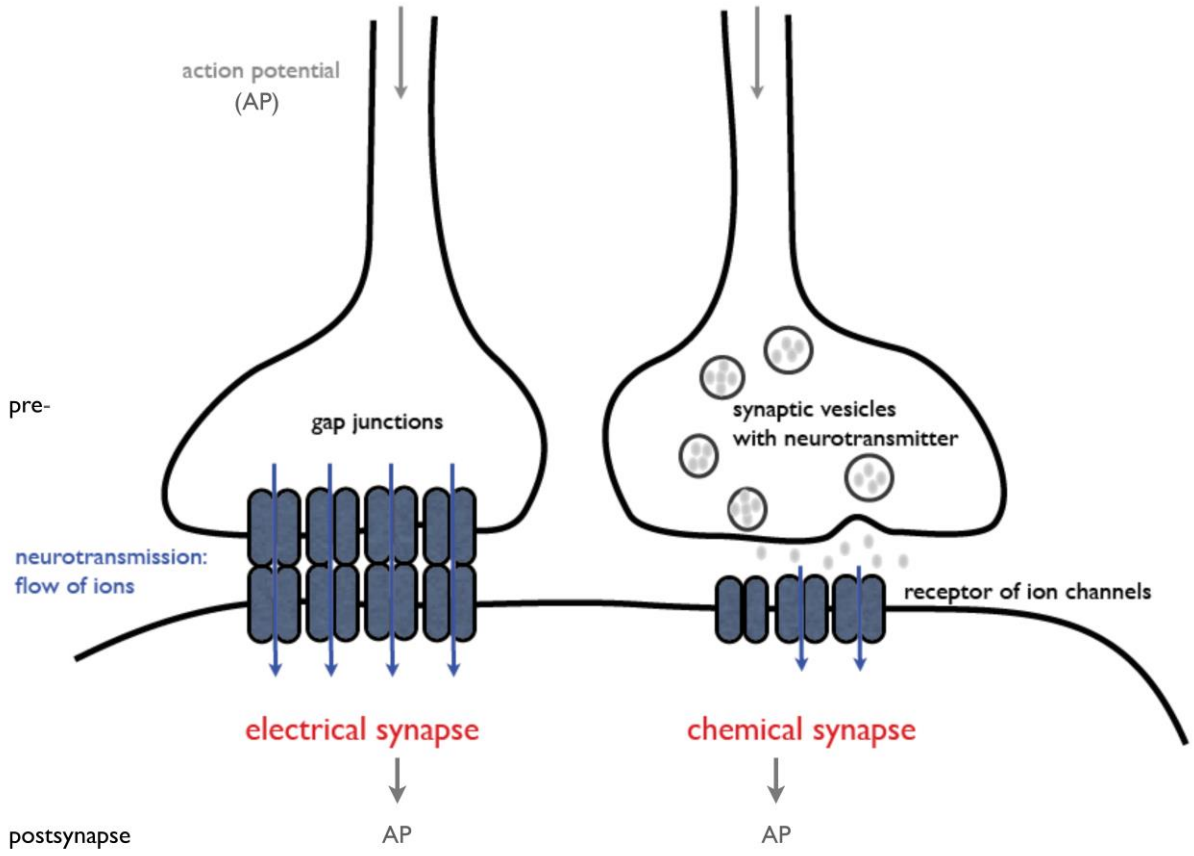

Fig. 1: **Neurotransmission of electrical and chemical synapses in the mammalian nervous system:** after an action potential (AP) arrives at a synapse, electrical signals are either directly transfered from the pre- to the postsynaptic site (electrical synapse) or first translated into a chemical signal in form of neurotransmitter (grey dots) before a new electrical signal can arise on the postsynaptic site (chemical synapse).

1.2 Neurotransmitters

There is a wide variety of different kinds of NTs with distinct functions including amino acids, amino acid derivates, amines and peptides (Kandel et al., 2000; Reichert, 2000). So far, over 100 NTs are identified (Purves et al., 2001). In the mammalian brain two main groups of NTs can be distinguished depending on the effect, when they bind to the postsynaptic receptor: inhibitory and excitatory NTs.

Inhibitory neurotransmitters decrease the likelihood that the neuron will fire an action potential. The most common inhibitory NT is gamma aminobutyric acid (GABA). The major excitatory NT, increasing the likelihood that the neuron will fire an action potential, is glutamate. Other excitatory NTs are for example acetylcholine and dopamine (Purves et al., 2001).

The concentration of NTs in the brain is highly regulated. Some studies revealed a strong correlation between the amount of NTs and the presence of specific psychiatric conditions. NT imbalance, for instance due to impaired NT filling into SVs, can alter the information transfer between neurons. NT imbalance is one hypothesis about the reason of mental diseases such as schizophrenia (Carlsson and Carlsson, 1990; Gargiulo and Landa, 2014) or Alzheimer`s disease (Garcia-Alloza et al., 2005; Lanari et al., 2006; Chen et al., 2011). Therefore, accurately SV recycling and NT refilling after SV fusion is necessary to maintain reliable neurotransmission (SV cycle).

1.3 The synaptic vesicle cycle of a chemical synapse

The SV cycle is a very important reliable process orchestrated by many synaptic proteins. The SV cycle can be divided into three main parts: exocytosis, endocytosis and refilling (fig.2).

Exocytosis is the process, where SVs fuse at a restricted zone of the plasma membrane, the active zone, and NTs are released into the synaptic cleft (Südhof and Jahn, 1991). The active zone, named by R. Couteaux and M. Pecot-Dechavassinein in 1970 (Couteaux and Pecot-Dechavassinein, 1970), is a specialized region of the presynaptic plasma membrane with an accumulation of cytoskeleton-associated proteins, such as Bassoon, Piccolo or Munc-13, called the cytomatrix of the active zone (CAZ) (Dresbach et al., 2001). The CAZ is seen under the electron microscope as a dark electron dense area (Dresbach et al., 2001; Zhai and Bellen, 2004).

Exocytosis occurs when an arriving AP depolarizes the synapse, resulting in activation of voltage-gated Ca^{2+}-channels and Ca^{2+}-influx. This Ca^{2+}-influx triggers the SV fusion machinery to release NTs by activation of the Ca^{2+}-sensor synaptotagmin (Baker and Knight, 1986, Brose et al., 1992)

Before SVs fuse with the presynaptic membrane and release NT into the synaptic cleft, two earlier steps occur defined as SV docking and priming (Südhof and Jahn, 1991; Südhof, 2004; fig.2). In the docking step specific synaptic proteins, the soluble N-ethylmaleimide-sensitive-factor (NSF) attachment receptors (SNAREs, fig.2), build a complex to bring the SVs close to the presynaptic membrane. SNARE proteins include the vesicle or v-SNARE, which is located at the SV membrane (synaptobrevin) and the target or t-SNAREs, which are located at the presynaptic cell membrane (syntaxin and SNAP-25; Betz and Angleson, 1998; Südhof, 1995). The priming step that follows an adenosine triphosphate (ATP)-dependent process, where molecular rearrangements of the SNAREs take place, makes the SVs competent to fuse after AP-induced Ca^{2+}-influx (2000; Südhof and Rizo, 2011).

All docked and primed vesicles, which can fuse immediately upon electrical stimulation, belong to the readily releasable pool (RRP). The RRP is the smallest pool about 1% of the total SV pool (Rizzoli and Betz, 2005) and empties very quickly. The size of the RRP determines the vesicular release probability (Pvr; Rosenmund and Stevens, 1996; Dobrunz, 2002). Depending on their position in the nerve terminal and their function in neurotransmission two other SV pools can be distinguished: the recycling pool and the reserve pool.

The recycling pool with SVs further away from the active zone is larger than the RRP (about 10-15% of the total pool) and releases SVs during moderate stimulation. The recycling pool is constantly refilled by newly recycled vesicles (Rizzoli and Betz, 2005).

The reserve pool is a depot of the majority of SVs and makes up about 80-90% of the total pool. The SVs of the reserve pool are released only during intense stimulation. However, it is not fully understood, but possibly those vesicles are seldom or never utilized during physiological activity (Alabi and Tsien, 2012; Rizzoli and Betz, 2005).

After SV fusion and NT release the SVs need to be recycled to maintain the vesicle supply. This happens by endocytosis and NT refilling of the SVs at sites flanking the active zone (fig.2). Diverse controversial theories exist concerning how SVs get endocytosed. One common scenario is slow clathrin-dependent SV endocytosis (about 30 s), where clathrin-coated pits together with several adapter proteins bud from the surface membrane,

so-called invaginations, and form early endosomes that later become functional SVs (Doherty and McMahon, 2009; Valtora et al., 2001).

Another theory is the fast non clathrin-dependent SV endocytosis (about 1 s), where SVs directly bud from the surface membrane after vesicle fusion, also called "kiss and run" theory (Jarousse and Kelly, 2001; Schneider, 2001; Valtora et al., 2001). Another study also describes the possibility of a clathrin-independent membrane retrieval, in particular under high-frequence stimulation conditions (Kononenko et al., 2014). Instead of clathrin, they propose dynamin 1/3- and endophilin-dependent mechanisms.

Granseth et al., 2006 suggest that the clathrin-mediated SV endocytosis is the dominant, maybe exclusive, mechanism of the SV retrieval at the hippocampal synapse, because experiments with a fluorescent reporter reveal only a slow mode of endocytosis (about 15 s), when SV fusion is triggered by a single nerve impulse. In contrast, Harata et al., 2005 using a novel quenching technique suggest "kiss and run" as the dominant mode.

Recent studies, where optogenetics are combined with electron microscopy (EM) (flash-and-freeze) to capture morphological changes during neurotransmission discovered a new form of recycling, the ultrafast endocytosis. Thereby, SV fusion was induced in channelrhodopsin-expressing neurons via a light flash and neurons were subsequently high pressure frozen 20 ms after the stimulation (Watanabe et al., 2013; Watanabe et al., 2014). The data illustrate that the ultrafast endocytosis seems to be specialized to restore the surface area of the membrane extremely fast within 50 to 100 ms and also in a clathrin-independent way (Watanabe et al., 2013; Watanabe et al., 2014).

The NT refilling of SVs is achieved by specific transporter proteins, the vesicular NT transporters (Südhof, 2004; Zimmermann et al., 1989; fig.2). These transporters are transmembrane proteins and their main function is to concentrate NTs in SVs.

Several vesicular NT transporters exist to transport different NT. For instance, GABA is transported into SVs by vesicular inhibitory amino acid transporters (VIAATs also termed vesicular GABA transporters, VGATs) and glutamate is transported by vesicular glutamate transporters (VGLUTs) (Bellocchio et al., 2000; Takamori et al., 2000).

Vesicular NT transporters rely on a proton (H^+) gradient created by an ATP-consuming vesicular ATP hydrolase (vATPase; Naito and Ueda, 1985; Hnasko and Edwards, 2012). Thereby, the pH inside the SVs becomes acidic (acidification). The subsequent remove of the protons from the SVs along an electrochemical gradient supports the NT transport into the vesicles (cotransport; Cidon and Sihra, 1989).

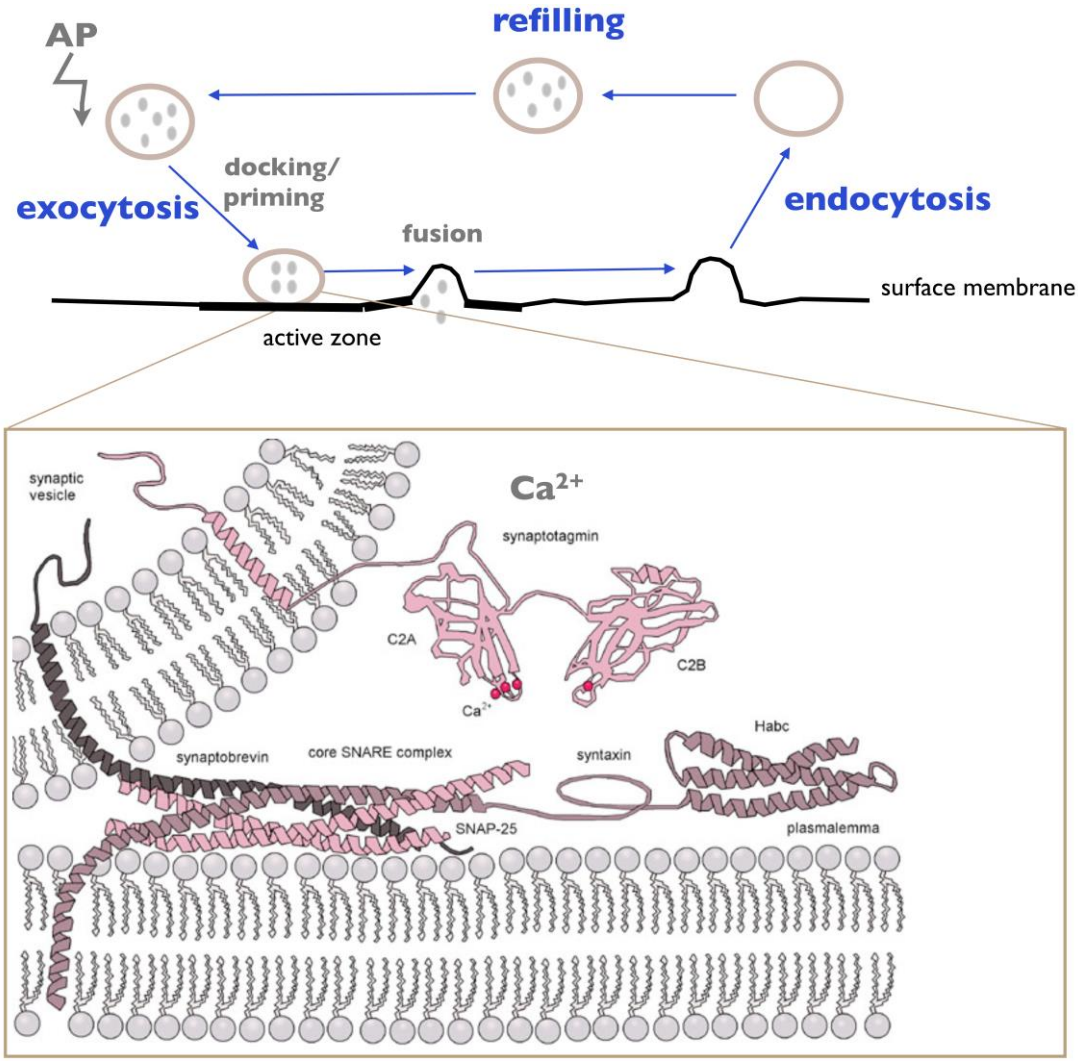

Fig. 2: **Exo- and endocytosis and the role of the SNARE proteins in the SV cycle:** the scheme illustrates that during exocytosis SVs, where prepared for fusion by docking and priming after an action potential (AP) arrived at the synapse. While then Ca^{2+} induces SNARE protein complex-mediated SV fusion and neurotransmitter release at the active zone. The SNARE protein complex consists of synaptobrevin, syntaxin and SNAP-25 that form a 4-α-helix bundle (box), which brings the SV close to the surface membrane. Synaptotagmin is a Ca^{2+} sensor. After SV fusion NT release at the active zone . SVs get retrieved by a machinery of different proteins (endocytosis) and refilled with NTs. (modified from illustration by Georgiev D. and Glazebrook J. from: Lyshevski S. (2007) Nano and molecular electronics Handbook, CRC Press, fig.17.4)

1.4 The role of vesicular glutamate transporters (VGLUTs) in the mammalian nervous system

VGLUTs are essential to fill SVs with L-glutamate. This process is driven by a proton electrochemical gradient across the SV membrane (Bai et al., 2001; Bellocchio et al., 2000; Masson et al., 1999; Schäfer et al., 2002; Takamori et al., 2000). The glutamate uptake by VGLUTs requires in addition a flux of chloride ions, which is a VGLUT specific transport

property compared with other vesicular NT transporters (Anne and Gasnier, 2014; Juge et al., 2006).

Glutamate uptake also occurs at the plasma membrane of neurons and glial cells by Na^{2+}-dependent excitatory amino-acid transporters (EAATs; Amara and Fontana, 2002; Kanai and Hediger, 1992; Seal and Amara, 1999). Thereby, the extracellular glutamate concentration is maintained below excitotoxic levels (Shigeri et al., 2004).

In mammals, three VGLUT isoforms (VGLUT1-3) exist. They belong to the type I phosphate transporter (solute carrier 17, SLC17)-family (Sreedharan et al., 2010). VGLUT1, VGLUT2 and VGLUT3 are highly similar in their substrate specificity, kinetics and pharmacology (Bellocchio et al., 2000; Frameau et al., 2001; Gras et al., 2002; Hayashi et al., 2001; Takamori et al., 2000 and 2002). However, they show spatiotemporally distinct protein expression patterns (fig. 3). VGLUT1 is mainly expressed in cerebral and cerebellar cortices and the hippocampus, whereas VGLUT2 predominates in the diencephalon, brainstem and spinal cord. A developmental shift from VGLUT2 to VGLUT1 expression occurs in the hippocampus and cortex (fig.3). VGLUT3 is only sparsely expressed, mostly in cholinergic, serotonergic and GABAergic neurons (Gras et al., 2005; Balschun et al., 2009). Moreover, coexpression of VGLUT3 and other transporters, e.g. GABA transporter, is suggested (Bulland et al., 2004; Stensrud et al., 2013).

The structure and amino acid (aa) sequence of the mammalian VGLUTs are highly similar. They consist of 560 to 582aa with 12 membrane-spanning domains, whereas the carboxy (C)- and amino (N)-terminus face the cytoplasmic site (Liefferinge et al., 2013; Anne and Gasnier, 2014; fig.4A). The amino acid sequence of the membrane-spanning segments of the VGLUT isoforms is with >75% identity highly homologous (Takamori, 2006, fig.4B). In contrast, the C- and N-terminal parts of VGLUTs show clearly more divergence in their amino acid sequence (fig.4B), which may indicate a contribution to potential isoform-specific functions. However, there are also similar segments. For instance, the VGLUT C-terminus exhibits some residues and motifs, which are conserved in all three mammalian VGLUT isoforms and even in other vertebrates or invertebrates like *Ceanorhabditis elegans* or *Drosophila melanogaster* such as a WA(X)PE motif sequence (fig.4B).

From reconstitution studies of VGLUT2 it is known that the residues R88, H128, R184, E191 and R322 are important for glutamate transport (Juge, 2006). For VGUT1 three arginine residues (R80, R176 and R314) are exposed to the pore (Almqvist et al., 2007). Whether equivalent residues in VGLUT3 are also pore building, is not known.

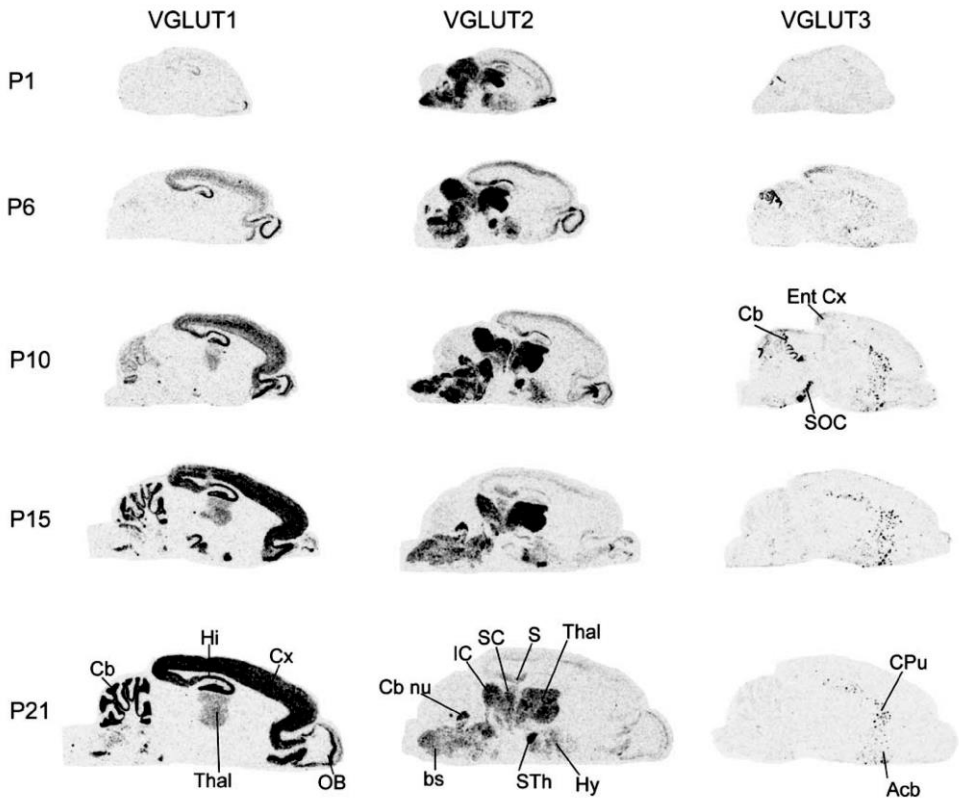

Fig. 3: **VGLUT expression in the mammalian brain during postnatal development:** VGLUT2 expression is dominant in the beginning of the brain development, especially in parts of the diencephalon and brainstem. Later also VGLUT1 is well expressed, mainly in the hippocampus and parts of the cortex. VGLUT3 is only sparsely expressed, mostly in cholinergic, serotonergic and GABAergic neurons (image from Gras et al., 2005; Acb, nucleus accumbens; bs, brainstem; Cb cerebellum; Cb nu, deep cerebellar nuclei; CPu, caudate putamen; Cx, cerebral cortex; Ent Cx, entorhinal cortex; Hi hippocampus; Hy, hypothalamus; IC, inferior colliculus; OB, olfactory bulb; S, subiculum; SC, superior collioculus; STh, subthalamic nucleus; Thal, thalamus nuclei; SOC, superior olivary complex).

A: Schematic VGLUT protein structure

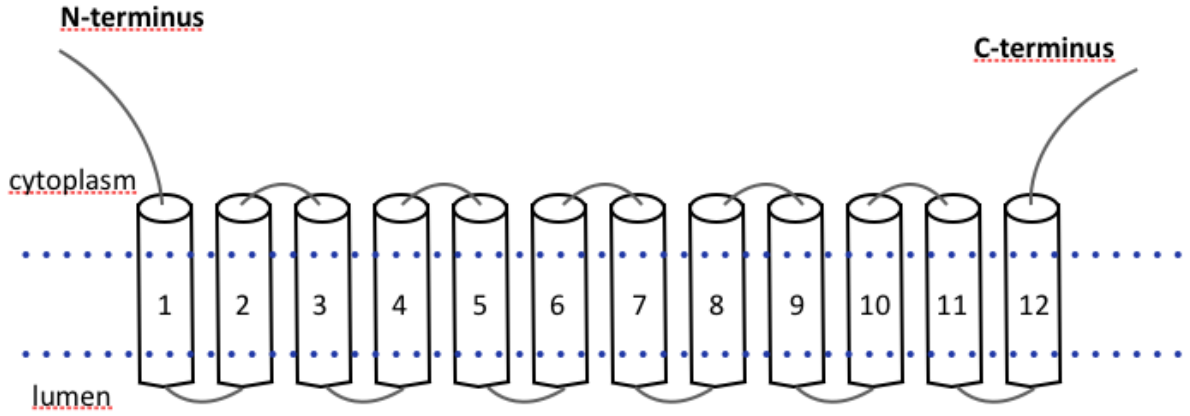

B: VGLUT sequence alignment

```
VGLUT1 1-------------MEFRQEEFRKLAGRALGRLHRLLEKRQEGAETLELSA 37
VGLUT2 1-----MESVKQRILAPGKEGIKNFAGKSLGQIYRVLEKKQDNRETIELTE 45
VGLUT3 1MPFKAFDTFKEKILKPGKEGVKNAVGDSLGILQRKIDGTNEEEDAIELNE 50
        :   :* .:: .* :** : * ::  ::  :::**.

        DGRPVTTHTRDPPVVDCTCFGLPR-------------RYIIAIMSGLGFC 74
        VDGKPLEVPEKKAPLCDCTCFGLPR-------------RYIIAIMSGLGF 82
        EGRPVQTSRAHRPVCDCSCCGIPKRYICDCSCCGIPKRYIIAVMSGLGFC 100
        :*:*: .   . *: **:* *:*:             *****:*******

        ISFGIRCNLGVAIVSMVNNSTTHRGGHVVVQKAQFNWDPETVGLIHGSFF 124
        ISFGIRCNLGVAIVDMVNNSTIHRGGKVIKEKAKFNWDPETVGMIHGSFF 132
        ISFGIRCNLGVAIVEMVNNSTVYVDGKPEIQTAQFNWDPETVGLIHGSFF 150
        **************.****** : .*:   :.*:*********:******

        WGYIVTQIPGGFICQKFAANRVFGFAIVATSTLNMLIPSAARVHYGCVIF 174
        WGYIITQIPGGYIASRLAANRVFGAAILLTSTLNMLIPSAARVHYGCVIF 182
        WGYIVTQIPGGFISNKFAASRVFGAAIFLTSTLNMFIPSAARVHYGCVMG 200
        ****:******:*..::**.**** **. ******:************:

        VRILQGLVEGVTYPACHGIWSKWAPPLERSRLATTAFCGSYAGAVVAMPL 224
        VRILQGLVEGVTYPACHGIWSKWAPPLERSRLATTSFCGSYAGAVIAMPL 232
        VRILQGLVEGVTYPACHGMWSKWAPPLERSRLATTSFCGSYAGAVVAMPL 250
        ******************:****************:*********:****

        AGVLVQYSGWSSVFYVYGSFGIFWYLFWLLVSYESPALHPSISEEERKYI 274
        AGILVQYTGWSSVFYVYGSFGMVWYMFWLLVSYESPAKHPTITDEERRYI 282
        AGVLVQYIGWASVFYIYGMFGIIWYMFWLLQAYECPAAHPTISNAERTYI 300
        **:**** **:****:** **:.**:**** :**.** **:*:: ** **




        EDAIGESAKLMNPVTKFNTPWRRFFTSMPVYAIIVANFCRSWTFYLLLIS 324
        EESIGESANLLGAMEKFKTPWRKFFTSMPVYAIIVANFCRSWTFYLLLIS 332
        ETSIGEGANLAS-LSKFNTPWRRFFTSLPVYAIIVANFCRSWTFYLLLIS 349
        * :***.*:* . : **:****:****:**********************

        QPAYFEEVFGFEISKVGLVSALPHLVMTIIVPIGGQIADFLRSRHIMSTT 374
        QPAYFEEVFGFEISKVGMLSAVPHLVMTIIVPIGGQIADFLRSKQILSTT 382
        QPAYFEEVFGFAISKVGLLSAVPHMVMTIVVPIGGQLADYLRSRKILTTT 399
        ********** *****::**:**:****:******:**:***::*::**

        NVRKLMNCGGFGMEATLLLVVGYSHSKGVAISFLVLAVGFSGFAISGFNV 424
        TVRKIMNCGGFGMEATLLLVVGYSHTRGVAISFLVLAVGFSGFAISGFNV 432
        AVRKIMNCGGFGMEATLLLVVGFSHTKGVAISFLVLAVGFSGFAISGFNV 449
        ***:*****************:**::**********************
```

```
NHLDIAPRYASILMGISNGVGTLSGMVCPIIVGAMTKHKTREEWQYVFLI 474
NHLDIAPRYASILMGISDGVGTLSGMVCPIIVGAMTKNKSREEWQYVFLI 482
NHLDIAPRYASILMGISNGVGTLSGMVCPLIVGAMTKHKTREEWQNVFLI 499
****************:***********:*******:*:***** ****

ASLVHYGGVIFYGVFASGEKQPWAEPEEMSEEKCGFVGHDQL-------- 516
AALVHYGGVIFYALFASGEKQPWADPEETSEEKCGFIHEDELDEETGDIT 532
AALVHYSGVIFYGVFASGEKQDWADPENLSEDKCGIIDQDELAEETELNH 549
*:****.*****.:******* **:**: **:***:: .*:*

-----AGSDESEMEDEAEPPGAPPAPPPSYGATHSTVQPPRPPPPVRDY- 560
QNYINYGTTKSYGATSQENGGWPNGWEKKEEFVQEGAQDAYTYKDRDDYS 582
ETFVSPRKKMSYGATTQNCEVQKTEWRQQRESAFDGEE-PLSYQAEGDFS 598
.  *      :          .   . .  : . .     *:

---     VGLUT1
---     VGLUT2
ETS 601 VGLUT3
```

Fig. 4 (A and B): **Protein structure and computer software predicted sequence alignment of mammalian VGLUT1-3:** schematic overview of VGLUT structure (A) with its 12 transmembrane domain. The N- and C-terminal ends face the cytoplasm. A computer software predicted sequence alignment of mammalian VGLUT1-3 (B) illustrate that there is a high homology of their amino acid sequences. Less analogy excists in the C- and N-terminal parts of the sequence (consensus symbols: ***** (asterisk): indicates positions, which have a single, fully conserved residue; **:** (colon): indicates conservation between groups of strongly similar properties; **.** (period): indicates conservation between groups of weakly similar properties; source: www.ebi.ac.uk/Tools/msa/clustalw2/).

1.5 The involvement of VGLUTs in neurological and psychiatric disorders

Glutamate is the most abundant excitatory NT in the mammalian CNS and an unimpaired glutamatergic neurotransmission is important to maintain general brain functions. Therefore, a reliable functionality of the VGLUTs is necessary to fill SVs with glutamate during vesicle recycling.

From previous studies, and our experiences, it is known that VGLUT1 KO mice die around three weeks after birth (Tordera et al., 2007). VGLUT2 KO mice die immediately after birth, because of absence of respiratory behavior (Wallén-Mackenzie et al. 2010). Several other studies show that mice lacking VGLUTs have addition problems in the sensory processing, motor coordination, learning and memory. They also show neuropathic pain and anxiety (Balchun et al., 2009; Fremeau et al., 2004; Moechars et al., 2006; Smear et al., 2007, Tordera et al., 2007, Wojcik et al., 2004). Moreover, impaired glutamatergic neurotransmission is believed to contribute to neurological and psychiatric diseases including: depressive disorder, bipolar disorder (Uezato et al., 2009), Alzheimer`s disease (Kashani et al., 2008; Liraz et al., 2013), epilepsy (Jahn, 2010, Juge et al., 2010, Schallier et al., 2009) and schizophrenia (Eastwood and Harrison, 2005; Uezato et al., 2009; Oni-Orisan et al., 2008). Another study reveals that increased VGLUT expression causes excitotoxic neuro-degeneration in fly (Daniels et al., 2011).

Further investigation of the relevance of VGLUTs in neurological and psychiatric disorders is important to develop ways for therapy and treatments to avoid the onset of disorders or to improve the effects of them. To understand the very complex correlation between protein dysfunction and functional consequences, for example failures in synaptic transmission by NT imbalance, it is important to understand the basic protein function. Therefore, structure-function analyses are a helpful tool. Thereby the protein structure is modified for example by induced mutations and the functional consequences are investigated.

1.6 The importance of VGLUT1 and its C-terminus

An important question is, whether VGLUTs have an additional function in glutamatergic neurotransmission besides their role in SV filling with glutamate and if so, which part of the protein regulates that function.

Evidence supporting a role of VGLUTs beyond SV filling are results from a previous study, which show that SVs carrying different isoforms of the VGLUT protein differ in their

efficiency to release glutamate (Weston et al., 2011). VGLUT1-expressing neurons have a lower vesicular release probability (Pvr), reflecting a lower chance of a fusion competent vesicle to be released, than VGLUT2 or VGLUT3-expressing neurons (Weston et al., 2011). A specific interaction between VGLUT1 and the synaptic protein endophilinA1 seems to play a role in regulating the release probability. In general, endophilins are known to be important in SV endocytosis functioning as a membrane-bending molecule, which is necessary in the clathrin-uncoating step (Bai et al., 2010; Kjaerulff et al., 2011; Sundborger et al., 2010). Imaging experiments of endophilinA1 knockout (KO) mice using a fluorescent reporter protein also reveal a slowing of endocytosis consistent with electrophysiological findings (Milosevic et al., 2011; Schuss et al., 2013).

The binding site of the VGLUT1-endophilinA1 interaction is one of two existing polyproline-rich domains (PRD2) in the VGLUT1 C-terminus with a C-terminal SH3 domain of endophilinA1 (DeGois et al., 2006; Vinatier et al., 2006, fig.5). PRDs do not exhist in VGLUT2 and VGLUT3. A single point mutation in VGLUT1 at the site P554 of PRD2 to alanine (A) causes a disruption of the VGLUT1 endophilinA1 interaction and leads to a higher Pvr (Weston et al., 2011). In addition, a recent study hypothesizes that the VGLUT1 interaction with endophilin influences the endocytic pathway as well (Foss et al., 2013). The idea is that VGLUT1 recycles directly from the plasma membrane versus through an endosomal or cisternal intermediate (Foss et al., 2013).

All three mammalian VGLUTs exhibit also non-isoform-specific, non-filling motifs, such as a C-terminal dileucine-like ((E/D)XXXL(L/I)) motif sequence, which consists of acidic residues at the positions -4 and -5 upstream of two hydrophobic residues. This sequence is known to be important for the trafficking of multispanning transmembrane proteins (Marks et al., 1996; Bonifacino and Traub, 2003). Other vesicular transporter proteins express dileucine-like motif structures as well, for example vesicular monoamine transporters (VMATs), vesicular acetylcholine transporters (VAChTs) and VGATs, where the motif plays an important role in protein trafficking and endocytosis (Tan et al., 1998; Santos, 2001; Santos et al., 2013).

In VGLUT1 the dileucine-like motif sequence is: $E_{505}EKCGFV_{511}$ (fig.5). VGLUT2 and 3 exhibit a similar sequence (fig.5). Previous studies have shown that the dileucine-like motif structure FV in the VGLUT1 C-terminus is crucial for VGLUT1 trafficking (Voglmaier et al., 2006). FV510/511AA mutation reveals a slower endocytosis rate compared to non-mutated VGLUT1 wildtype (WT) protein (Foss et al., 2013; Voglmaier et al., 2006). Additionally, the

surface expression after 30 Hz stimulation is higher in FV510/511AA (Foss et al., 2013). The trafficking of VGLUT2 also depends on the conserved C-terminal dileucine-like motif sequence (Foss et al., 2013). Data about VGLUT3 and a role of its dileucine-like motif sequence do not exist.

A similar effect of impaired trafficking is also known from VGAT. Here, a mutated FA of the dileucine-like motif sequence $E_{39}EAVGFA_{45}$ shows a slower endocytosis rate as well. Mutated EE of the VGAT dileucine-like motif sequence shows slower endocytosis as well. Both VGAT mutant versions, FA/AA and EE/GG, also exhibit a higher surface expression (Santos, et al. 2013). Likewise, all mammalian VGLUTs contain EEs in their C-terminal dileucine-like motif sequence, but their functional role is not known.

A recent study describes that the mammalian VGLUT1 N-terminus also contains dileucine-like motif sequences (Foss et al., 2013), which are not well conserved in the other two VGLUT isoforms. Mutations of the two N-terminal VGLUT1 dileucine-like motif sequences cause impaired protein accumulation at the synaptic sites (Foss et al., 2013). Moreover, this study shows that VGLUT1 trafficking is mediated by different adaptor proteins. The VGLUT1 C-terminal dileucine-like motif sequence operates mainly by adaptor protein 2, whereas the N-terminal dileucine-like motif sequences use adaptor protein 1 (Foss et al., 2013).

Recent data also propose a day-time depentent sorting of VGLUT1 to the plasma membrane, which might be to modulate glutamate transmission (Darna et al., 2009), but further studies to elucidate this possibility are required.

Moreover, a VGLUT1 C-terminal serine (S) at the position 504 (S504) flanks the dileucine-like motif upstream of the sequence. The other two VGLUT isoforms also contain a dileucine-like motif sequence flanking serine (fig.4B).

S504 as well as three other VGLUT1 C-terminal serine sites are potential phosphorylation sites, as prognosticated by phosphorylation site prediction software (NetPhos2.0 by Center for Biological Sequence (CBS) analysis). S519 and S522 are located in front of the PRD1 of VGLUT1. S540, located between the VGLUT1 PRD1 and PRD2, is part of a SYGAT motif (fig.5). A recent study using the radioactive isotope $^{32}P_i$ to label VGLUT1 constructs and autoradiography can strengthen the idea that S519 and S522 are phosphorylation sites (Santos et al., 2014).

However, if phosphorylated, the VGLUT1 S504 residue would become negatively charged. Several other vesicular NT transporters also contain a charged residue upstream of the

dileucine-like motif sequence such as VMAT and VAChT, which exhibits the positively charged residues lysine (K) and arginine (R) (Erickson et al., 1994; Tan et al., 1998). VGAT also contains a negatively charged residue, the aspartic acid 38 (D38), flanking the dileucine-like motif sequence (Blagoveshchenskaya et al., 1999, Santos et al., 2013). Mutation of D38 to glycine (G) alters the recycling kinetics of VGAT (Santos et al., 2013).
In principle, phosphorylation sites in other vesicular NT transporters such as VAChT play a role in regulating transporter trafficking (Krantz et al., 2000, Cho et al., 2000). For instance phosphorylation of VMATs has different regulatory roles, for example in transporter expression, activity, trafficking and degradation (Krantz et al., 1997; Ramamoorthy et al., 2011). However, NT uptake seems to be not necessarily affected by different protein phosphorylation states of vesicular NT transporters, at least not for the vesicular loading of GABA in VGAT (Bedet et al., 2000).

Besides the dileucine-like motif sequence all three mammalian VGLUT isoforms exhibit some other similar motifs such as the WA(X)PE motif sequence a few amino acids away from the last 12th transmembrane domain and a SYGAT motif sequence containing two potential phosphorylation sites S540 and the tyrosine (T) T544 (fig.5). Even invertebrates such as *Drosophila melanogaster* express the highly conserved SYGAT motif sequence, but nothing is known about a potential functional role for VGLUTs.
Furthermore, a recent study described an additional web-based predicted C-terminal VGLUT domain, the so-called PEST domain. Both, VGLUT1 and VGLUT2, contain two lysine residues flanking a sequence, which is rich in proline (P), glutamic acid (E), serine (S) and threonine (T) residues, called PEST (Santos et al., 2014). Usually, PEST domains can direct ubiquitination or calpain cleavage (Rogers et al., 1986; Chummy et al., 1999). This study suggests that ubiquitination occurs in VGLUT1 (Santos et al., 2014). The study also identified several other interaction partner of the VGLUT1 C-terminus such as tyrosine kinases, cytoskeletal adaptors and ubiqutitin ligases, but their role in VGLUT1 function and synaptic transmission need to be further investigated (Santos et al., 2014).

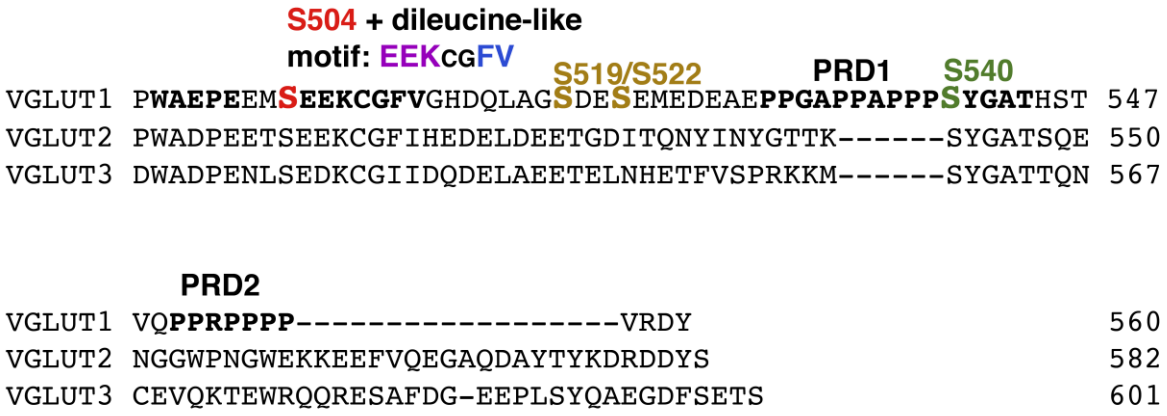

Fig. 5: **Sequence alignment of mammalian VGLUT1-3 C-termini with VGLUT1 related structures and potentially important residues:** shown is the amino acid sequence of the C-terminus from all three VGLUT isoforms starting right after the predicted 12th transmembrane. Highlighted are in color putative VGLUT1 serine phosphorylation sites (S504 in red, S519/S522 in brown, S540 in green), the dileucine-like motif (black) with the FV structure (blue) and (S)EEK motif (S red and EEK purple), the WAEPE motif (black), the polyproline-rich motifs 1 and 2 (PRD1 and 2, black) and the highly conserved SYGAT motif (black) (all in bold) (sequence alignment by www.uniprot.org).

1.7 Aim of this thesis

Different studies of synaptic proteins and vesicular NT transporters show that the C- and N-terminus have a high relevance for their protein function. For example a mutation at the C-terminus of the serotonin transporter disrupts brain serotonin function (Zhao et al., 2006). In the dopamine transporter discrete epitopes in the C-terminus are involved in protein targeting to the cell surface (Bjerggaard et al., 2004).

As already mentioned a previous study has shown that the VGLUT1 C-terminus is crucial for the protein trafficking through its dileucine-like FV structure. A FV510/511AA mutation slows the endocytosis rate of VGLUT1 significantly (Voglmaier et al., 2006), but if the speed of VGLUT1 recycling might be a limiting factor for maintaining baseline synaptic transmission is unknown and needs to be investigated.

Moreover, a recent study (Santos et al., 2014) and software-based predictions show multiple serine (S) sites in the VGLUT1 C-terminus to be phosphorylation sites, but so far no studies exist testing their role in VGLUT1 function. Therefore, another focus of this research project was to investigate, whether mutations of the C-terminal serine sites S504, S519, S522 and S540 alter VGLUT1 functionality. The serine sites were substituted with alanine (A) to mimic permanent dephosphorylation (phosphodeficient mutants) or replaced by glutamic acid (E) to mimic permanent phosphorylation (phosphomimetic mutants).

Generally, it is important to understand how phosphorylation might influence VGLUT1 function, but also whether other special motifs of the VGLUT1 C-terminus such as the WAEPE motif sequence are important for proper VGLUT1 operation in synaptic transmission and SV cycling.

Furthermore, nothing is known, whether VGLUT1 is functional without its C-terminus. Therefore, another object of investigation in this study is to test the functional consequences of a truncated VGLUT1.

To address these questions structure-function analyses of the VGLUT1 C-terminus were performed using the whole-cell voltage clamp technique in combination with fluorescence-based imaging on single neurons, so called autaptic cultures. With such elctrophysiological recordings the physiology of a neuron can be investigated. The use of a pH-sensitive green fluorescent fusion protein (pHluorin), which is directly coupled with VGLUT1, allows to study the VGLUT1 cycling in real time. The advantage of the autaptic culture system, where all synapses that contact the dendrite of the neuron are formed by the axon of the same neuron, is a direct control and measurement of input by electrical cell stimulation and output (postsynaptic response).

Gain-of-function rescue experiments by specific lentiviral infection were used to restore VGLUT1 wildtype (WT) protein or mutant variants in VGLUT1 KO hippocampal neurons, which allows a direct comparison of different VGLUT1 constructs. Mutant constructs of specific VGLUT1 residues and motifs were created by site-directed mutagenesis and also include C-terminal truncation and deletion versions.

In addition, to investigate potential changes of the SV morphology and number, EM was used. EM analyses help to see if there are any correlations of structural changes of SVs to potential functional alterations in VGLUT1 mutants. Impaired SV endocytosis for example by blocking dynamin, a protein important in the scission of newly formed vesicles, leads to changes in the SV morphology (Kirchhausen et al., 2008; Newton et al., 2006).

The used techniques of this study are in detail described in the following chapter „Material and methods“.

2. Material and Methods

Introduction of the main techniques

2A: Whole-cell voltage clamp recordings in autaptic culture to study neurotransmission

One main interest in this study is to investigate the function of VGLUT mutants in synaptic transmission. To monitor synaptic transmission the voltage clamp technique can be used, which allows the investigation of ion currents through the plasma membrane of neurons, but also of other excitable cells such muscle fibers.

A refinement of the voltage clamp technique is the patch clamp technique developed by E. Neher and B. Sakmann in the 1970s. In 1991, both received the Nobel prize of physiology and medicine for their invention (Kandel et al., 2000).

For patch clamp recordings a single glass micropipette with a small tip about one micrometer to enclose a certain area of the neuronal surface membrane, the so-called "patch", is used (fig.6). This allows for example the investigation of single or multiple ion channels.

The most commonly used patch clamp mode is the whole-cell configuration. Here, the micropipette is pressed against the membrane patch and by suction a high electrical resistance seal between the glass and the cell membrane is formed, so-called "gigaseal", since the resistance is about one gigaohm. With more suction the membrane patch of the neuron gets disrupted providing access to the intracellular part of the neuron.

Other patch clamp configurations are the cell-attached mode, where the membrane patch is left intact or the loose-patch mode, where the pipette is only loosely attached to the membrane (Numberger and Draghun, 1996; Reichert, 2000).

The micropipette is filled with a conducting internal electrolytic solution, which can be for example a potassium chloride (KCl)-containing solution. A chlorinated silver wire inside the micropipette (electrode, fig.6), that is in contact with the internal solution, can conduct electric currents, which are monitored with a computer. A reference electrode is located in the external solution surrounding the cells, which usually contains among others a high concentration of sodium ions similar to the physiological environment of a neuron.
A differential amplifier allows to keep the voltage constant, while observing changes in current (voltage clamp). Alternatively, the neuron can be also current clamped to observe changes in membrane voltage (Numberger and Draghun, 1996).

In the present study whole-cell voltage clamp recordings were performed in autaptic cultures. This model system was invented by J. Bekkers and C. Stevens and further developed by C. Rosenmund (fig.6, Bekkers and Stevens, 1991; Pyott and Rosenmund, 2002). Here, a single neuron grows on a small island of glial cells (microculture) and forms synapses onto itself, so-called autaptses (fig.6). This special culture technique excludes communication between adjacent neurons (network activity), which is different from mass cultured neurons or slice preparations. The autaptic culture system helps to elucidate basic mechanisms of the single cell neurotransmission, because both, the pre- and postsynaptic function of a neuron, can be monitored by a single recording micropipette and thereby electrical input and output properties can be easily controlled.

To induce AP-evoked SV fusion a brief voltage step can be applied and postsynaptic currents (PSCs) can be measured. The PSC charge represents all released SVs during one AP. Other synaptic release characteristics, including the probability of a vesicle to release (Pvr) or the number of readily releasable SVs, can be simply studied as well. The RRP contains the subset of all docked and primed vesicles that are immediately ready for release upon electrical stimulation. The RRP can be triggered by use of 500 mM hypertonic sucrose solution (Rosenmund and Stevens, 1996). The Pvr is calculated as the ratio of the size of the PSC charge and the size of the RRP charge. Spontaneous miniature PSCs (mPSCs), representing the response to a single released vesicle, can be equally monitored. Also high frequent AP-trains, mostly 10 Hz stimulations, can be applied.

An advantage of the autaptic culture system is the direct control and measurement of PSCs during presynaptic cell stimulation. The spatial restriction of the autaptic neurons also allows an easy exchange of the external solution or the application of different drugs by a so-called fast flow perfusion system. Thereby, drug concentrations can be precisely varied during the experiments.

A limitation of the autaptic culture system is that the neurons are prepared from young animals, such as mice, and therefore only represent an immature physiological state of the cells. In this study hippocampal neurons from newborn mice (around 0-2 days after birth) were mainly used, because about 90% of the hippocampal neurons express VGLUT1. A small fraction of hippocampal neurons about 12% also express VGLUT2. VGLUT3-expressing cells in the hippocampus are very rare with less than 1% (Wojcik et al., 2004). Besides excitatory neurons, the hippocampus also contains a variety of inhibitory interneurons, but they are also rare in cell number. In cell culture inhibitory neurons can be distinguished from excitatory ones by their typical morphology or their PSC kinetics (Benson et al., 1994).

Another disadvantage of the autaptic culture system, compared to mass cultured neurons or slice preparations, is that the cell environment is supposedly different without network activity of neighboring neurons. This may influence the cell physiology in unexpected ways (Amara S., 1998). For instance, hippocampal autaptic neurons or neurons in a network exhibit distinct synaptic transmission phenotypes in absence of synaptotagmin I, represented by different mEPSC frequencies (Liu et al., 2009)

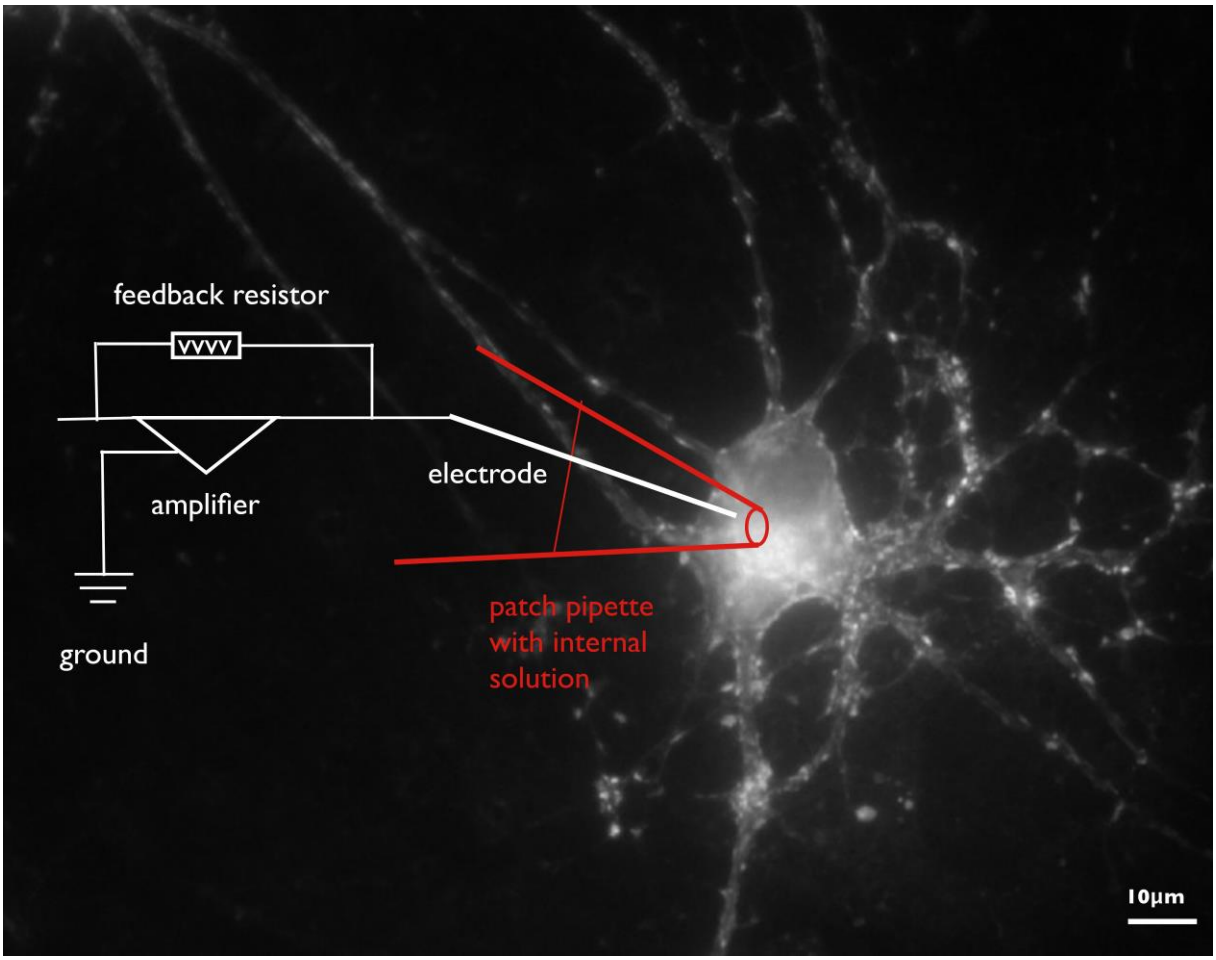

Fig. 6: **Scheme of voltage clamped whole-cell recording on a single (autaptic) neuron:** shown is a circuit diagram showing an electrode, a feedback resistor, an amplifier and a ground. A micropipette with the electrode is filled with a conducting solution and connected to the amplifier and feedback resistor to measure the membrane potential and send compensation currents back to the neuron. The idea is to keep the voltage constant, typically at -70 mV, while observing changes in current during electrical stimulation. The ground is to minimize electrical noise. The shown autaptic VGLUT1 KO neuron expresses virus-mediated mkate tagged VGLUT1. The punctate fluorescence pattern illustrates synaptic VGLUT1 expression in the dendrites (4% PFA fixed neuron, red fluorescence protein (RFP) antibody staining to recognize the mkate tag, 60x magnification).

2B: pH-sensitive green fluorescent protein (pHluorin)-based live cell imaging to monitor synaptic vesicle cycling

With whole-cell voltage clamp recordings it is possible to obtain information about spontaneous or by electrical stimulation evoked changes of PSCs of a neuron, but the functional activity of single synapses remains inaccessible. To directly investigate changes in SV exo- or endocytosis of individual synaptic boutons, imaging techniques are more beneficial. Especially, the pH-sensitive green fluorescent protein (pHluorin)-based imaging assay allows to study the SV cycle in a synapse in real-time. The combination of both techniques, whole-cell voltage clamp and pHluorin-based imaging, permits a perfect control of defined neuron stimulation and monitoring the SV cycling.

pHluorin is a pH-sensitive green fluorescent protein (GFP)-variant developed by G. Miesenböck and colleagues in 1998 (Miesenböck et al., 1998). The idea of the pHluorin asssay is to detect fluorescence changes (ΔF) of the pHluorin molecule caused by changes of the pH during SV cycling (cf. fig7).

In the present study the VGLUT1 (mutant) constructs are directly linked to pHluorin molecules (fusion proteins) and thereby expressed on the SV surface. The VGLUT1-pHluorin constructs express the pH-sensitive fluorophore on the luminal side of the SVs, where an acidic pH of about 5.5 quenches the fluorophore fluorescence. This low pH is provided by a vATPase, which transports protons into the vesicles using energy of ATP hydrolysis (acidification, Cidon and Shira, 1989). When the SVs undergo exocytosis, where they fuse with the plasma membrane, the fluorophore is exposed to the outside of the neuron, where the pH is neutral (<7.4). This leads to an increase of the detectable fluorophore fluorescence (unquenching). After SV exocytosis, subsequently endocytosis occurs (SV recycling). Thereby the fluorophore fluorescence is quenched again apparent by a decrease of the fluorescence. This is possible, because the SVs are refilled with NT and re-acidified, which results again in an acidic pH of about 5.5 inside the SVs (re-acidification; Cidon and Sihra,

1989; Miesenb\ck et al., 1998, fig.7). The SV re-acidification is a fast process about 4 s. So, the decline in the pHluorin fluorescence signal gives a measure of SV endocytosis that is close to real-time (Royle et al., 2008).

The change in the pHluorin signal can be used for monitoring the cycling of VGLUT1-pHluorin constructs during electrical stimulation and the retrieval after stimulation. The change in the pHluorin signal can be also used for estimating the rate of VGLUT1-construct release. Additionally, the pHluorin fluorescence is a function of the amount of unquenched pHluorin molecules that are already on the cell surface (surface expression) as well as the rate at which these molecules are internalized into SVs and thereby quenched (Dreosti and Lagnado, 2010).

Another commonly used pHluorin-based reporter is a fusion protein of synaptophysin, which is exclusively expressed on SVs (Kwon and Chapman, 2011) and the most abundant SV protein with about 10% of the total vesicle proteins (Takamori et al., 2006).

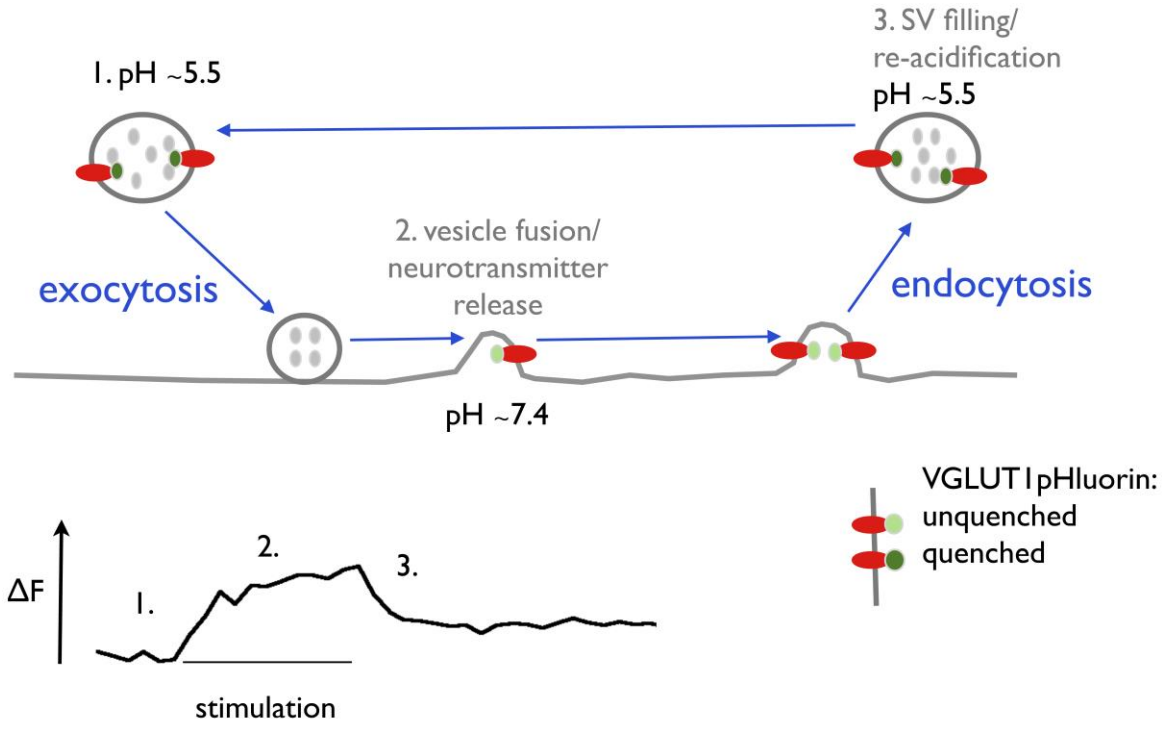

Fig. 7: **Scheme of pHluorin-based imaging:** the schematic diagram in the upper part illustrates the SV cycling: exo-, endocytosis, SV filling with NT (grey dots)/re-acidification. The graph on the bottom shows changes in pHluorin fluorescence levels (⊗F) over time in a single bouton during events described in the scheme with the corresponding numbers. The pHluorin molecules on the SVs (red and green dots) are quenched by low pH of <5.5 inside the vesicles (dark green) and a baseline pHluorin fluorescence can be measured (1). During electrical stimulation (black bar) vesicle fusion with the surface membrane occurs (exocytosis) and the pHluorin fluorescence increases due to changes of the pH (<7.4), thus unquenching the pHluorin molecules (light green) (2). NTs are released. After SV retrieval (endocytosis), NT refilling and SV re-acidification the pHluorin fluorescence declines usually up to baseline fluorescence (3), because pHluorin molecules are quenched again by a pH <5.5 inside the SVs. The SV cycle can start again.

2C: Electron microscopy to investigate the synaptic vesicle morphology

To investigate microscopic very small cell structures a high magnification at best about more than 10,000 times is necessary. In 1926, H. Busch invented the first electromagnetic lenses and a few years later the first electron microscope was built using a beam of electrons as the light source to create an image (Kandel et al., 2000). This prototype was constructed by E. Ruska and M. Knoll in 1931 with a magnification about four hundred times. This invention was awarded by the Nobel prize in 1986. Today electron microscopes achieve resolution in a picometer range and magnifications up to 10,000,000 times. For decades scientists used electron microscopy (EM) to explore the morphology of cells and cell structure. In the 1950s, the first images of nerve cells and SVs were taken by EM (Palay and Palade, 1954; DeRobertis and Bennett, 1955). Since then many new insights in the SV morphology were obtained and sample fixation and embedding techniques were optimized for better resolution and contrast.

The commonly used classical fixatives of proteins are formaldehyde or glutaraldehyde. Lipids are usually fixed with osmium tetroxide. Newly, high-pressure freezing or the so-called cryofixation technique, which means a rapid sample freezing with liquid nitrogen, were developed to achieve a closer native state with less fixation artefacts (Ryan, 1992; Dahl and Staehelin, 1989).

For classical tissue fixation the samples are dehydrated and embedded mostly by resins such as epon. Afterwards the tissue is sectioned in ultra-thin slices. The samples can be treated with uranyl acetate to increase the contrast of the images. Thereby, the uranyl ions bind to proteins and lipids with carboxyl groups such as glycoproteins and ganglioside, which are concentrated on cell membranes, as well as to phosphate groups of deoxyribonucleotide acid (DNA) and ribonucleic acid (RNA). As a result, uranyl acetate delivers a good contrast of

membranes, nucleic acids and nucleic acid-containing protein complexes such as ribosomes (Watson, 1958).

In the present study EM was used to compare the SV morphology and vesicle number of different VGLUT1 mutant constructs with a VGLUT1 full-length rescue construct (WT rescue) and KO conditions.

From previous findings it is known that in VGLUT1 KO neurons SVs look significantly smaller and deformed after classical EM fixation and embedding compared to VGLUT1 WT. A lower number of vesicles was also observed in VGLUT1 KO synapses (Siksou et al., 2013). Interestingly, after high pressure freezing instead of aldehyde fixation the SVs of VGLUT1 KO neurons are not deformed. The reason for this phenotype is the missing VGLUT1 protein causing a reduction in the osmotic pressure in the vesicles, which results in a less stable cell membrane. The appearance of deformed looking SVs in VGLUT1 KO neurons can be prevented by viral-induced VGLUT1 rescue (Siksou et al., 2013).

From other proteins, which are involved in SV cycling, for example endophilin, it is known that a KO can also lead to changes in vesicle number and an enrichment of endocytic or cisternal structures in the synapse (Milosevic et al., 2011; Schuske et al., 2003; Verstreken et al., 2002). A KO of the adapter protein 2 or a depletion of clathrin results in an increase of endosomal-like vacuoles as well (Kononenko et al., 2014).

Therefore, it is important to also investigate potential alterations in the SV morphology and number or other synaptic structures in VGLUT1 mutants.

Performance and evaluation of the experiments

2.1 Neuronal culture

Murine autaptic microisland cultures from VGLUT KO mice were prepared similarly as previously described (Pyott and Rosemund, 2002). VGLUT1 KO mice were earlier described by Wojcik et al., 2004.

Briefly, the hippocampal or thalamic neuron preparation from newborn mice (postnatal, P0-2) were quickly done in 4°C cooled Hank's Balanced Salt Solution (HBSS, Gibco Life technologies, Germany). The neurons were dissected using a sterile filtered papain-containing enzyme solution (50 mM L-cystein, 100 mM $CaCl_2$, 50 mM EDTA, Carl Roth, Germany, 20-25 U papain, Worthington, USA; for pH adjustment CO_2 was applied to the solution for 5 min.) and incubated for 45 minutes. The reaction of the enzyme solution was stopped by 5 min. incubation of sterile filtered inactivating solution (25 mM albumin, 25 mM trypsin, Sigma-Aldrich, Germany in Dulbecco's Modified Eagle's Medium, DMEM, Gibco Life technologies, Germany). Afterwards, the cells were counted and cultured in neuronal basal A (NBA)-containing solution (500 ml NBA, 10 ml B27 supplement, 5 ml glutamax, Gibco Life technologies, Germany, 1 ml penicillin/streptavidin solution, Roche, Germany).

For autaptic neuron cultures used for electrophysiology or pHluorin-based imaging experiments 3,000 neurons were seeded per 35 mm diameter well of a 6 well culture plate. For immunocytochemical quantifications or EM experiments 500,000-1,000,000 neurons, so-called mass cultures, were seeded on a 12 well plate with 22 mm diameter per well or also on a 6 well culture plates. The experiments were usually performed at 12-16 days *in vitro* (DIV) at room temperature (RT). If not extra mentioned in the text, VGLUT1 hippocampal KO cells were used for the experiments, especially for lentiviral achieved gain-of-function rescue experiments of VGLUT1 WT or mutant variants. The virus design and production is detailed described in the paragraph 2.3 "Lentivirus constructs and production". In some experiments VGLUT1 WT or thalamic neurons were used as well.

The autaptic cultured neurons grew on glial microislands, achieved by a stamping technique using a poly-D-lysin coating mixture (1:1:1 mix of poly-D-lysine, acedic acid, Sigma Aldrich, Germany and collagen I, Gibco Life technologies, Germany) similar to Burgalossi et al., 2012. The glial cells are mainly astrocytes derived from P0-2 cortex tissue at a density of 3,000 cells per 6 well culture plate. The astrocytes grew for one week in DMEM solution before the neurons were seeded. Therefore, to stop the glia cell devision after one week a

sterile filtered 5-fluoro-2-deoxyuridine (FUDR)-containing solution was applied to the cells (8.1 mM FUDR, 20.4 mM uridine, Sigma-Aldrich, Germany).
A part of the brain tissue during the hippocampal or thalamic neuron preparation was kept for polymerase chain reaction (PCR, see the next paragraph) to quantify the genotype of the tissue.

2.2 PCR for genotyping

Most of the experiments were done in VGLUT1 or VGLUT2 KO background. For some experiments neurons from VGLUT WT mice were also used.
To examine the genotype of the used animals from the VGLUT mouse line polymerase chain reaction (PCR) was done to amplify extracted DNA from brain tissue. To extract the DNA, the cell tissue was incubated in lysis buffer (10mM Tris HCL, 100 mM NaCl, Carl Roth, Germany) for 5 min. at 55°C. Thereby, the cell membranes were destroyed to open the nucleus. To stop the enzyme reaction the tissue was heated up to 99°C for 10 min.
The components of the solutions necessary to run the PCR as well as the PCR conditions are listed in the tables 1-3. The total amount necessary to run the PCR is 25 µL with 24 µL "mastermix" and 1 µL DNA. The PCR was realized with a MastercyclerPro PCR machine (Eppendorf, Germany).

Tables 1-3: **Overview of PCR conditions to quantify VGLUT1 genotypes:** in table 1 are listed the chemicals, which are needed to run the PCR. Table 2 contains the description of the PCR primer. Table 3 shows the required PCR cycling conditions.

1:

"WT-PCR"	**"KO-PCR"**	**concentration (each)**	**1x (in µL)**
Primer 4172	Primer 4173	10 pmol/µl	0,5
Primer 4173	Primer 4174	10 pmol/µl	0,5
Buffer (1)	Buffer (1)	10x	2,5
NTPs (2)	NTPs (2)	2,5 mM each	1
Taq polymerase (1)	Taq polymerase (1)	5 U/µL	0,2
H_2O	H_2O		19,3
mastermix WT	mastermix KO		24

(1) from New England Biolabs, USA

(2) nucleoside triphosphate s (NTPs): from Biosystems, Switzerland

2:

Primer	**Primer name**	**Primer abbrevation**	**Primer sequence**
forward *	WT-BNP1 NEO 4172	4172	ttc agc agc ccg cgt tca cta tgg
reverse *	WT&KO-BNP1 NEO 4173	4173	ccc agc tca gcc ctc ctc gca caa
forward *	KO-BNP1 NEO 4174	4174	cgc atc gcc ttc tat cgc ctt ctt

* from Metabion, Germany

3:

PCR cycle Steps (N°)	**Temperature**	**Time**
1	95°C	3min
2	95°C	15sec
3	65°C	15sec
4	72°C	30sec
5	72°C	1min
6	12°C	∞
repeat: steps: 2-4		
total cycles: x30		

2.3 Lentivirus constructs and production

The virus preparation was done similarly to Loius et al., 2002. Briefly, HEK293T cells were co-transfected with 10 µg shuttle vector-containing complementary DNA (cDNA) for the different VGLUT constructs and the helper plasmids CMVdR8.9 and pVSV.G (5 µg each) using x-tremeGENE 9 DNA transfection reagent (Roche diagnostics, Germany).

To obtain the virus, the supernatant of virus-containing HEK cell cultures were collected and purified by filtration 72 hours after transfection. Aliquots of the virus-containing supernatants were fresh frozen in liquid nitrogen and stored at -80°C. Estimation of the titer, to guess the virus efficiency for the neuron infection, was done on WT hippocampal mass cultures. For infection of the neurons about 100-500 µl of the virus-containing solution was used after DIV1.

A neuron specific synapsin promotor was used for controlled expression of VGLUT WT rescue or mutant variants. For the study of VGLUT1 or VGLUT2 C-terminal mutants, to detect virus infected neurons, the protein expression cassette also consists of a nuclear localization green fluorescent protein (NLS-GFP) coupled to the VGLUT constructs by a self-cleaving P2A peptide (Kim et al., 2011) or a pHluorin tag (with a linker sequence at aa100). Especially, for the investigation of different VGLUT C-terminus truncation constructs other tags for protein detection and immunocytochemistry experiments were used (a myc tag at aa100 and a mkate tag directly linked after the C-terminal end).

The full VGLUT1 C-terminus truncation construct (VGLUT1Δ496-560) is a deletion of all amino acids right after the last 12th transmembrane domain (Freameau et al., 2001). A shorter C-terminus truncation construct consists of eight more amino acids after the last transmembrane domain including a conserved VGLUT1 WAEPE motif sequence (VGLUT1Δ504-560). For a VGLUT1 chimera construct the VGLUT1 C-terminal end was substituted with the C-terminal sequence of the common SV marker synaptophysin (aa225-aa314). The importance of the VGLUT C-terminus truncation was further tested by using a myc tagged VGLUT2 C-terminus deletion construct (VGLUT2Δ493-582).

To study protein phosphorylation of serines (S) permanent dephosphorylation was mimicked by substituting the S with alanine (A) to prevent potential phosphorylation by kinases. Permanent phosphorylation was mimicked by substituting the S with glutamic acid (E).

Different putative VGLUT1 C-terminal serine phosphorylation sites were mutated: S504 belongs to a $S_{504}EEK_{507}$ motif, which is part of the dileucine-like motif sequence. A double mutation of S519 and S522 was created, because this amino acids are located very

close together and S540 belongs to a conserved VGLUT1 SYGAT motif sequence. Other constructs used for this study are a deletion construct of the $S_{504}EEK_{507}$ motif and the earlier described FV510/511AA mutation (Voglmaier et al., 2006).

2.4 RNA interference by shRNA for protein knockdown

In hippocampal neuron cultures about 12% of the cells express VGLUT2 (Wojcik et al., 2004). To reduce the expression of VGLUT2 in culture VGLUT2 knockdown (KD) was induced by ribonucleic acid (RNA) interference.

RNA interference is a common cellular method of gene regulation. In 1998, Fire et al. described the RNA interference the first time in *Caenorhabditis elegant.* They awarded the Nobel prize for that invention 2006.

To silence the target gene expression short hairpin RNA (shRNA) is used, which is directly expressed in neurons typically via plasmids or, as in this work, by lentiviral cell infection. shRNAs usually consist of a sense and antisense sequences (each about 19–21aa in length). They are synthesized in the nucleus of the target neuron and form a hairpin-like loop structure. This loop structure of the shRNA together with several proteins, the RNA-induced silencing complex (RISC), acts on the cellular mRNA resulting in a subsequent degradation of the targeted mRNA. Thereby, further expression of the target protein is blocked, which in turn leads to a decrease in its expression levels.

The VGLUT2 shRNA was produced similar to the other lentiviral constructs (cf. paragraph 2.3 "Lentivirus constructs and production"). Two shRNA-based KD constructs with the numbers 1 and 2 were created. The shRNA sequence for construct N° 1 is: GGATCCCGTCACTTGGATATTGCTCCATTCAAGAGATGGAGCAATATCCAAGTGATTTTTTTCCAATTAATTAA.

The shRNA sequence for construct N°2: GGATCCCGCAGCACTATCCACCGCGGATTCAAGAGATCCGCGGTGGATAGTGCTGTTTTTTCCAATTAATTAA. For control also an empty unspecific vector was created. For the experiments in this study the KD virus number 1 was used.

2.5 Electrophysiology

Whole-cell voltage clamp recordings were mainly performed from VGLUT WT rescue or KO neurons (control groups) and mutant VGLUT variants in parallel on the same days (between DIV 12-16, at RT). Recordings were done in 2 mM Ca^{2+}/4 mM Mg^{2+} external solution (molecular composition, see below) using a patch clamp amplifier (Multi Clamp 700B, molecular devices, USA) and digitizer (Digidata, Axon instruments, USA) under control of Clampex 9.2 (Mil Devices, USA). Data were acquired at 10 kHz and low pass filtered at 3 kHz. The series resistance was compensated at 70% and only cells with a series resistance below 10-15 mOhm were analyzed. Otherwise data from patched neurons were excluded. Patch pipettes, to access the neurons, had a resistance about 2-4 mOhm.

AP-induced excitatory postsynaptic currents (EPSCs, example fig.8A) were triggered by a 2 ms somatic depolarization from the holding potential of -70 mV to 0 mV. The EPSCs were baselined and integrated for about 1 s to calculate the charge of the transient synaptic current. Measured was also the amplitude of the recorded EPSCs. The size of all fusion competent vesicles, the RRP, was determined by application of SV pool depleting 500 mM hypertonic sucrose solution for 5 s (in external solution, example fig.8B). The use of hypertonic sucrose solution to release the RRP was invented by C. Rosenmund and others (Rosenmund and Stevens, 2006). The RRP was quantified by first baselining the steady state current at the end of the response and then integrating the charge of the transient synaptic current. To determine the release probability of the fusion competent SVs (Pvr) the ratio of the charge of the EPSCs to the RRP charge was calculated (Pvr = EPSC charge/RRP, in %). To avoid rundown affects of the evoked postsynaptic responses over time, which might influence the Pvr calculation, EPSC and RRP was measured at the same time. If the measured EPSC was zero or no RRP could be recorded no Pvr was calculated for that neuron. Short-term plasticity, to get an idea, whether neurons tend to facilitate or depress, was examined either by high frequency stimulation at 10 Hz (50APs, normalized to the 1st response) or by evoking two synaptic responses (paired pulses, PP) with an electrical stimulation interval of 25 ms. Neurons tend to facilitate if the release probability is low or they depress if the release probability is high. The PP were measured to calculate the ratio of the amplitude of the second to first pulse (PP ratio, PPR = EPSC2/EPSC1). A PPR <1 indicates a low Pvr and facilitation. A PPR >1 indicates a high Pvr and depression. For analysis of spontaneous activity, the miniature events (mEPSCs, example fig.8A), neurons were detected with and without kynurenic acid solution for later background noise subtraction (similar to Clements and Bekkers, 1997). For each cell,

the mEPSC data were filtered at 1 kHz and analyzed by using a template-based detection algorithm implemented in the data analyzing software Axograph X version 1.31 (Axograph scientific, Australia) including a rise time of each event of 0.5 ms and decay time of 3 ms. To investigate potential changes during depletion of the SV pool by VGLUT1 mutation, a high stimulation protocol with 1,000AP stimulation and 20 Hz frequency was also used. Afterwards the subsequent recovery of the first 24AP-induced EPSCs (0.2 Hz stimulation) was monitored.

All electrophysiological data were analyzed by using Axograph X and Prism 5 version 5.0 (GraphPad software, USA).

Neurons could be identified as excitatory by the kinetics of the EPSC amplitude, but usually they were identified by application of 3 mM kynurenic acid (in external solution; Tocris Bioscience, USA), an antagonist of ionotropic AMPA-, NMDA- and kainate glutamate receptors. Excitatory (glutamatergic) hippocampal neurons have a 5-10 times faster decay time of the peak of the EPSC amplitude after electrical stimulation to come back to baseline levels (about 5-10 ms) than inhibitory (GABAergic) neurons, which were excluded.

The standard extracellular solution contained (concentration, mM): NaCl (140); KCl (2.4); HEPES (10); glucose (10); $CaCl_2$ (2) and $MgCl_2$ (4) (all Carl Roth, Germany; 300 mOsm, pH 7.4). The standart internal solution contained (concentration, mM): KCl (136); HEPES (17.8); EGTA (1) (Carl Roth, Germany); $MgCl_2$ (0.6); ATP-Mg^{2+} (4); GTP-Na (0.3) (Sigma-Aldrich, Germany); phosphocreatine (12) (Calbiochen, MERCK, Darmstadt, Germany) and phosphocreatine kinase (50 U/ml; Sigma-Aldrich, Germany) (all 300 mOsm, pH 7.4).

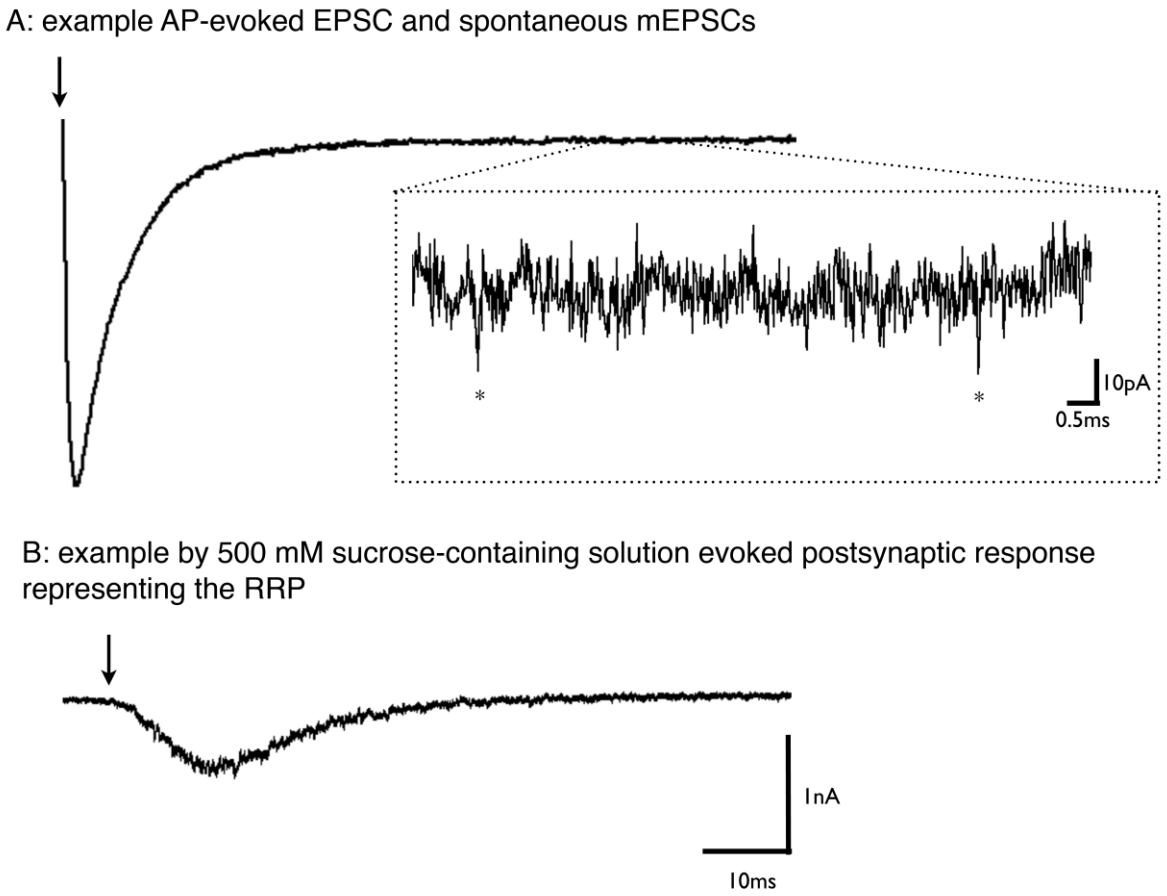

Fig. 8 (A and B): **Example traces of electrophysiological recordings:** illustrated are an AP-evoked EPSC by somatic depolarization for 2 ms (black arrow) and exemplary two spontaneous miniature events (mEPSCs; indicated by a star in the zoom in, black box) (A). The EPSC charge reflects the release of all SVs by one AP. To determine the RRP 500 mM hypertonic sucrose solution is applied for 5 s (black arrow) that all fusion competent vesicles close to the active zone are released (B). The charge of this sucrose-evoked postsynaptic response represents the RRP and can be quantified by first baselining the steady state current at the end of the response and then integrating the area of the transient synaptic current. The probability of a SV to be released, the Pvr, can be calculated by devision of the EPSC charge and the RRP charge.

2.6 pHluorin imaging

To monitor SV cycling the pHluorin-based imaging technique was used. Thereby, the fusion of pHluorin directly to the VGLUT1 protein allows to investigate VGLUT1 during SV exocytosis and recycling (endocytosis with NT refilling) in real-time (Miesenböck et al., 1998). The pHluorin molecule was fused to different VGLUT1 constructs at the position 100aa right after the first transmembrane domain (cf. paragraph 2.3 “Lentivirus constructs and production”).Lentiviral infected neurons in rescue experiments with different mutant VGLUT1-pHluorin constructs in VGLUT1 KO background were compared to VGLUT1 WT-pHluorin.

To test if the general SV cycling is altered in some experiments a synaptophysin-pHluorin (SypHl) construct, similar to Zhu et al., 2009, was used. Here, the pHluorin molecule is directly tagged to synaptophysin. In this experiments VGLUT1 KO neurons were double infected with SypHl and a NLS-GFP expressing VGLUT1 mutant construct. The recorded groups were also compared to pure VGLUT1 KO neurons, which were infected with SypHl and a control virus only expressing a NLS-GFP tag for detection.

Fluorescence changes of the pHluorin molecules were monitored during 5 Hz stimulation for 1 min. (300AP), similar to Voglmaier et al., 2006, followed by application of 50 mM NH_4Cl-containing external solution to alkalinize all synaptic compartments. Thereby the total fraction of pHluorin molecules on SVs could be determined. Afterwards, an acidic external solution with a pH of 5.5 was applied to dim the pHluorin fluorescence at the surface membrane. Thereby, the surface expression could be calculated as the ratio of the peak pHluorin fluorescence of pH 5.5-possessing solution application with the peak fluorescence of NH_4Cl-containing solution application.

The NH_4Cl-containing external solution contained of (concentration, mM): NaCl (90), NH_4Cl (50), KCl (2.4), Hepes (10), $CaCl_2$ (2), $MgCl_2$ (4), glucose (10) (all Carl Roth, Germany; 300 mOsm, pH 7.3). The pH 5.5 external solution contained of (concentration, mM): NaCl (140), KCl (2.4), MES hydrate (10), $CaCl_2$ (2), $MgCl_2$ (4), glucose (10) (all Carl Roth, Germany; 300 mOsm).

Images were acquired with an Andor iXon camera (16 µm x 16 µm pixel size, 2x2 binning, 150-250 ms exposure time) at a rate of 0.5 Hz (300AP stimulation) or 2.5 Hz (NH_4Cl/pH 5.5 application) using a 60x magnification water objective and a band-pass filter with an emission of 500-550 nm. The light source was a polychrome monochromator from Till Photonics, Germany.

The average fluorescence of the regions of interest (ROI) at synaptic boutons was measured with a circle about 3x3 pixels over the center of the bouton by ImageJ 64 (Wayne Rasband National Institutes of Health, USA). For background subtraction the rolling ball option with a ball radius of 50 pixels of ImageJ was used. For data analysis the acquired data were graphically illustrated by AxographX version 1.3.1 and Prism5 version 5.0. The data were baselined from three frames before the electrical stimulation occurs and normalized to either the peak fluorescence of the 300AP stimulation to investigate potential changes in SV exo- or endocytosis or the peak fluorescence of NH_4Cl-containing solution application to become an idea about the total amount of released SVs during the 300AP stimulation. To investigate the SV endocytosis with VGLUT1 retrieval, important to fill newly formed SVs with NT, a single

exponential fit was used to measure the decay time of the pHluorin fluorescence decline. The SV exocytosis, reflected by the rise time during stimulation, was also investigated by use of a single exponential fit. In addition, fluorescence changes of baselined 300AP traces ($\Delta F/F_0$) of the investigated groups after a certain time post stimulus were compared with each other as well.

An advantage of the combination of electrophysiology and pHluorin-based imaging was that the EPSCs during 300AP stimulation can be recorded in parallel to the acquisition of the images. The plotted EPSC amplitudes could be used for analysis of the synaptic strength and plasticity. PP measurements before the imaging protocol started were also used to judge from the kinetics of the PSCs, whether the recorded neuron was excitatory or inhibitory. Inhibitory neurons have a much slower decay time of the peak amplitude of their AP-evoked inhibitory postsynaptic current (IPSC) to come back to baseline levels than excitatory neurons and were excluded.

From the literature it is known that mutated VGLUT1 FV510/511AA slows the VGLUT1 recycling after 5 Hz stimulation (for 1 min.) and increases the cell surface expression (Foss et al., 2013; Voglmaier et al., 2006), which reveals that FV510/511 is important for VGLUT1 retrieval. Therefore, this mutation was used as a control for the VGLUT1-pHluorin experiments in the present study.

2.7 Immunocytochemistry and ratiometric imaging

To determine protein expression levels antibody-based staining (immunecytochemistry, ICC) was used that target specific protein antigens in paraformaldehyde (PFA, Sigma-Aldrich, Germany) fixed neuron cultures. In this study antibodies were used to especially recognize VGLUT1 directly or a myc or mkate tagged VGLUT1 version and usually synaptophysin 1 as control. For quantification of the fluorescence intensities between the analyzed groups, ratiometric imaging was used. Thereby, the fluorescence intensity of the first channel (protein of interest, e.g. VGLUT1) was divided by a second channel (control protein, e.g. synaptophysin) to correct for unequal expression levels between the analyzed groups. The fluorescence intensities of the virus infected neurons are a degree for the protein expression levels of the protein of interest.

Therefore, autaptic or mass cultures were fixed usually at DIV 12-16 with 4% PFA (in phosphate buffered saline (PBS) solution, pH 7.4; Sigma-Aldrich, Germany) for 15 min. and three times washed with PBS solution at RT. The neurons were permeabilized with

0.02% Tween-20 (Sigma-Aldrich, Germany) in PBS solution (PBST) for about 20 min. After a blocking step with 4% normal goat serum (NGS; Jackson Immuno Research, UK) in PBST for 1 h at RT, the samples were incubated with either guinea-pig (gp) VGLUT1 antibody (1:4000, Synaptic Systems, Germany) or rabbit (rb) VGLUT1 N-terminus antibody (1:1000, Abcam, Germany) as well as rabbit or respectively mouse (m) synaptophysin 1 antibody (1:1000, Synaptic Systems, Germany) over night at 4°C. For myc tagged VGLUT1 constructs anti-myc antibodies from Millipore (Germany) and Santa Cruz (USA) were tested in different concentration (1:100-1:5000). None of these antibodies worked specific enough for the experiments (fig.17). For mkate tagged VGLUT1 constructs an anti rb red fluorescence protein (RFP) antibody (Invitrogen, USA) was used. After the incubation with the first antibody, the samples were three times washed with PBST for each time 10 min. Then the neurons were incubated with the corresponding secondary antibody (1:1000, against gp, rb or m with different wavelength fluorophores: Alexa-555 or Alexa 647 to not interfere with the GFP signal from the NLS virus expression or Alexa-488 to not interfere with the mkate signal, Molecular Probes, USA) for 2 h at RT. The fluorescence signals of representative ROIs of the cultured neurons were visualized using an Olympus IX 81 microscope with a 20x objective and a CCD camera with a chip of 1300x1300 pixel size (Princeton, Roper Scientific, Germany). The ratiometric imaging analyses of the ROIs and the statistics were done using ImageJ 64 and Prism 5 version 5.0.

2.8 Electron microscopy

Besides studying synaptic neurotransmission and SV cycling by electrophysiology and combined pHluorin-based imaging the SV morphology of different VGLUT1 mutants was also investigated. Therefore, a high magnification above 10,000 times is required achieved by using dedicated electron beams of EM.

For EM samples of mass cultured neurons were embedded using the epoxy resin epon. The cells were first fixed with 4% PFA solution containing 0.25% glutaraldehyde (GA, Sigma-Aldrich, Germany) in 0.1 M phosphate buffer (PB, pH 7.4, Sigma-Aldrich, Germany) for 45 min. at RT. After four washing steps (each 15 min.) with PB, the neurons were further fixated with 0.5% osmium containing solution (in PB, Carl Roth, Germany) for 45 min. at 4°C. Afterwards the samples were again washed two times with PB and four times with distilled water (ddH_2O, each time for 10 min.), followed by a third fixation step with 2% uranyl acetate (in ddH2O) for 45 min. at 4°C. The uranyl acetate-containing solution needed

to be freshly prepared and sterile filtered using a 2 µm filter. The next step was again a washing step for 4 times in ddH_2O at 4°C. Then, the cells were dehydrated by using different percentage of alcohol (30% for 15 min., 50% for 15 min., 70% over night, 70%, 90%, 96% ethanol, EtOH, each time for 15 min. and 100% EtOH two times for 15 min.; all steps at 4°C). Thereafter, the neurons were incubated with hydroxypropyl methacrylate (HPMA, Sigma-Aldrich, Germany) for 10 min. at RT and afterwards with an HPMA-epon mixture (1:1) for 1 h at RT. The HPMA-epon mixture consists of 5.35 g epon 812, 3.9 g hardener dodecenyl succinic anhydride (DDSA), 3.25 g hardener methyl nadic anhydride (MNA) and 0.25 g accelerator dipropylene glycol monomethyl ether (DMP-30) (all Sigma-Aldrich, Germany). Here, the very exact composition of the substances is important. Then the HPMA-epon mixture was exchanged to fresh HPMA-epon mixture (1:1) and incubated over night at RT. The same mixture was exchanged two more times for 3 h each time and incubated again over night at RT (this last over night incubation step is not necessary, but leads to bettwer embedding results). After one more HPMA-peon mixture exchange for 3 h at RT a polymerization step followed for 18 h at 60°C. Here, it is important that the neurons are oriented to the bottom.

After the epon embedding the resin block was cutted into 40-60 µm thin slices, which were carefully mounted on copper grids with 200 square mesh (G2200N Agar Scientific, UK). The grids were coated and dried before use with 0.75% formvare (in 100% chloroform; Agar Scientific, UK). Then the grids with the slices were counterstained using 2% uranyl acetate (in ddH_2O; Sigma-Aldrich, Germany) for 5 min. at RT. After brief washing steps of each time 10 s ddH_2O the neuron-containing grids were dried and examined under an electron microscope with 30,000 times magnification.

The images were analyzed and statistics performed using ImageJ 64 and Prism 5 version 5.0. The shape of the SVs was investigated by encircling the membrane of the vesicles and analyzing the following parameter: area, perimeter, roundness (with the formula 4π*area/(π*major axis2) and the meaning: 1= perfect circle and 0= increasingly elongated shape). The SV density reflecting the number of the vesicles per square with a length of the active zone (example, fig.9) was analyzed as well. When the active zone could not be precisely determined the SV density was not measured. The Feret`s diameter, which considers the longest distance between two points along the selected vesicle boundary was also measured. The diameter results were grouped into three classes: <30nm, 30-50nm and >50nm.

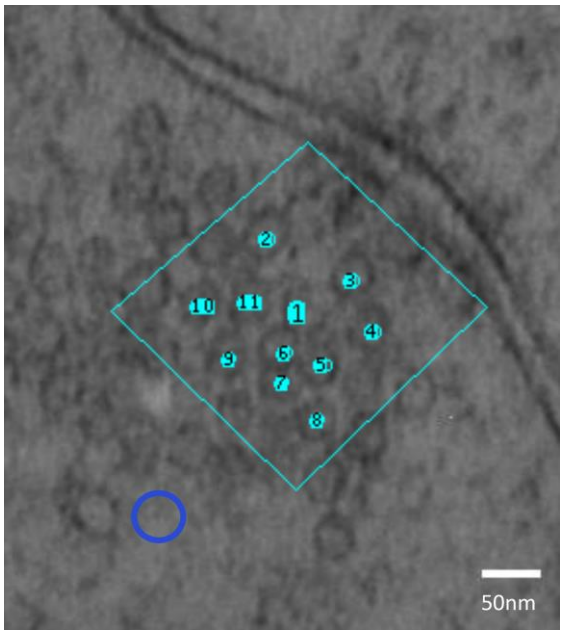

Fig. 9: **Example EM image of SV morphology and density analyses:** the SVs (region of interests, ROIs) were marked and quantified using ImageJ. To measure the SV density a square with the length of the active zone (electron dense membrane) was defined and all vesicles in that square were counted. The SV density is the ratio of the number of ROIs to the size of the square. In blue is an example of a perfect round circle described by the formula 4π*area/(π*major axis2) and defined as "1" (magnification of 30,000x, scale bar 50nm).

2.9 Statistics

Data results from electrophysiology, pHluorin-based imaging and EM experiments were pooled from independently recorded neuronal cultures, as long the values did not vary significantly across different experiments, for example due to bad cell culture quality. Then this cell culture was excluded from the results.

For data analyses of EM images all SV per synapse were quantified. At least ten synapses per investigated group and cell culture were analyzed.

Data were shown as absolute values in comparison to the VGLUT WT rescue or KO neurons (control groups) or normalized to the mean value of the corresponding control group to allow a comparison of divers VGLUT1 mutants across different experiments at distinct timepoints. The normalization was done for each cell culture and altogether the average was calculated for the control or mutant groups. For comparison of two normally distributed groups, statistical significance was tested by using Student`s t test. Otherwise, for three ore more groups statistics were performed by use of One-way ANOVA with tukey`s multiple comparison post hoc test (* P<0,05, ** P<0,001, *** p<0,0001). To illustrate error bars the standard error of means (s.e.m.) was used.

All statistical information as well as the sample number (n number) are mentioned in the figures.

3. Results

3.1 Mutations of the C-terminal VGLUT 1 dileucine-like motif impair VGLUT1 recycling without affecting neurotransmission

The VGLUT1 C-terminus contains a dileucine-like motif sequence, E_{505}EKCGFV_{511}. Generally, the short linear dileucine-like motif sequence, which is present within cytosolic domains of different transmembrane proteins, is known to be important for protein sorting and trafficking (Bonifacino and Traub, 2003). From other vesicular transporters, such as VMAT and VAChT, it is known that dileucine-like motif sequences are important for their trafficking as well (Tan et al., 1998). Previous studies have shown that the VGLUT1 C-terminus is crucial for trafficking through its dileucine-like $F_{510}V_{511}$ structure as well (Voglmaier et al., 2006). pHluorin-based imaging experiments show that mutation of that FV motif to AA results in a delayed VGLUT1 endocytosis. A FV/GG mutation leads to an even slower VGLUT1 endocytosis (Foss et al., 2013). Whether differences in VGLUT1 recycling influence NT release properties, is unknown. Likewise, the functional role of the other amino acids of the VGLUT1 dileucine-like motif sequence were not investigated yet.

Therefore, combined whole-cell patch-clamp recordings with pHluorin-based imaging were performed to further investigate the relevance of the VGLUT1 trafficking motif sequence E_{505}EKCGFV_{511} in neurotransmission and cycling. Hippocampal autaptic VGLUT1 KO neurons were lentiviral infected to express either the VGLUT1 FV510/511AA construct (similar to Voglmaier et al., 2006) or a VGLUT1 C-terminus construct lacking the S_{504}EEK_{507} domain in comparison to a VGLUT1 full-length construct (WT rescue, control). EM images of the VGLUT1 dileucine-like motif sequence mutants were also examined to test if potential alterations in VGLUT1 recycling or NT release might lead to changes in their SV morphology or density.

3.1.1 FV510/511AA mutation and $S_{504}EEK_{507}$ deletion results in slower VGLUT1 retrieval

In this study it can be confirmed in pHluorin experiments (example images, fig. 10A) that the C-terminal VGLUT1 FV510/511AA mutation causes a slower VGLUT1 recycling as previously described by Voglmaier et al., 2006 and Foss et al, 2013. This is apparent in a slowed decay time analyzed by use of a single exponential fit of the pHluorin fluorescence decline in the to 300AP normalized traces (fig.10B). Therefore, VGLUT1 FV510/511AA-pHluorin was used as a positive control in all following VGLUT1-pHluorin experiments. Interestingly, the decay time of FV510/511AA-pHluorin is not slowed to the same extent in autaptic cultured mouse neurons compared to mass cultured rat neurons, which Voglmaier et al, 2006 and Foss et al., 2013 used.

The $S_{504}EEK_{507}$ deletion-pHluorin construct also shows a little slower VGLUT1 recycling compared to the WT rescue (exponential fit (τ): 10.5± 0.18s in WT rescue (WT resc.), 11.3± 0.25s in $S_{504}EEK_{507}$ del., 14.8± 0.24s in FV510/511AA, fig.10B). In addition, investigation of the fluorescence canges ($\Delta F/F_0$) of the $S_{504}EEK_{507}$ deletion 125 s post stimulus (t_{150s}) strengthen the results found by the exponential fit analyses. Here, higher pHluorin fluorescence values of FV510/511AA and the $S_{504}EEK_{507}$ deletion illustrate that less VGLUT1-pHluorin molecules are recycled during endocytosis, at which the pHluorin fluorescence is normally quenched (t_{150s} $\Delta F/F_0$: 0.2 in WT resc., 0.27 in $S_{504}EEK_{507}$ del., 0.3 in FV510/511AA, fig.10B). Analyzing the rise time in the to 300AP normalized traces by exponential fit and the pHluorin fluorescence change 25 s post stimulus (t_{50s}) also reveal differences between the recorded groups (fig.10B). The rise time of FV510/511AA-pHluorin is significantly slower than the rise time of the WT rescue-pHluorin, but only slightly slower of the $S_{504}EEK_{507}$ deletion-pHluorin construct (exponential fit (τ): 5.3± 1s in WT resc., 7.1± 1s in $S_{504}EEK_{507}$ del., 12.4± 1s in FV510/511AA; t_{50s} $\Delta F/F_0$: 0.98 in WT resc., 0.88 in $S_{504}EEK_{507}$ del., 0.72 in FV510/511AA, fig.10B).

Investigating the peak pHluorin fluorescence from the traces normalized to NH_4Cl-containing solution application of FV510/511AA-pHluorin and the $S_{504}EEK_{507}$ deletion-pHluorin show no significant differences compared to WT rescue (fig.10C).

The calculated surface expression levels show no differences between the VGLUT1 $S_{504}EEK_{507}$ deletion-pHluorin construct and the WT rescue-pHluorin as well. In contrast, the surface expression of FV510/511AA-pHluorin is significantly higher than the WT rescue-pHluorin (1± 0.11% in WT resc., 1.04± 0.11% in $S_{504}EEK_{507}$ del., 1.46± 0.13% in

FV510/511AA, fig.10D). The total amount of expressed pHluorin molecules in the synapses is reduced in FV510/511AA compared to WT rescue levels, but not different in the $S_{504}EEK_{507}$ deletion construct (1± 0.1 in WT, 0.74± 0.09 in $S_{504}EEK_{507}$, 0.42± 0.05 in FV510/511AA, fig.10E).

A: Examples fluorescence changes of VGLUT1-pHluorin constructs

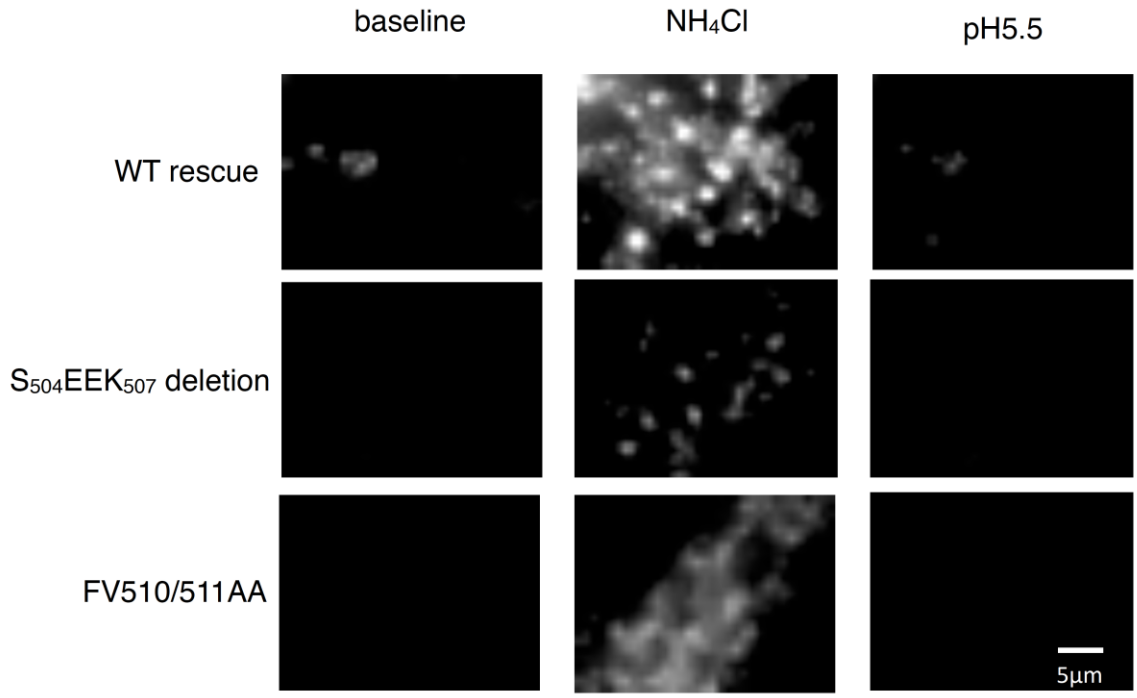

B: Fluorescence changes normalized to the peak of 300AP stimulation

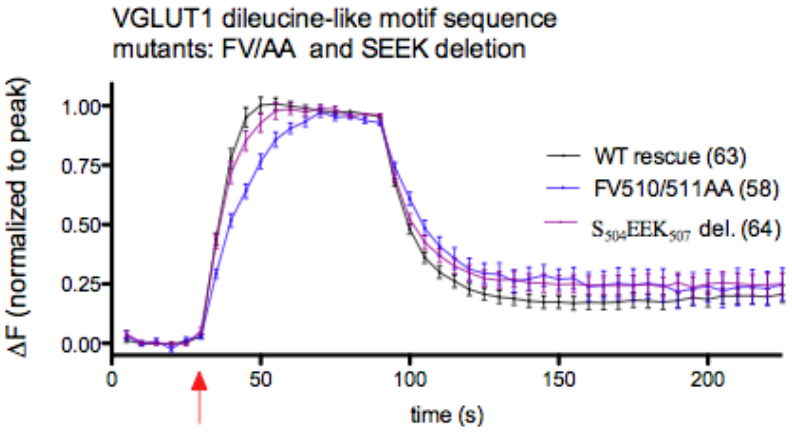

C: Fluorescence changes normalized to the peak of NH_4Cl-induced fluorescence

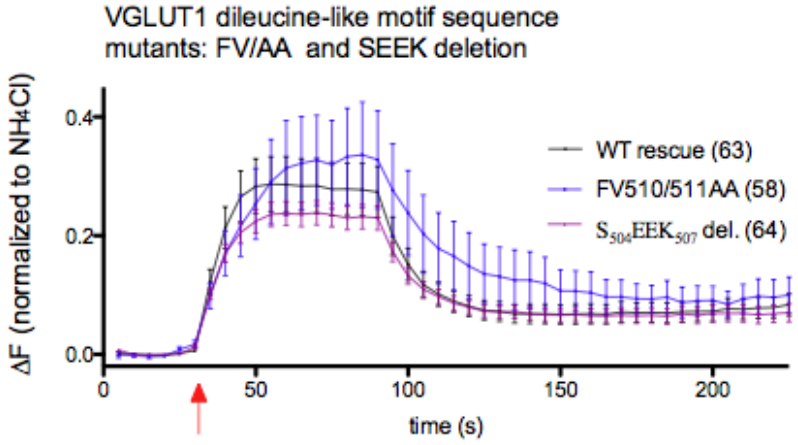

D: Surface expression

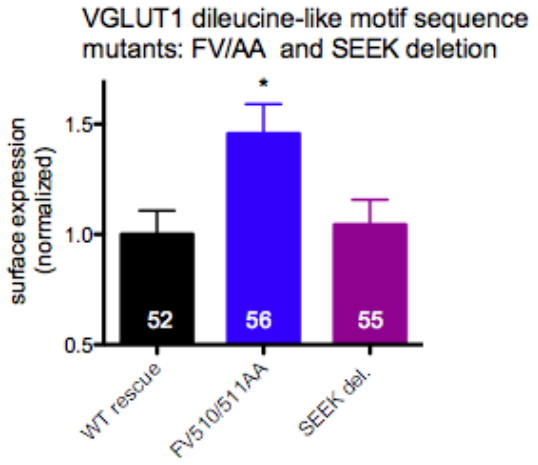

E: Total pHluorin expression

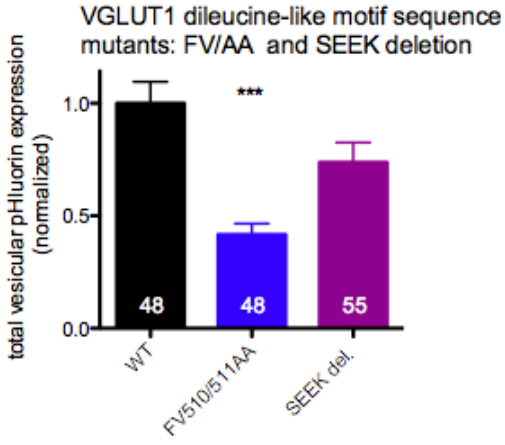

Fig. 10 (A-E): **pHluorin-based SV cycling analysis of C-terminal VGLUT1 FV510/511AA mutant and $S_{504}EEK_{507}$ deletion:** $S_{504}EEK_{507}$ and FV motif belong to the C-terminal dileucine-like motif $S_{504}EEKCGFV_{511}$. To monitor potential fluorescence changes after high frequency stimulation (5 Hz, 300AP, start red arrow) VGLUT1 mutant constructs ($S_{504}EEK_{507}$ deletion (purple) and FV510/511AA (blue)) were tagged with a pHluorin molecule and expressed in VGLUT1 KO neurons. The pHluorin fluorescence was detected during baseline conditions (F_0), during NH_4Cl- and pH 5.5-containing solution application to analyze fluorescence changes ($\Delta F/F_0$) (examples, A). The plotted data were normalized to either the pHluorin peak fluorescence during 300AP train stimulation (B) or the peak fluorescence during application of NH_4Cl-containing solution (C), which reflects the total amount of VGLUT1 pHluorin-tagged molecules. The VGLUT1 recycling is slower in both C-teminal dicleucine-like motif sequence mutants compared to the WT rescue (black, A). Also the rise time during stimulation is slower in FV510/511AA (B). FV510/511AA and the $S_{504}EEK_{507}$ deletion show no obvious changes in their peak fluorescence of traces normalized to the peak fluorescence of NH_4Cl-containing solution application (C). The calculated surface expression of the $S_{504}EEK_{507}$ deletion (red) is not different to the WT rescue (black), whereas FV510/511AA (blue) shows as reported before by Voglmaier et al., 2006 a significantly increased surface expression (D). The total expression of pHluorin molecules is decreased in FV510/511AA compared to WT rescue levels, but not in the $S_{504}EEK_{507}$ deletion (E) (A: zoom in of synaptic boutons with 60x magnification, n number marked in the figure legend/ bargraphs, bars indicate mean±SEM, One way ANOVA with tukey`s multiple comparison test: *p<0.05, ***p<0.001).

In addition, during the pHulorin-based imaging experiments, the electrophysiology of the VGLUT1 $S_{504}EEK_{507}$ deletion and the FV510/511AA mutant were analyzed. The action potential (AP)-evoked excitatory postsynaptic current (EPSC) amplitudes and paired pulse (PP) ratio, measured before starting the imaging protocol, are not different between the mutant and WT rescued neurons (EPSCs: 1± 0.08 in WT resc., 1.30± 0.14 in $S_{504}EEK_{507}$ del., 1.07± 0.09 in FV510/511AA; PP ratio: 1± 0.03 in WT resc., 1.00± 0.02 in $S_{504}EEK_{507}$ del., 1.01± 0.02 in FV510/511AA, fig.11A, B). The paired pulse (PP) ratio is calculated by dividing the measured amplitude of the second to the first EPSC after stimulation with two APs with 25 ms interstimulus interval.

Further detailed electrophysiological analyses done by pure whole-cell voltage clamp recordings without pHluorin imaging are shown in the following paragraph.

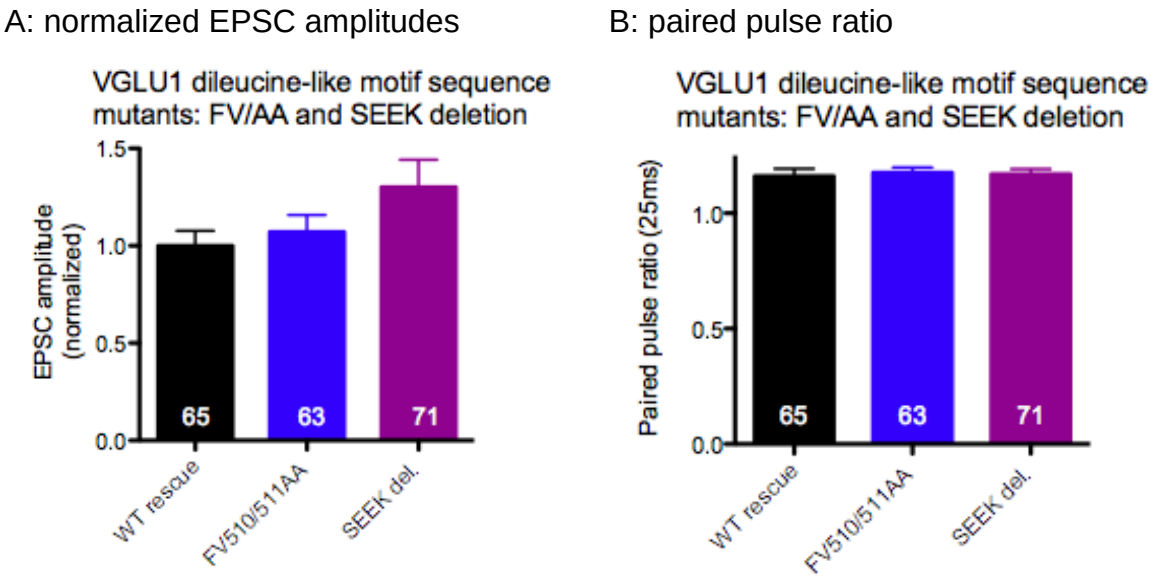

Fig. 11 (A and B): **Analysis of the electrophysiology of VGLUT1 C-terminal FV510/511AA mutation and $S_{504}EEK_{507}$ deletion during pHluorin-based imaging experiments:** before the imaging protocol started EPSCs and the PP ratio of VGLUT1 KO neurons lentiviral rescued with the FV510/511AA construct or $S_{504}EEK_{507}$ deletion construct were measured in comparison to VGLUT1 WT rescued neurons (A-B). There are no obvious changes between the VGLUT1 C-terminal dileucine-like motif sequence mutants and the WT rescue (n number marked in the bargraphs, bars indicate mean±SEM, One way ANOVA with tukey`s multiple comparison test).

Altogether, the pHluorin-based imaging results show, as expected from previous data (Foss et al., 2013; Voglmaier et al., 2006), a slower recycling of VGLUT1 in FV510/511AA resulting in a higher surface expression. The data suggest that $S_{504}EEK_{507}$ seems to play a role for the retrieval of VGLUT1 as well, because a loss of the $S_{504}EEK_{507}$ motif sequence causes a little

slower VGLUT1 recycling as well, which is apparent in a slower pHluorin fluorescence decline after 300AP stimulation.

3.1.2 Mutating the C-terminal VGLUT1 dileucine-like motif sequence not affects neurotransmission

The VGLUT1-pHluorin data show slower VGLUT1 recycling in the FV510/511AA mutation and the $S_{504}EEK_{507}$ deletion. A remaining question is whether impaired VGLUT1 retrieval might also affect neurotransmission. The electrophysiology data besides the pHluorin data acquisition suggest no changes in neurotransmission of both VGLUT1 dileucine-like motif sequence mutants (fig.11). However, further NT release properties were measured by pure whole-cell voltage clamp measurements in both VGLUT1 mutants in comparison to the WT rescue as control.
The kinetics of the AP-evoked postsynaptic currents (PSCs) were analyzed to determine the identity of the neurons, whether the postsynaptic responses are from glutamatergic or GABAergic neurons. Glutamatergic (excitatory, E) neurons have a fast decay time of the EPSC amplitude (about 5-10 ms) to come back to baseline after being evoked by electrical stimulation. GABAergic (inhibitory, I) neurons have a slower IPSC amplitude decay time about 30-40 ms. GABA-expressing interneurons were excluded from all measurements.

Evoked postsynaptic responses, the EPSCs, as well as the spontaneous activity (miniature events, mEPSCs) of neurons expressing the VGLUT1 FV510/511AA mutation are not different in comparison to neurons rescued with VGLUT1 WT (EPSCs: 4.7± 0.7nA in WT resc., 3.7± 0.53nA in FV510/511AA; mEPSC amplitude: 31.6± 2.87pA in WT resc., 24.7± 1.5pA in FV510/511AA; mEPSC frequency: 4.9± 0.68Hz in WT resc., 4.7± 0.63Hz in FV510/511AA, fig.12 A, F, G). All other analyzed electrophysiological parameters (the readily releasable pool (RRP), the vesicular release probability (Pvr), PP ratio, 10 Hz train stimulation) are the same between VGLUT1 FV510/511AA and the WT rescue as well (RRP: 626.3± 97.91pC in WT resc., 443.6± 49.54pC in FV510/511AA; Pvr: 5.6± 0.78% in WT resc., 5.6± 0.55% in FV510/511AA; PP ratio: 1.4± 0.07 in WT resc., 1.2± 0.06 in FV510/511AA, fig.12 B, C, D, E).
The RRP includes all SVs that are fusion competent evoked by extracellular 500 mM hypertonic sucrose solution application. The Pvr is defined as the ratio of all SVs released by a single AP (EPSC charge) and the number of vesicles released during hypertonic sucrose

solution application (RRP charge). The PP ratio is, as already mentioned, calculated by dividing the measured amplitude of the second to the first synaptic response (with 25 ms interstimulus interval). Whether postsynaptic responses tend to depress or facilitate, when the neurons were stimulated with a train of 50APs (10 Hz), was also analyzed.

A: Evoked postsynaptic responses

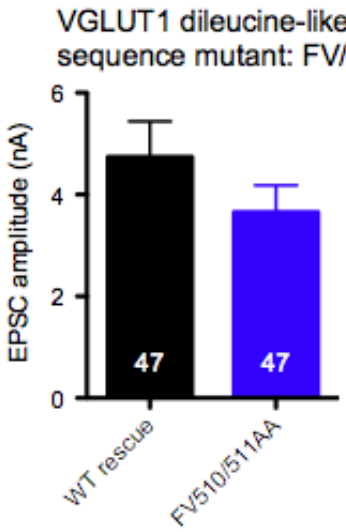

B: Readily releasable pool

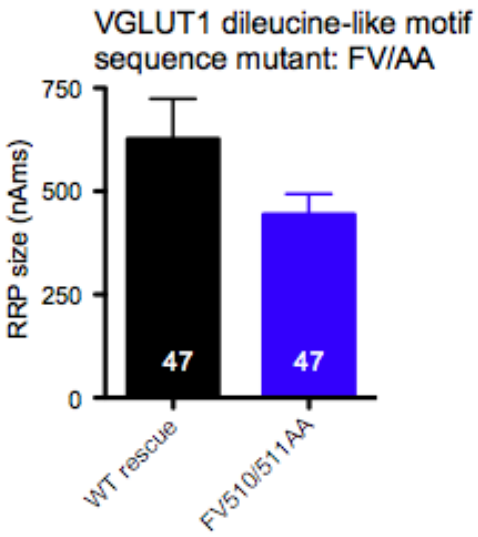

C: Vesicular release probability

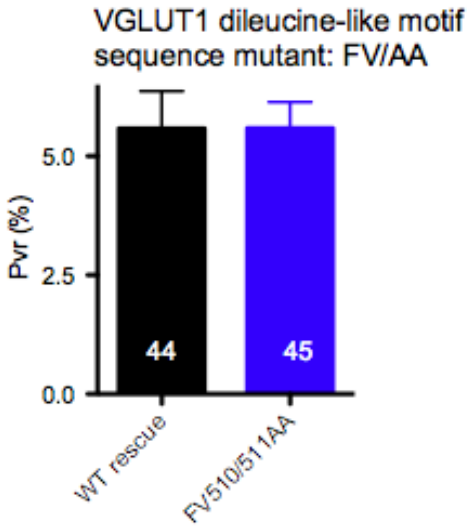

D: Paired pulse ratio

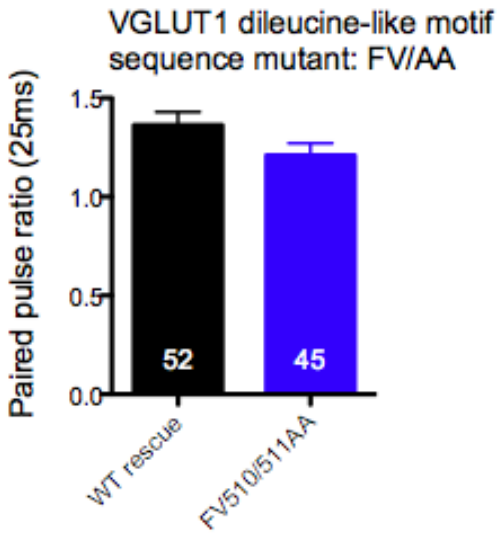

E: 10 Hz train stimulation

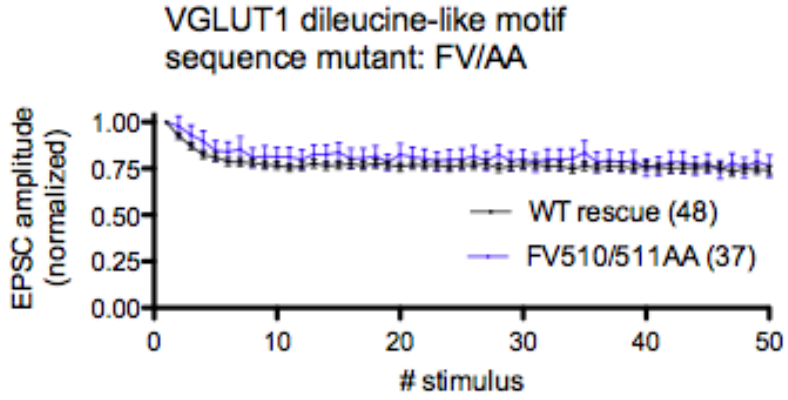

F: spontaneous activity
(mEPSC amplitude)

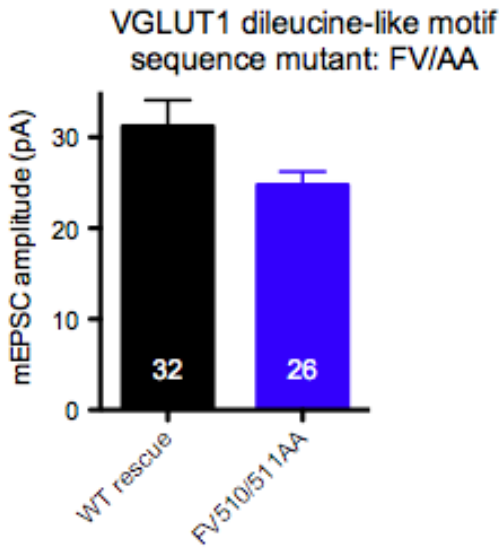

G: spontaneous activity
(mEPSC frequency)

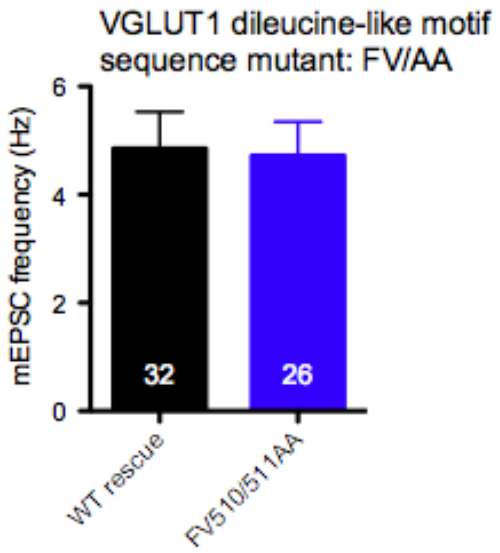

Fig. 12 (A-G): **Electrophysiological analysis of the neurotransmission of VGLUT1 C-terminal FV510/511AA mutant:** the FV motif is part of the C-terminal VGLUT1 dileucine-like motif sequence. To investigate the neurotransmission hippocampal VGLUT1 KO neurons were infected with a FV510/511AA mutant rescue construct in comparison to the WT rescue. EPSC amplitudes (A) as well as the RRP (B) of FV510/511AA are not different compared to the WT rescue. The Pvr (C) and the PP ratio (D) do also not show any changes as well as the 10 Hz train stimulation (E). The mEPSC amplitude (F) and mEPSC frequency (G) are also not different to WT rescue levels (G) (n numbers correspond to 3 cell cultures, bars indicate mean±SEM, Student`s t-test).

The VGLUT1 $S_{504}EEK_{507}$ deletion was compared to VGLUT1 WT rescue and at the same time to a mutation of the serine S504, which is part of the $S_{504}EEK_{507}$ motif sequence. S504 is predicted by computer software to be a putative phosphorylation site of VGLUT1 (http://kinasephos2. mbc.nctu.edu.tw). A mutation of the VGLUT1 serine S504 to alanine A (S504A) prevents potential phosphorylation and consequently mimics permanent dephosphorylation (phosphodeficient mutant). Detailed characterizations of the putative

phosphorylation site S504 and other VGLUT1 serine sites are shown in the results chapter three.

The EPSCs and RRP of the VGLUT1 $S_{504}EEK_{507}$ deletion are not altered in comparison with the WT rescue, but S504A shows significantly increased EPSC amplitudes (EPSCs: 4.3± 0.45nA in WT resc., 5.1± 0.58nA in $S_{504}EEK_{507}$ del., 6.5± 0.93nA in S504A; RRP: 820.1± 85.64pC in WT resc., 1001± 114.9pC in $S_{504}EEK_{507}$ del., 1034± 158.6pC in S504A, fig.13A, B). The calculated Pvr of the $S_{504}EEK_{507}$ deletion is not different to WT rescue levels as well. The Pvr of S504A is by trend increased (3.9± 0.3% in WT resc., 3.7± 0.36% in $S_{504}EEK_{507}$, 4.79± 0.41% in S504A, fig.13C). The PP ratio is unchanged of the $S_{504}EEK_{507}$ deletion construct compared to the WT rescue. According to the Pvr results, the PP ratio of S504A is slightly reduced (0.87± 0.03 in WT resc., 0.8 0.03 in $S_{504}EEK_{507}$ del., 0.92± 0.04 in S504A, fig.13D). The 10 Hz train stimulation of both, the $S_{504}EEK_{507}$ deletion and S504A, are not different in comparison to the WT rescue (fig.13E). The mEPSC amplitudes and frequencies are not changed in neurons rescued with both mutant dileucine-like motif sequence constructs as well (mEPSC amplitude: 28.34± 1.05pA in WT resc., 31.8± 1.43pA in $S_{504}EEK_{507}$ del., 31.62± 1.45pA in S504A; mEPSC frequency: 6.8± 0.8Hz in WT resc., 8.7± 1Hz $S_{504}EEK_{507}$ del., 8.5± 1Hz in S504A, fig.13F, G).

The data illustrate that a deletion of the VGLUT1 $S_{504}EEK_{507}$ motif, which is part of the C-terminal dileucine-like motif sequence, does not affect neurotransmission, wheres a mutation of the putative phosphorylation site S504 suggests higher NT release.

A: Evoked postsynaptic responses

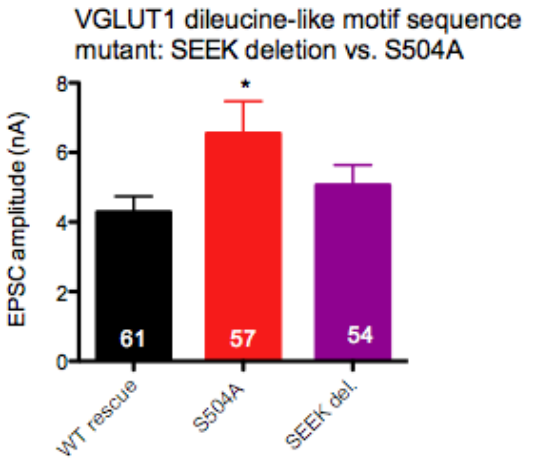

B: Readily releasable pool

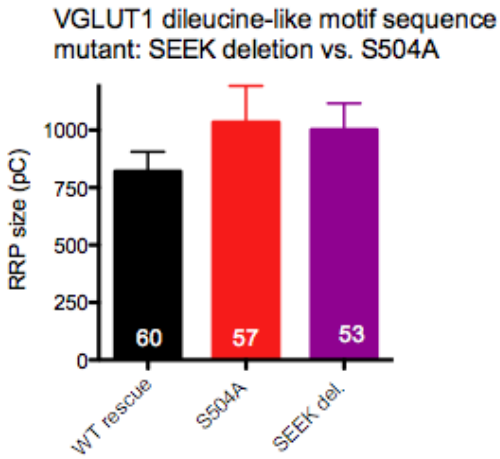

C: Vesicular release probability

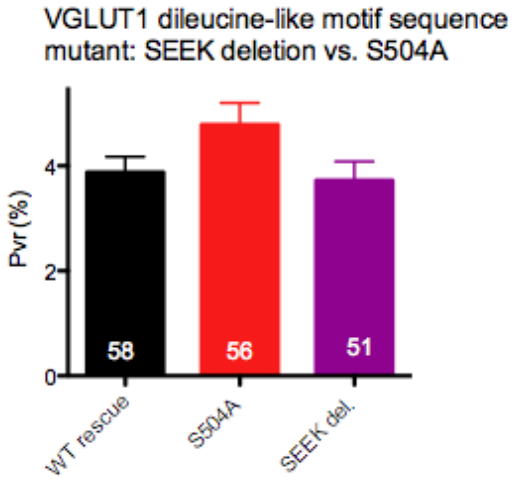

D: Paired pulse ratio

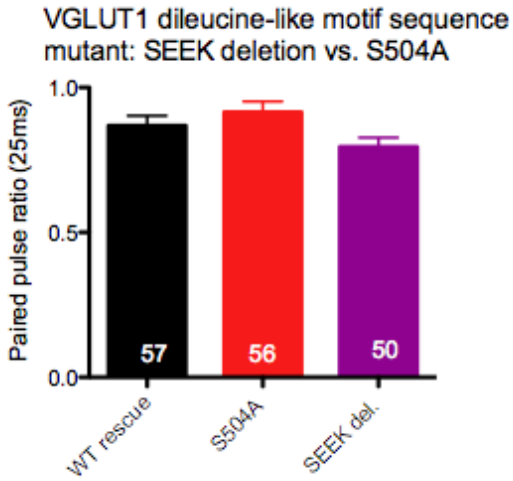

E: 10 Hz train stimulation

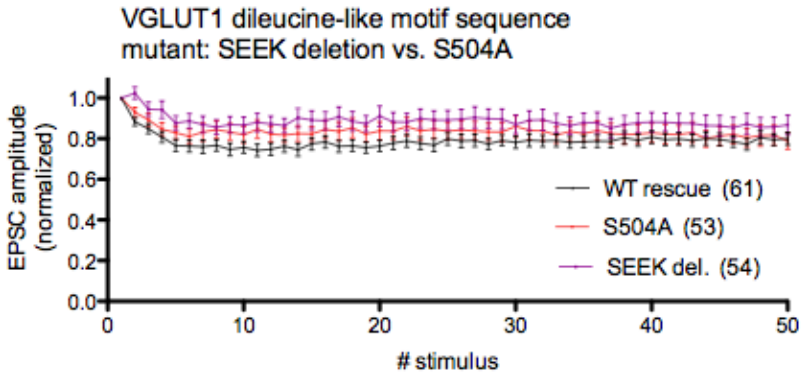

F: spontaneous activity
(mEPSC amplitude)

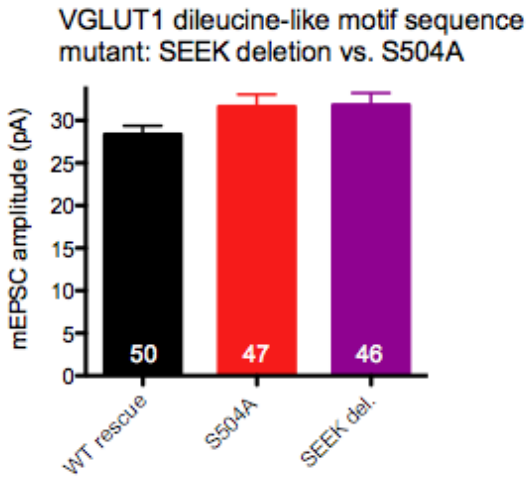

G: spontaneous activity
(mEPSC frequency)

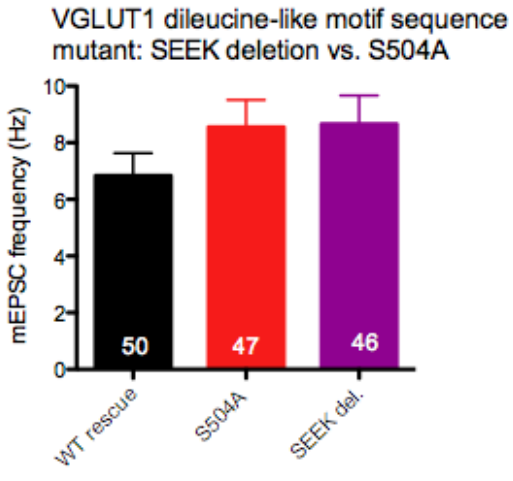

Fig. 13 (A-G): **Electrophysiological analysis of the neurotransmission of VGLUT1 C-terminal $S_{504}EEK_{507}$ deletion in comparison to S504A mutation:** besides the FV motif, the $S_{504}EEK_{507}$ motif is also part of the C-terminal VGLUT1 dileucine-like motif sequence. S504 is flanking the dileucine-like motif sequence upstream. To investigate the neurotransmission hippocampal VGLUT1 KO neurons were infected with a $S_{504}EEK_{507}$ deletion rescue construct or a S504A mutant construct in comparison to the WT rescue. Direct comparison of the VGLUT1 C-terminus mutants with the WT rescue reveal no differences in the EPSC amplitudes (A) as well as the RRP (B) of the $S_{504}EEK_{507}$ deletion construct. S504A shows a significantly increase in the EPSC amplitudes (A). The Pvr of S504A shows a trend towards an increase as well (C). The Pvr of the $S_{504}EEK_{507}$ deletion is not different compared to the WT rescue (C). The PP ratio of both, S504A and the $S_{504}EEK_{507}$ deletion, show no changes compared to the WT rescue (D). The 10 Hz train stimulation also reveals no differences between the recorded groups (E). The mEPSC amplitudes (F) and mEPSC frequencies (G) are not changed as well (n numbers correspond to 3 cell cultures, bars indicate mean±SEM, One way ANOVA with tukey`s multiple comparison test: *<0.05).

Quantifications of immunofluorescence staining data (ICCs) show unexpected high protein expression levels in FV510/511AA and low expression levels in the $S_{504}EEK_{507}$ deletion construct in comparison to the WT rescue or the S504A mutant (1± 0.12 in WT, 1.5± 0.14 in FV510/511AA, 0.59± 0.4 in $S_{504}EEK_{507}$ del., fig.37E, appendix and 1± 0.05 in WT, 0.96± 0.08 in S504A, 0.59± 0.04 in $S_{504}EEK_{507}$ del., fig. 37F, appendix). Maybe a higher sample size might lead to different results. Nevertheless, the electrophysiology results do not illustrate any alterations in the neurotransmission of both dileucine-like motif sequence mutants, suggesting that these differences in VGLLUT1 expression do not affect the physiology.

3.1.3 Electron microscopy analyses of VGLUT1 FV510/511AA mutation and $S_{504}EEK_{507}$ deletion reveal no alterations on synaptic vesicle morphology or density

The electrophysiology and pHluorin-based imaging data of the C-terminal VGLUT1 FV510/511AA mutation and $S_{504}EEK_{507}$ deletion illustrate that VGLUT1 recycling is slower in both cases, but the neurotransmission is unaffected. To further investigate, whether a slowed VGLUT1 retrieval comes along with changed morphological properties of the SVs or vesicle number per synapse, EM images of the FV510/511AA mutant and $S_{504}EEK_{507}$ deletion were also quantified.

EM is helpful to achieve high resolution of very small cell ultrastructures, because one SV is about 40-50 nm diameter (Kandel et al., 2000; Südhof and Jahn, 1991). With EM images the SV number (density), but also the shape (area, perimeter, Feret`s diameter, roundness) were analyzed. The occurrence of abnormal structures such as enlarged vesicular structures or accumulations of so-called multivesicular bodies (MVBs) were investigated as well.

To acquire EM images, the cultured neurons were classically fixed and embedded using 0.25% glutaraldehyde and epon resin. Samples were cutted into 40-60 µm thin sections, contrasted with 2% uranyl acetate and imaged with 30,000 times magnification to provide overview images of synaptic boutons (example images, fig.15A, B).

The SV morphology is not different in VGLUT1 FV510/511AA or $S_{504}EEK_{507}$ deletion mutants compared to VGLUT1 WT rescue (area: 1± 0.03 in WT resc., 0.92± 0.03 in $S_{504}EEK_{507}$ del.; 0.97± 0.05 in FV510/511AA, 0.83± 0.02 in KO; perimeter: 1± 0.02 in WT resc., 0.97± 0.02 in $S_{504}EEK_{507}$ del., 0.98± 0.04 in FV510/511AA, 0.93± 0.01 in KO; roundness: 1± 0.01 in WT resc., 0.97± 0.01 in $S_{504}EEK_{507}$ del., 0.95± 0.03 in FV510/511AA, 0.85± 0.01 in KO; density (#SV/area above active zone): 1± 0.05 in WT resc., 1.1± 0.1 in $S_{504}EEK_{507}$ del., 0.96± 0.09 in FV510/511AA, 0.97± 0.1 in KO, fig.14A-D). The SV density per synapse is also not changed in both mutant groups (fig.14E). Interestingly, the $S_{504}EEK_{507}$ deletion shows a decreased number of enlarged vesicular structures, whereas the KO exhibits significantly more enlarged vesicles (diameter <50nm: 14.4± 2.1% in WT resc., 6.1± 0.71% in $S_{504}EEK_{507}$ del., fig.14E). At all, VGLUT1 KO neurons show alterations in the SV morphology and number of "normal" sized vesicles about 30-50 nm. Their vesicles are significantly smaller and less round than SVs of WT rescued neurons (fig. 14A, C). Likewise, the number of SVs with a diameter about 30-50 nm per synapse is reduced in KO neurons ("KO phenotype“, fig.14E), whereas the number of SVs close to the active zone is not different compared to WT rescued neurons (fig.14D). These results are consistent with previously published data from Fremeau et al., 2004, Siksou et al., 2013 and Tordera et al., 2007. In contrast, the FV510/511AA mutant shows no noticeable changes in SV number.

A: vesicle area

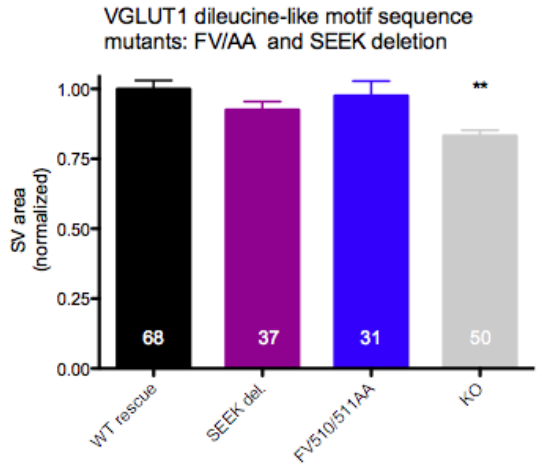

B: vesicle perimeter

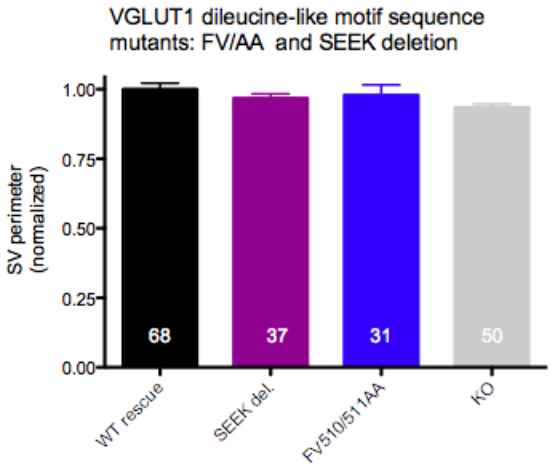

C: vesicle roundness

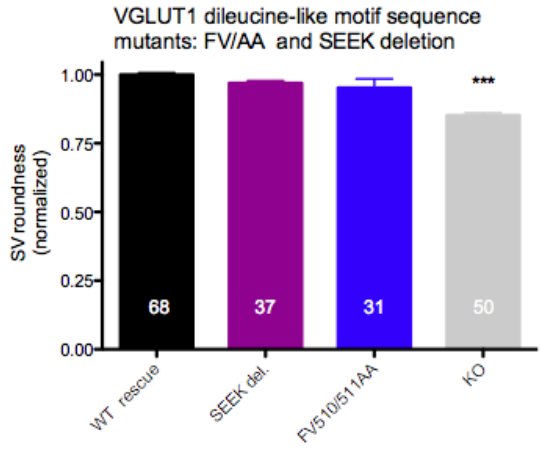

D: vesicle density

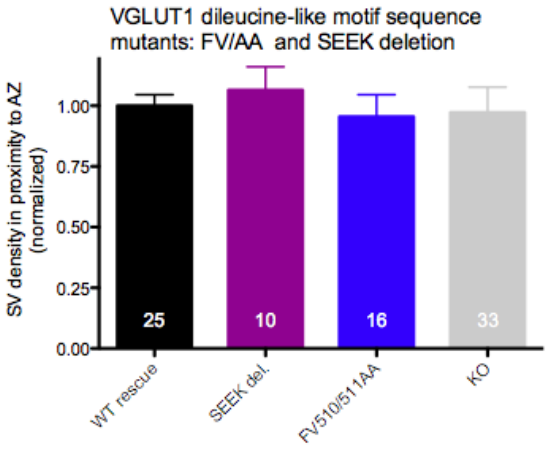

E: grouped vesicle size

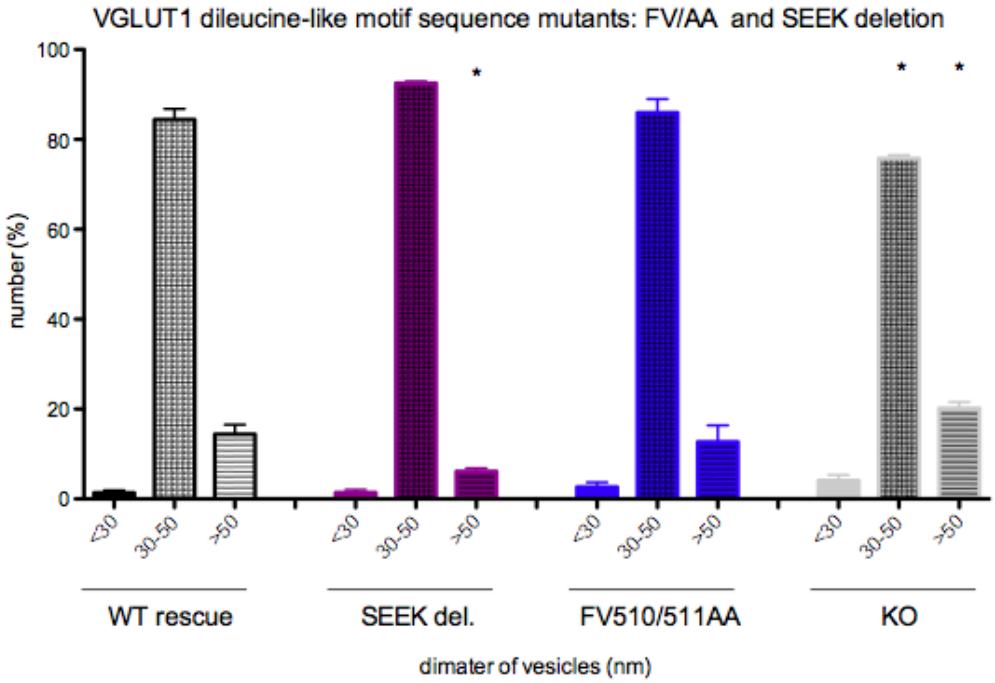

Fig. 14 (A-E): **Morphological quantification of SVs from VGLUT1 C-terminal FV510/511AA mutation and $S_{504}EEK_{507}$ deletion by EM**: to investigate the SV morphology and denstity by EM hippocampal VGLUT1 KO neurons were lentiviral infected to express either a VGLUT1 FV510/511AA construct or $S_{504}EEK_{507}$ deletion construct in comparison with a VGLUT1 WT rescue construct. Both VGLUT1 mutants belong to the C-terminal dileucine-like motif sequence. Analyses of the SV shape including the area (A), perimeter (B), Feret`s diameter (E) and roundness (C) (by formula 4π*area/(π*major axis2) with the meaning 1= perfect circle and 0= increasingly elongated) do not show changes in the VGLUT1 $S_{504}EEK_{507}$ deletion (purple) or the FV510/511AA mutant (blue). Similarly, the vesicle density in proximity to the active zone (AZ) (D) is not changed in the dileucine-like motif sequence mutants. The SV density was calculated as the ratio of the number of vesicles of a defined area (a square with the length of the active zone) including mainly readily releasable and docked vesicles. The diameter of the SVs was investigated as well and classified into three groups: <30 nm, 30-50 nm, >50 nm. The number of SVs with a diameter >50 nm are decreased in the $S_{504}EEK_{507}$ deletion, but not in the FV510/511AA mutant (E). In contrast, VGLUT1 KO neurons (light grey) show changes in the SV morphology and number compared to the WT rescue (black). Their SVs are amaller and less round (deformed shape). The density of „normal“ sized SVs per synapse is also reduced in KO neurons, whereas the number of enlarged vesicular structures is increased (n number mentioned in the bar graphs, bars indicate mean±SEM, for A-D: One way ANOVA with tukey`s multiple comparison test: **p<0.01, ***p<0.001; for E: Student`s t-test: *p<0.05).

Further investigations show that in both, the $S_{504}EEK_{507}$ deletion and the FV510/511AA mutant, an accumulation of supposedly MVBs (no example images shown) and large endosomal-like (tubular) or vesicular structures (example images, fig.15) occurs.

A more detailed characterization of the mentioned structures, for example by ICC for endosome marker such as antibodies against the early endosome antigen 1 (EEA1) (Mu et al., 1995) or Rab4 (Chavrier et al., 1990), was not done. MVBs, whose size is with up to 600 nm

huge compared to SVs (Hanson and Cashikar, 2012), usually function in endocytosis and endosomal trafficking. They are part of the endosomal sorting machinery playing a role in the biosynthetic secretory pathway and for lysosomes. MVBs are also important for sorting internalized macromolecules and membrane proteins (Stahl and Barbieri, 2002). Tubular/endosomal-like structures are known to be involved in protein sorting as well, but also in endocytic and recycling pathways (Mellman, 1996).

A: synapse of a hippocampal VGLUT1 KO neuron expressing VGLUT1 $S_{504}EEK_{507}$ deletion

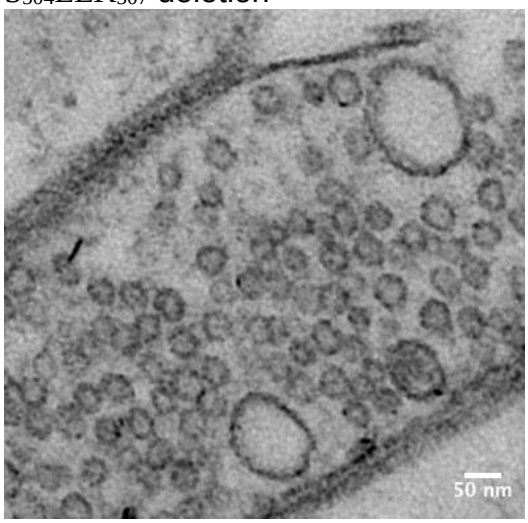

B: synapse of VGLUT1 FV510/511AA

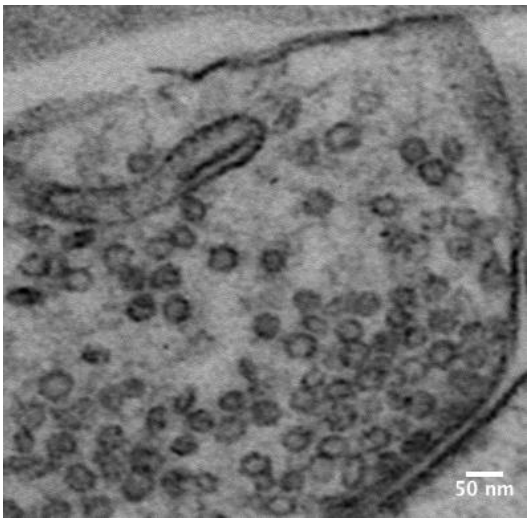

Fig. 15 (A and B): **Example EM images of enlarged vesicular structures of the C-terminal VGLUT1 FV510/511AA mutation and $S_{504}EEK_{507}$ deletion:** hippocampal VGLUT1 KO neurons were lentiviral infected to express VGLUT1 C-terminal dileucine-like motif sequence mutant constructs (FV510/511AA mutation and $S_{504}EEK_{507}$ deletion). The EM data of both mutant VGLUT1 constructs show no distinct alterations in their SV appearance, but an accumulation of enlarged endosomal (tubular)/vesicular structures (magnification about 30,000x).

3.2 C-terminus truncation constructs illustrate the importance for VGLUT1 recycling during endocytosis

The relevance of the mammalian VGLUT1 C-terminus for VGLUT1 protein function was further investigated by different C-terminus deletion constructs: a full VGLUT1 C-terminus truncation construct, which ends directly after the proposed last transmembrane domain (Freameau et al., 2001) at aa496 (VGLUT1Δ496-560) and a shorter C-terminus truncation construct with eight additional amino acids including a WAEPE motif sequence, which ends at aa504 (VGLUT1Δ504-560). In addition, a VGLUT2 C-terminus truncation construct (VGLUT2Δ493-582) was created. The idea was to study, whether the importance of the C-terminus is VGLUT isoform-specific.
To investigate the role of the VGLUT C-terminus in neurotransmission and SV cycling whole-cell voltage clamp recordings in combination with pHluorin-based imaging were performed again. EM imaging data to discover potential changes in SV morphology and density were also examined. Therefore, in most cases hippocampal VGLUT1 KO neurons were lentiviral infected to express VGLUT1 mutant rescue constructs in comparison with a WT rescue construct (control). In some experiments investigating VGLUT2Δ493-582 thalamic cells were used as well. For protein detection by immunofluorescence stainings the VGLUT C-terminus constructs were designed with a fluorescent tag, which was directly linked to the VGLUT protein (cf. paragraph 2.3 "Lentivirus constructs and production") and thereby equally to VGLUT expressed in the synapses.

3.2.1 Quantifications of VGLUT1 full C-terminus truncation expression reveal protein mislocalization

The full C-terminus truncation version VGLUT1Δ496-560 and similarly the WT rescue construct were designed with a monomeric far-red fluorescence protein (RFP) tag, the mkate tag. An advantage of the mkate tagged VGLUT1 constructs was that the fluorescence of the fusion protein was already visible during whole-cell voltage clamp recordings. Thereby, virus infected VGLUT1/mkate-expressing neurons could be distinguished from not infected ones.
To determine the lentivirus infection efficiency of the VGLUT1 constructs, reflecting the protein expression levels, immuncytochemistry (ICC) in combination with ratiometric imaging was performed (cf. chapter 2.3 „Lentivirus constructs and production“). Therefore,

virus infected hippocampal mass cultured VGLUT1 KO neurons from the same cell culture as the recorded neurons were fixed with 4% PFA and stained with either an antibody detecting the RFP (mkate tag) or an antibody against the VGLUT1 N-terminus as well as an antibody against synaptophysin 1 for control. Synaptophysin is exclusively localized to SVs and a common SV marker.

The ICC results illustrate a less punctate (synaptic) protein expression pattern of the mkate tagged VGLUT1Δ496-560 (fig.16B) compared to the WT rescue (fig.16A). The expression of mkate tagged VGLUT1Δ496-560 is more cytosolic and not excusively in synaptic boutons, but also in dendrites. Instead, the corresponding synaptophysin 1 control staining of VGLUT1Δ496-560 shows a punctuate (synaptic) protein expression pattern, indicating normal distribution of synaptophysin to synapses. The less punctate (synaptic) and more extrasynaptic expression pattern of mkate tagged VGLUT1Δ496-560 indicates impaired VGLUT1 localization to synapses.
However, the overall protein expression levels quantified by ratiometric imaging of VGLUT1Δ496-560 and the control protein synaptophysin 1 are not different to WT rescue levels (2.04± 0.5a.u. in WT rescue, 1.67± 0.51a.u. in C-terminus truncation (C-term trunc.), fig.16D). As expected, the VGLUT1 protein expression levels in KO neurons are drastically decreased (0.68± 0.11a.u., fig.16D). Remaining very weak fluorescence signals of antibody stainings in VGLUT1 KO cells are presumably background signals.

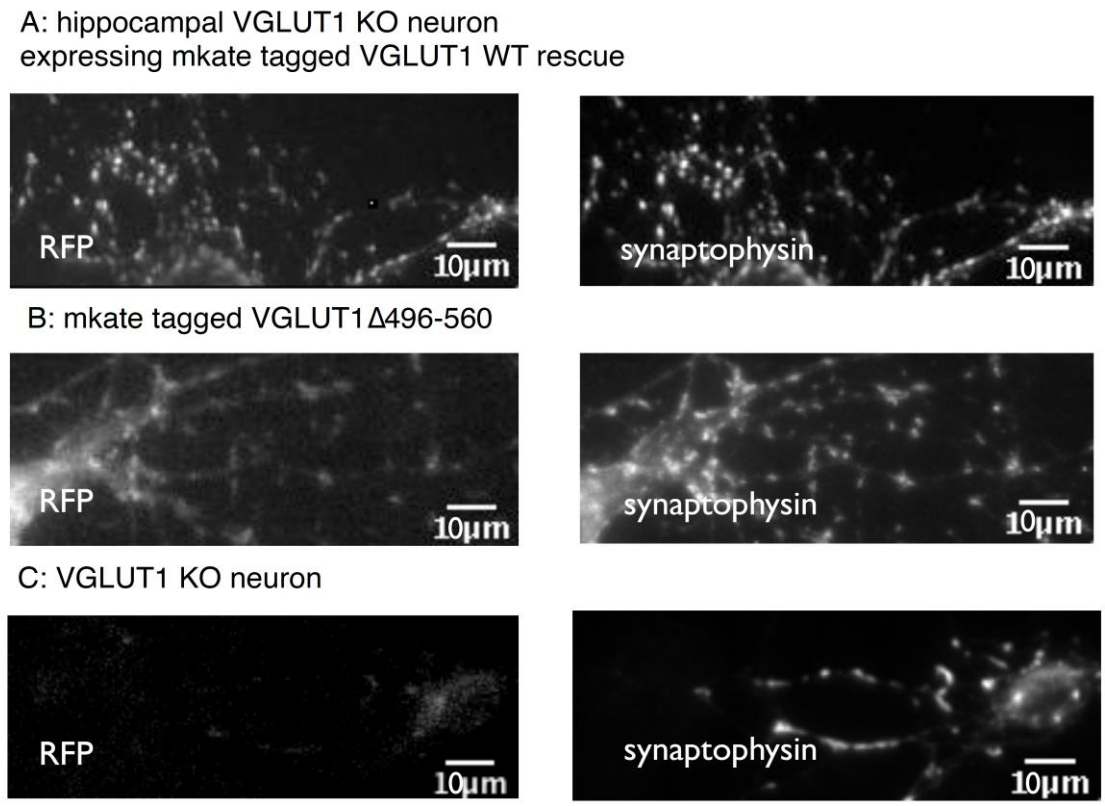

D: protein expression levels

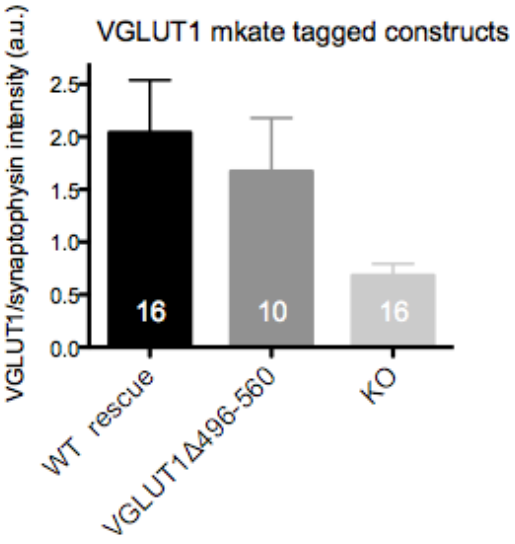

Fig. 16 (A-D): **Example images of VGLUT1Δ496-560 and WT rescue-expressing VGLUT1 KO neurons for ratiometric imaging:** for ICC analyses a mkate-expressing C-terminus truncation VGLUT1Δ496-560 construct or a VGLUT1 WT protein construct were used to rescue hippocampal VGLUT1 KO neurons by lentiviral infected. Mass cultured cells were stained by using an anti-RFP antibody for detecting mkate or an anti-VGLUT1 N-terminus antibody in combination with an anti-synaptophysin 1 antibody for control. Synaptophysin is a common SV marker. The results show that VGLUT1 WT rescued neurons (A) have a punctate (synaptic) RFP staining pattern. VGLUT1Δ496-560 (B) exhibits a mainly cytosolic RFP fluorescence signal with a less punctate staining pattern. KO neurons (C) with no mkate tag show no RFP staining signals confirming the specificity of the RFP antibody.

The protein expression levels were quantified by ratiometric imaging of VGLUT1 in relation to synaptophysin 1 expression and show no differences between the WT rescue (black) and VGLUT1Δ496-560 (dark grey) (D). The protein expression of VGLUT1 KO neurons (light grey) is reduced (A-C: zoom in of neuronal extensions with 20x magnification, D: n numbers correspond to 1 cell culture, bars indicate mean±SEM, One way ANOVA with tukey`s multiple comparison test).

A myc tagged VGLUT1Δ496-560 construct was also tested in this study, but VGLUT1 KO neurons showed unspecific punctate fluorescence signals (example images, fig.17B). KO neurons should have no fluorescence signals, because no VGLUT1 protein is expressed (cp. anti-RFP mkate ICC results in VGLUT1 KO neurons, fig.16C). In contrast, WT rescued VGLUT1 KO neurons showed as expected a punctate (synaptic) staining pattern (fig.17A). Therefore, trustable specific staining results, to draw conclusions about protein expression levels of myc tagged VGLUT1 constructs, were not possible. Consequently, data with myc constructs (not shown and only mentioned in the text) have to be carefully discussed.

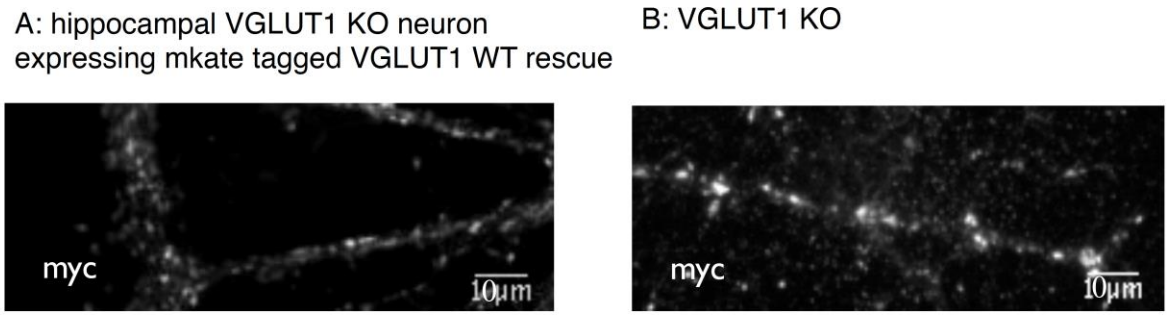

Fig. 17 (A and B): **Example images of anti-myc antibody stained WT rescued VGLUT1 KO neurons:** a myc tag was also used in this study to label VGLUT1 constructs, which were used for VGLUT1 rescue in hippocampal VGLUT1 KO neurons by lentivirus. ICC of mass cultured cells using an anti-myc antibody illustrates that myc tagged VGLUT1 WT rescued neurons (A) exhibit, as expected, a punctate (synaptic) staining pattern. However, KO neurons (B) with no myc tag also show a punctate staining pattern indicating unspecific antibody binding (zoom in of a section of neuronal extensions with 20x magnification).

3.2.2 Electrophysiology data of the VGLUT1 full C-terminus truncation construct reveal impaired neurotransmission

To investigate the physiology of the full C-terminus truncation construct VGLUT1Δ496-560, electrophysiological measurements of the mkate and myc tagged versions were compared with those from WT rescued and VGLUT1 KO neurons (controls).

The EPSC amplitudes of the mkate tagged C-terminus truncation VGLUT1Δ496-560 are substantially reduced compared to EPSCs of WT rescued neurons and reach almost KO levels (4.81± 0.61nA in WT resc., 0.93± 0.22nA in C-term trunc., fig.18A). The EPSC amplitudes of VGLUT1 KO neurons are even further reduced, close to "0" (0.29± 0.08nA, fig.18A). This VGLUT1 „KO phenotype“ was already earlier described. Wojcik et al., 2004 reported that many recorded KO neurons are "silent", expressing no detectable EPSCs (statistically

measured as "0"). Remaining postsynaptic activity, from "responding" cells, seems to be due to VGLUT2-expressing neurons in the VGLUT1 hippocampal cell culture (about 12%). Therefore, the EPSC data of the KO neurons are the mean of all measured EPSCs including "silent" and "responding" cells.

The RRP is correspondingly reduced in the mkate tagged C-terminus truncation VGLUT1Δ496-560 as well as in the KO neurons (7824.4± 107.2pC in WT resc., 311.5± 143.8pC in C-term trunc., 92.9± 21.59pC in KO, fig.18B). The calculated Pvr as well as the PP ratio show no significant changes in the mkate tagged C-terminus truncation VGLUT1Δ496-560 compared to the VGLUT1 WT rescue (Pvr: 4.27± 2.92% in WT resc., 2.98± 0.56% in C-term trunc., PP ratio: 1.42± 0.11 in WT resc., 1.98± 0.32 in C-term trunc., fig.18C and D). These data only indicate a lower release probability in VGLUT1Δ496-560-expressing neurons. Similarly, the KO neurons show no obvious differences in Pvr and PP ratio (Pvr: 4.06± 1.13%, PP ratio: 1.48± 0.12, fig.18C and D). In contrast, the 10 Hz train stimulation of the mkate tagged VGLUT1 C-terminus truncation and the KO neurons show a trend of less depression (fig.18E) indicating a lower release probability similar to Wojcik et al., 2004. The mean mEPSC frequency is also altered in neurons expressing the mkate tagged C-terminus truncation VGLUT1Δ496-560, showing a trend of reduction (4.87± 0.81Hz in WT resc., 2.95± 1.09Hz in C-term trunc., fig.18G), whereas the mean mEPSC amplitude is not different in VGLUT1Δ496-560 compared to the VGLUT1 WT rescue (31.11± 2.04pA in WT resc., 29.39± 2.76pA in C-term trunc., fig.18F). However, KO neurons show a reduction in both, mean mEPSC amplitude and frequency (mEPSC amplitude: 20.26± 1.89pA, mEPSC frequency: 1.51± 0.42Hz, fig.12F and G). This phenotype of a highly decreased mEPSC frequency of VGLUT1 KO-expressing neurons has also been shown by Wojcik et al., 2004.

A: Evoked postsynaptic responses

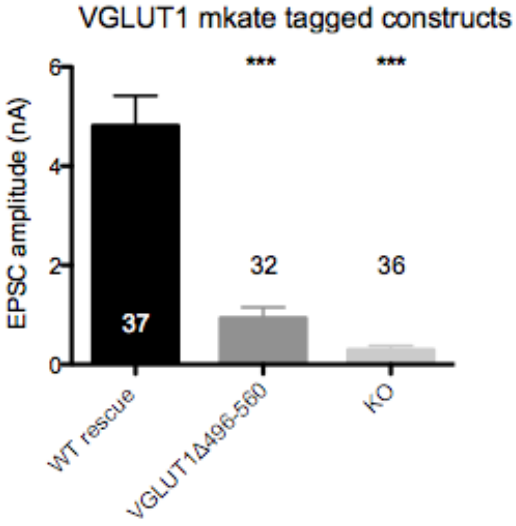

B: Readily releasable pool

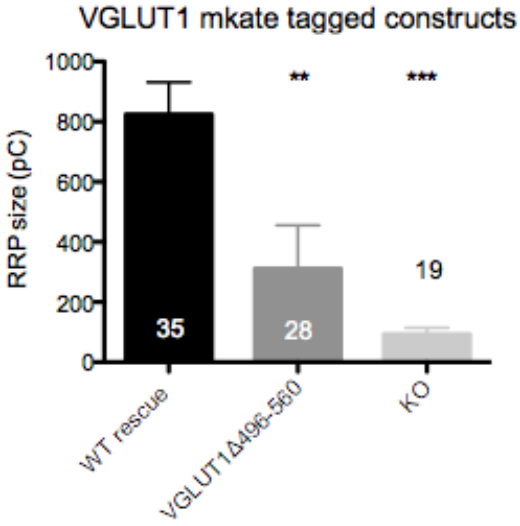

C: Vesicular release probability

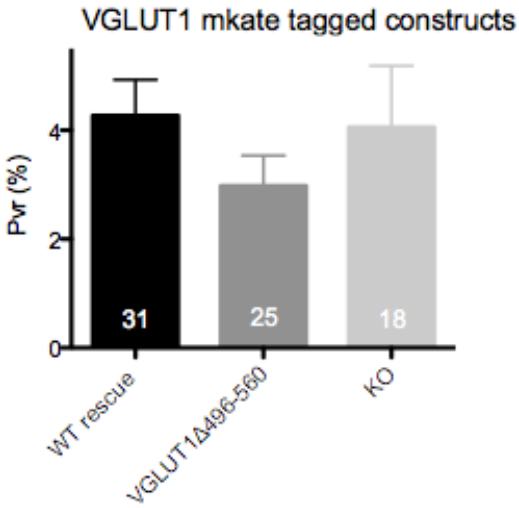

D: Paired pulse ratio

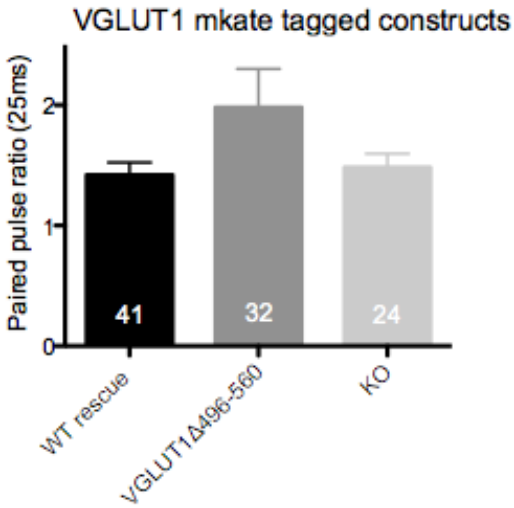

E: 10 Hz train stimulation

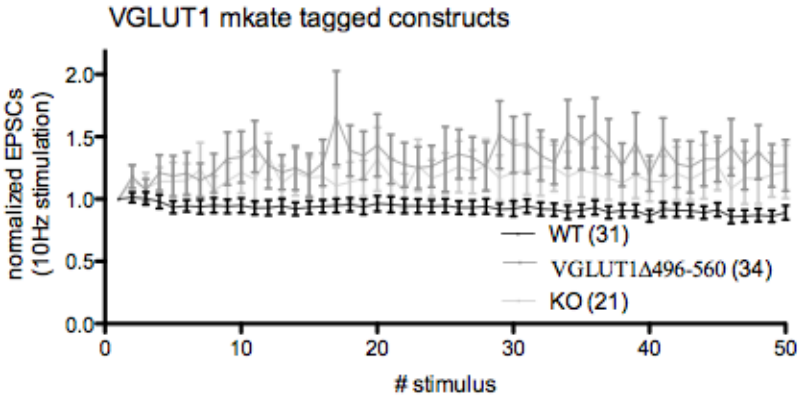

F: spontaneous activity
(mEPSC amplitude)

G: spontaneous activity
(mEPSC frequency)

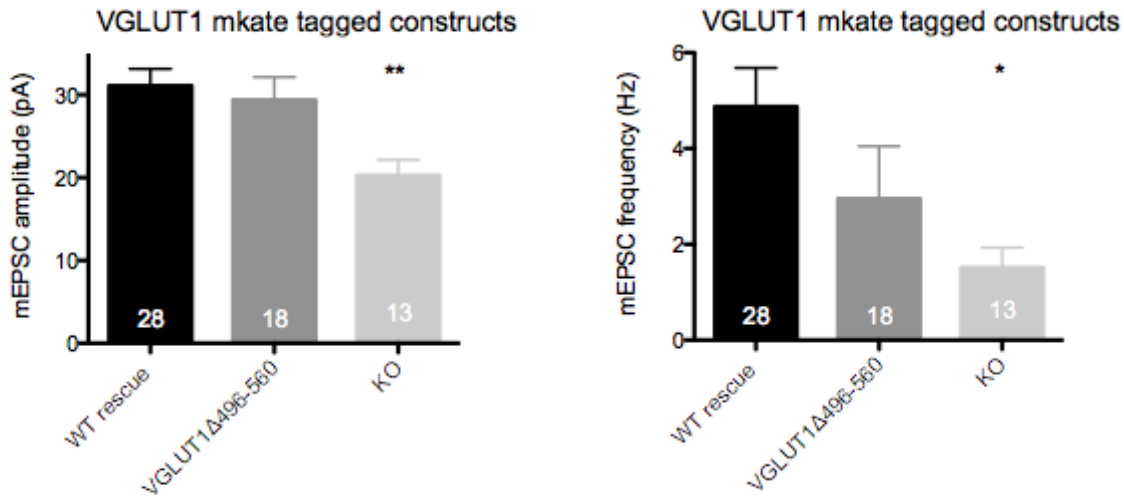

Fig. 18 (A-G): **Electrophysiological analysis of mkate tagged full C-terminus truncation VGLUT1Δ496-560 with WT rescued and VGLUT1 KO neurons:** to investigate the neurotransmission hippocampal VGLUT1 KO neurons were lentiviral infected to express a C-terminus truncation construct VGLUT1Δ496-560 in comparison with a WT rescue construct. EPSCs (A) and RRP (B) are significantly reduced in VGLUT1Δ496-560 (dark grey) to almost KO levels (light grey). Pvr (C) and PP ratio (D) show no obvious changes in VGLUT1Δ496-560 compared to the WT rescue (black). The 10 Hz train stimulation reveal slightly less depression in VGLUT1Δ496-560 and KO neurons (E). The mEPSC amplitude (F) and frequency (G) are significantly reduced in VGLUT1 KO compared to the WT rescue. The mEPSC frequency is also by trend decreased in VGLUT1Δ496-560, whereas the mEPSC amplitude is not different to the WT rescue (n numbers correspond to 3 independent cell cultures, bars indicate mean±SEM, One way ANOVA with tukey`s multiple comparison test: *p<0.05, ** p<0.001, ***p<0.0001).

A reduction of EPSCs and the RRP of a myc tagged C-terminus truncation VGLUT1Δ496-560 version could be detected as well. Since protein expression levels of the myc tagged C-terminus truncation VGLUT1Δ496-560 cannot be determined, due to the mentioned unspecific antibody staining problems (cf. fig.17), it cannot be explained if the reduction in the electrophysiological parameters are a result of impaired protein expression or maybe a consequence of functional or protein trafficking problems. Therefore, the electrophysiology results of the myc tagged VGLUT1 truncation construct are not shown.

In summary, both full VGLUT1 C-terminus truncation constructs (until aa496), the myc and the mkate tagged version, fail to rescue postsynaptic responses to WT rescue levels. The mkate data of VGLUT1Δ496-560 show only low remaining rescue activity. The postsynaptic currents of VGLUT1Δ496-560 are significantly reduced to almost VGLUT1 KO levels.

A missing VGLUT1 C-terminus seems to cause a drastic impairment of the glutamatergic neurotransmission (fig.18) presumably due to incorrect protein translocation to synaptic boutons (fig.16B). However, the total protein expression level of VGLUT1Δ496-560 is unaffected (fig.16D).
Overall, the results suggest an important role of the VGLUT1C-terminus for its performance in synaptic tranmsission. Therefore, further investigations were performed, among others testing a VGLUT2 C-terminus truncation and a chimeric VGLUT1 C-terminus construct (following paragraphs).

3.2.3 A C-terminus truncation of VGLUT2 demonstrates a non-isoform-specific effect of impaired neurotransmission

The C-terminus of mammalian VGLUTs is highly diverse, although conserved sequences can be found (cf. fig.4). The sequence of the VGLUT2 C-terminus is 12 amino acids longer (aa582) than the VGLUT1 C-terminus (aa560). One question is, whether the detected failure of VGLUT1Δ496-560 to rescue the VGLUT1 KO phenotype of significantly reduced postsynaptic responses (fig.12) is isoform-specific or not.
To address this question, a myc tagged C-terminus truncation construct of VGLUT2 was investigated. This VGLUT2 construct ends similar to the truncation construct of VGLUT1 after the last transmembrane domain, here at the amino acid 493.
VGLUT1 KO neurons expressing the VGLUT2 C-terminus truncation construct (VGLUT2Δ493-582) were recorded in comparison to a VGLUT2 full-length rescue version (VGLUT2 WT rescue) as well as VGLUT1 WT expressing neurons. A comparison with endogenous VGLUT1 WT neurons is useful to show that the VGLUT2 WT rescue construct reach similar levels of evoked postsynaptic responses illustrating that the rescue construct is functional and localizes to SVs. In fact, neurons expressing the VGLUT2 WT rescue construct show EPSC sizes, which reach almost VGLUT1 WT levels (fig.19A).

The results of the myc tagged VGLUT2 C-terminus truncation are similar to the myc and mkate tagged VGLUT1 C-terminus truncation data, in which the evoked and spontaneous postsynaptic responses are reduced (fig.18A and G). The EPSCs of the C-terminus truncation VGLUT2Δ493-582 are significantly reduced as well (1.57± 0.52nA in VGLUT1 WT, 1.17± 0.24 nA in VGLUT2 WT resc., 0.20±0.2nA in VGLUT2 C-term trunc., fig.19A), but interestingly the RRP is only by trend smaller in VGLUT2Δ493-582 compared to the

VGLUT2 WT rescue (109.6± 33.7pC in VGLUT1 WT, 107.3± 36.9pC in VGLUT2 WT resc., 55.6± 18.9pC in VGLUT2 C-term trunc., fig.19B). To judge the Pvr of the VGLUT2 truncation construct too few data are available, but the PP ratio, also reflecting potential short-term plasticity changes of synaptic responses, is not changed in the truncation construct VGLUT2Δ493-582 (0.97± 0.11 in VGLUT1 WT, 1.02± 0.08 in VGLUT2 WT resc., 0.69± 0.04 in VGLUT2 C-term trunc., fig.19D). Due to low sample size and therefore big error bars, also no results from 10 Hz train stimulation are shown. mEPSC recordings were also not analyzed, because their data had too much background noise, which makes the detection and evaluation of this small events difficult. ICC analyses were not performed as well.

Since the EPSC values of the C-terminus truncation VGLUT2Δ493-582 are significantly reduced, the data from only one culture were analysed.

Nevertheless, with these results the findings of reduced EPSCs of the myc and mkate tagged full VGLUT1 C-terminus truncation (Δ496-560) can be confirmed. In addition, the data illustrate that an impaired neurotransmission by VGLUT C-terminus truncation is not isoform-specific, but rather an effect provoked by the structural changes of the VGLUTs or more likely incorrect protein localization.

A: Evoked postsynaptic responses

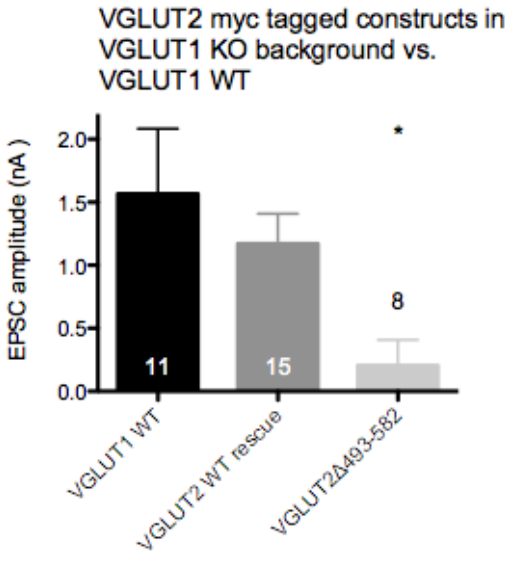

B: Readily releasable pool

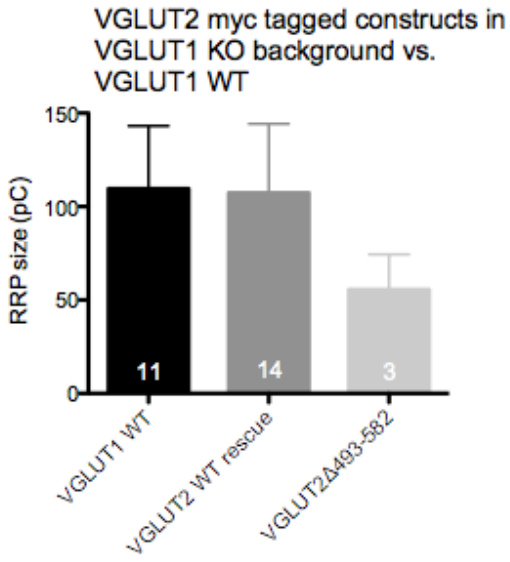

C: Vesicular release probability

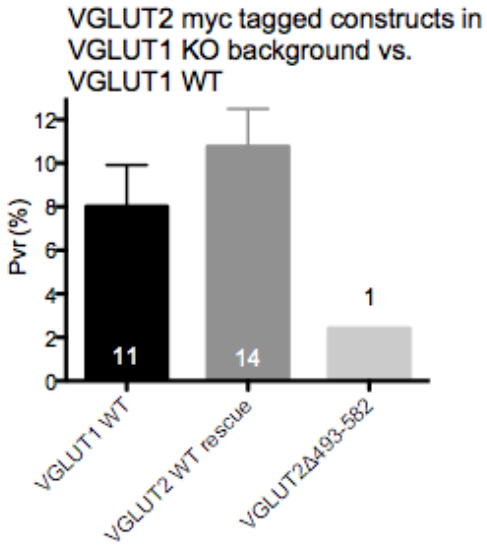

D: Paired pulse ratio

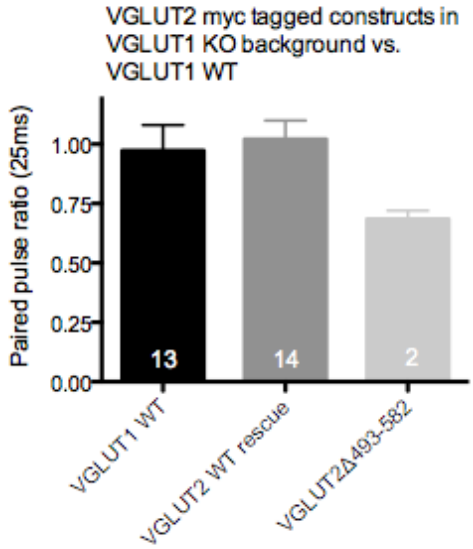

Fig. 19 (A-D): **Electrophysiological analysis of a myc tagged VGLUT2 C-terminus truncation construct (VGLUT2Δ493-582) and a VGLUT2 full-length construct (WT rescue) in VGLUT1 KO background in comparison with endogenously expressed VGLUT1 WT:** to investigate the neurotransmission of myc tagged VGLUT2 constructs hippocampal VGLUT1 KO neurons were lentiviral infected to express these constructs in comparison to endogenously expressing VGLUT1 WT neurons. Both, the VGLUT1 WT (black) and the VGLUT2 WT rescue (dark grey), reach almost the same extent of EPSC sizes (A) indicating that the VGLUT2 WT rescue construct is functional. EPSCs (A) and RRP (B) of the C-terminus truncation VGLUT2Δ493-582 construct (light grey) show a similar reduction of postsynaptic responses as the already described VGLUT1 full C-terminus truncation construct VGLUT1Δ496-560 (cf. fig.18A). The Pvr (C) and PP ratio (D) show no significant differences between the recorded groups (n numbers correspond to 1 cell culture, bars indicate mean±SEM, One way ANOVA with tukey`s multiple comparison test: * $p<0.05$).

3.2.4 A C-terminus chimera can also not rescue the impaired protein function of a VGLUT1 full C-terminus truncation

To further investigate, whether a rescue effect to VGLUT1 WT rescue levels depends on an existing C-terminal tail after the last transmembrane domain, electrophysiological recordings were also performed from VGLUT1 KO neurons expressing a chimeric VGLUT1 C-terminus version. Here, the C-terminal end right after the 12th VGLUT1 transmembrane domain (cf. fig.4 and 5) was substituted with the terminal amino acid sequence of another vesicular protein, synaptophysin (cf. paragraph 2.3 "Lentivirus constructs and production"). This chimeric C-terminus construct as well as the corresponding WT rescue control construct express in addition a green fluorescent protein (GFP) as a nuclear localization signal (NLS-GFP) to recognize virus infected cells.

Similarly to the myc or mkate tagged VGLUT1 full C-terminus truncation constructs, the chimeric construct fails to rescue the VGLUT1 KO phenotype to WT rescue levels. The EPSCs of the chimera are reduced by more than half compared to the WT rescue, but the EPSCs of the KO neurons are even further reduced (1.88± 0.19nA in WT resc., 0.82± 0.23nA in chimera, 0.06± 0.03nA in KO, fig.20A). The RRP of the VGLUT1 C-terminus chimera-expressing neurons as well as the VGLUT1 KO neurons are also significantly reduced (323.4± 32.18pC in WT resc., 138.5± 26.66pC in chimera, 57.92± 18.99pC in KO, fig.20B). Likewise, the mean mEPSC frequency is reduced in both, the chimera and KO group compared to the WT rescue (3.19± 0.4Hz in WT resc., 1.78± 0.24Hz in chimera, 0.71± 0.17Hz in KO, fig.20G). Pvr, PP ratio and mEPSC amplitudes are unchanged in the chimeric VGLUT1 construct compared to the WT rescue and KO neurons (Pvr: 3.45± 0.31% in WT resc., 2.65± 0.6% in chimera, 2.12± 0.82% in KO, PP ratio: 1.38± 0.13 in WT resc., 1.68± 0.23 in chimera, 1.25± 0.35 in KO, mEPSC amplitude: 28.47± 1.01pA in WT resc., 28.23± 2.50pA in chimera, 24.29± 5.31pA in KO, fig.20C, D, F). The 10 Hz train stimulation data indicates a little less depression in the VGLUT1 chimera compared to the WT rescue (fig.20E). ICC quantification data suggest impaired protein expression of the VGLUT1 chimera as well, because the fluorescence signals are similar low compared to the KO group (1± 0.06 in WT resc., 0.6± 0.06 in chimera, 0.56± 0.1 in KO, fig.37A, appendix).

Altogether, these findings are similar to results of the mkate tagged full C-terminus truncation VGLUT1Δ496-560 and the VGLUT2 C-terminus truncation VGLUT2Δ493-582 version, which showed that a rescue of the KO phenotype is not possible when the VGLUT C-terminus is missing. A substituted VGLUT1 C-terminus with the C-terminal end of synaptophysin can also not rescue the reduction of postsynaptic responses compared to the WT rescue. The data of the VGLUT1 chimera underline the importance of the VGLUT C-terminus for a regular performance in synaptic transmission.

A: Evoked postsynaptic responses

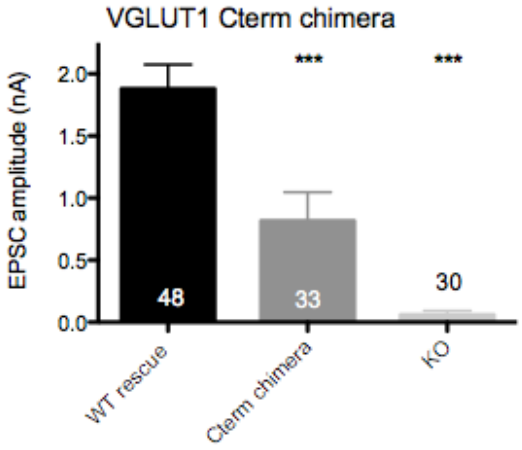

B: Readily releasable pool

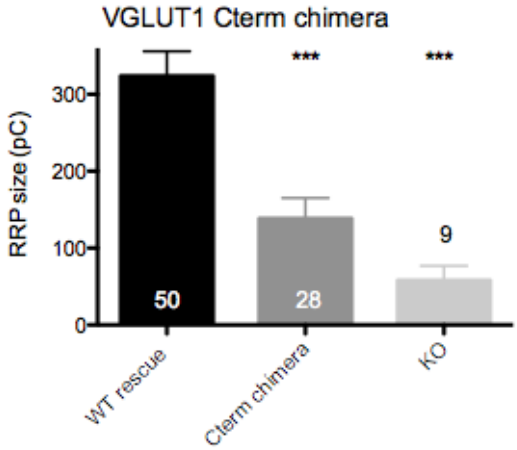

C: Vesicular release probability

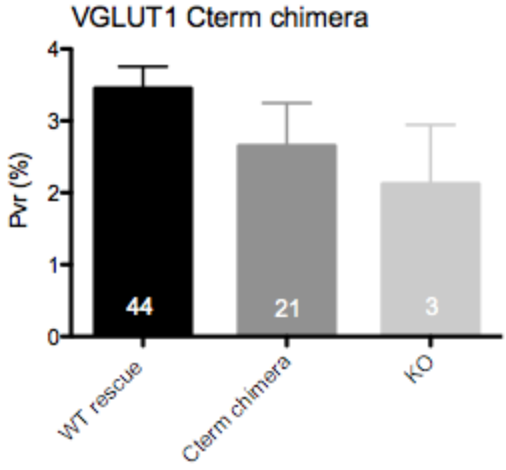

D: Paired pulse ratio

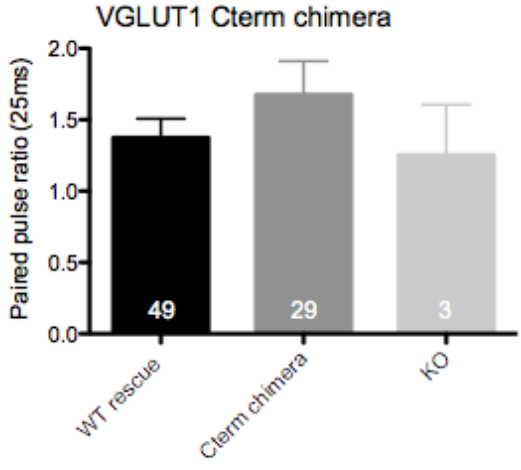

E: 10 Hz train stimulation

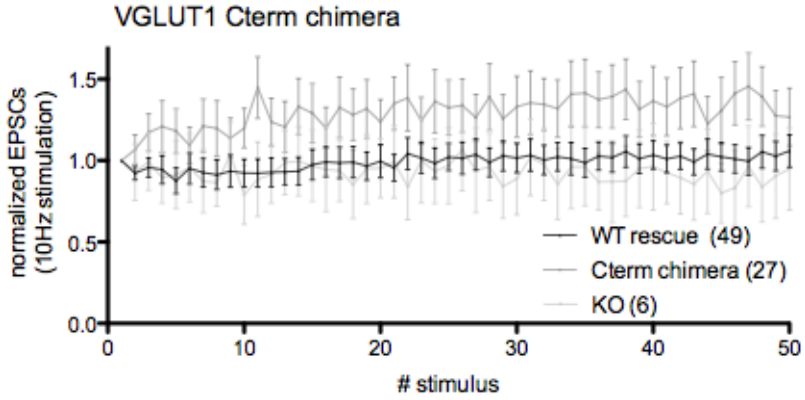

F: spontaneous activity
(mEPSC amplitude)

G: spontaneous activity
(mEPSC frequency)

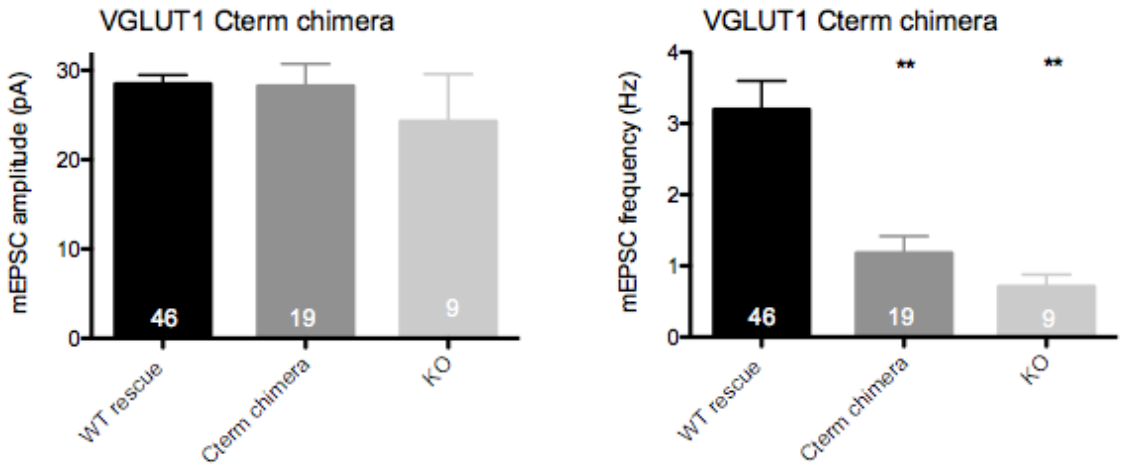

Fig. 20 (A-G): **Electrophysiological analysis of a VGLUT1 C-terminus chimera with WT rescue and VGLUT1 KO neurons:** the neurotransmission of a VGLUT1 C-terminus truncation construct substituted with the C-terminal amino acid sequence of synaptophysin, another common SV protein, was also investigated. Therefore, hippocampal VGLUT1 KO neurons were lentiviral infected to express a VGLUT1 chimera rescue construct in comparison to the WT rescue. EPSCs (A) and RRP (B) are significantly reduced in the VGLUT1 C-terminus chimera construct (dark grey) compared to the WT rescue (black), which is also the case in VGLUT1 KO neurons (light grey). The calculated Pvr (C) and measured PP ratio (D) are not different in the VGLUT1 chimera or VGLUT1 KO compared to the WT rescue. The 10 Hz train stimulation (E) shows small alterations in the VGLUT1 chimera apparent by less depression compared to the WT rescue and VGLUT1 KO neurons. mEPSC amplitudes (F) show no differences in the recorded groups, whereas the mEPSC frequencies (G) are significantly reduced in both groups, the VGLUT1 chimera and VGLUT1 KO (n numbers correspond to 3 independent cell culture, bars indicate mean±SEM, One way ANOVA with tukey`s multiple comparison test: ** $p<0.001$, ***$p<0.0001$).

3.2.5 VGLUT2 knockdown in hippocampal neurons validates the reduced neurotransmission in the VGLUT1 C-terminus chimera

From previous work (Wojcik et al., 2004) it is known that besides VGLUT1 about 12% of the hippocampal neurons express VGLUT2 and less than 1% of the cells express VGLUT3, which is negligible. Whether this VGLUT2 expression influences the mean size of the recorded postsynaptic responses of the different VGLUT C-terminus constructs, was explored in an additional experiment.

The previous experiments show that the EPSC amplitudes of the VGLUT1 and 2 C-terminus truncation constructs and the VGLUT1 C-terminus chimera construct were significantly smaller than the EPSCs of WT rescues, but still larger than the postsynaptic responses of KO neurons. These data indicate a low rescue activity of the different VGLUT C-terminus constructs (fig.18-20), which might be as mentioned before due to VGLUT2 expressing in the cell culture. Therefore, the chimeric VGLUT1 C-terminus construct was used together with a VGLUT2 knockdown (KD), which was induced by small hairpin RNA (shRNA, cf. paragraph 2.4 „RNA interference by shRNA for protein knockdown“). The idea was to reduce the VGLUT2 protein expression of the hippocampal cell culture to almost zero.

In this experiment lentivirus infected VGLUT1 KO neurons expressing either the chimeric VGLUT1 or the WT rescue construct plus in addition VGLUT2 shRNA were recorded. The VGLUT1 constructs were also compared with VGLUT1 KO neurons that were infected with VGLUT2 shRNA as well.

The VGLUT2 KD quantification is described in the appendix (fig.34-36).

The EPSC amplitudes of the VGLUT1 chimera rescue construct plus VGLUT2 shRNA are about 20% of the WT rescue plus VGLUT2 shRNA (fig.21A). The postsynaptic responses of the KO cells plus shRNA are even further reduced and almost zero (4.8± 1.7nA in WT resc.; 1.1± 0.2nA in chimera; 0.23± 0.1nA in KO all plus VGLUT2 shRNA, fig.21A). Corresponding, the RRPs are also significantly reduced in the VGLUT2 sRhNA co-infected VGLUT1 chimera and KO neurons compared to the VGLUT2 shRNA co-infected WT rescue (793.0± 262.9pC in WT resc.; 202.4± 55.9pC in chimera; 56.3± 12.2pC in KO all plus VGLUT2 shRNA, fig.21B). The Pvr and PP ratio do not show significant changes between the investigated groups (Pvr: 4.2± 1.6% in WT resc.; 3± 0.6% in chimera; 3.3± 1% in KO; PP ratio: 0.9± 0.1 in WT resc.; 0.8± 0.1 in chimera; 0.7± 0.1 in KO all plus VGLUT2 shRNA, fig.21C, D). The mEPSC amplitudes are not changed in any of the recorded groups as well

(33.8± 3.7pA in WT resc.; 27.3± 3.6pA in chimera; 25.3± 2.6pA in KO all plus VGLUT2 shRNA, fig.21F). There were also no significant changes in 10 Hz train stimulation (fig.21E). In contrast, the mEPSC frequencies are significantly decreased in the VGLUT2 sRhNA co-infected VGLUT1 chimera construct and KO neurons (10.7± 2.3Hz in WT resc.; 1.9± 0.7Hz in chimera; 1.1± 0.5Hz in KO all plus VGLUT2 shRNA, fig.21G). ICC quantifications were not performed for this experiment.

The results of this experiment, using additionally VGLUT2 shRNA to reduce the VGLUT2 expression in hippocampal VGLUT1 KO cell culture, confirm that the detected postsynaptic responses are still larger in the VGLUT1 chimera than the responses from recorded VGLUT1 KO neurons. These data indicate that the remaining rescue activity of the chimera is indeed VGLUT1 dependent and not an effect of VGLUT2 expression in hippocampal cell culture.

A: Evoked postsynaptic responses

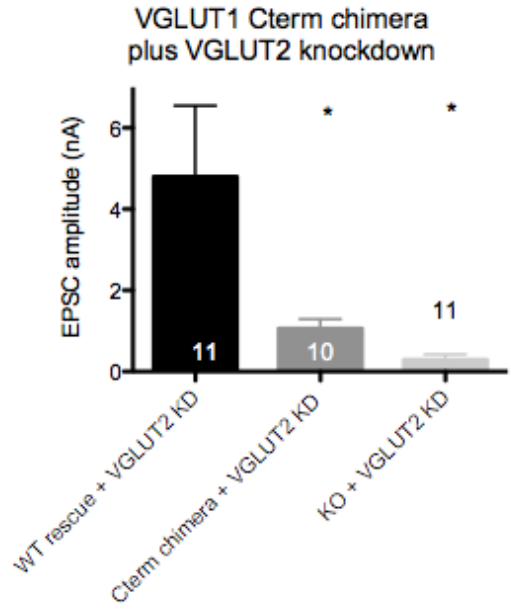

B: Readily releasable pool

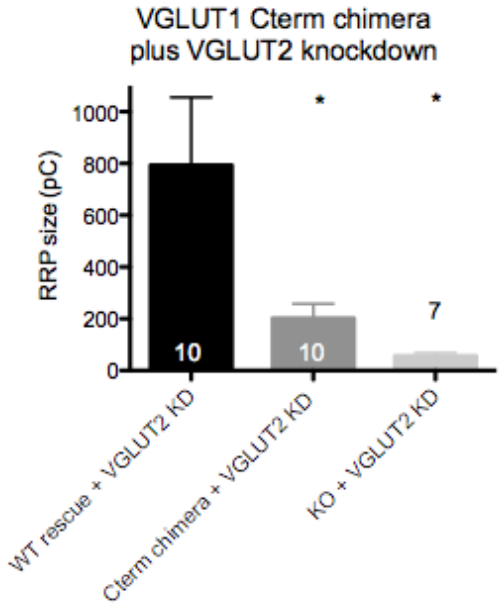

C: Vesicular release probability

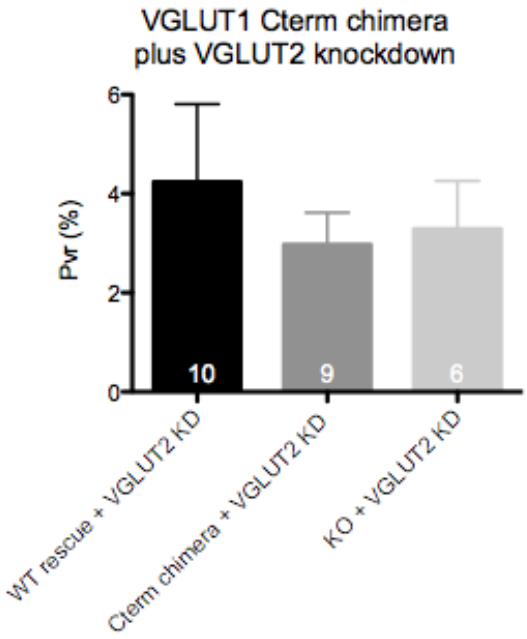

D: Paired pulse ratio

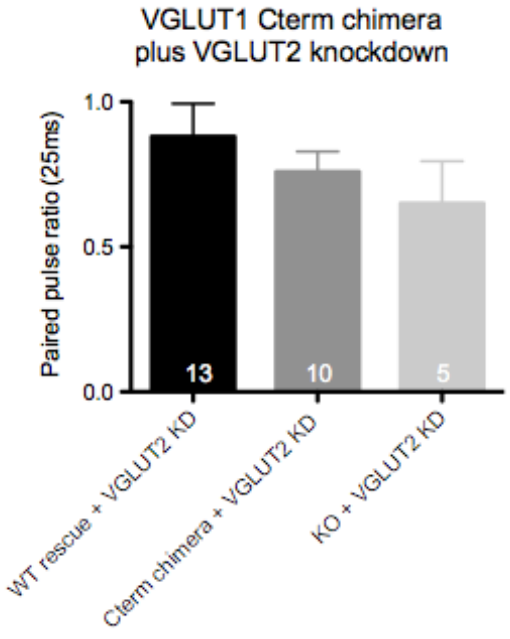

E: 10 Hz train stimulation

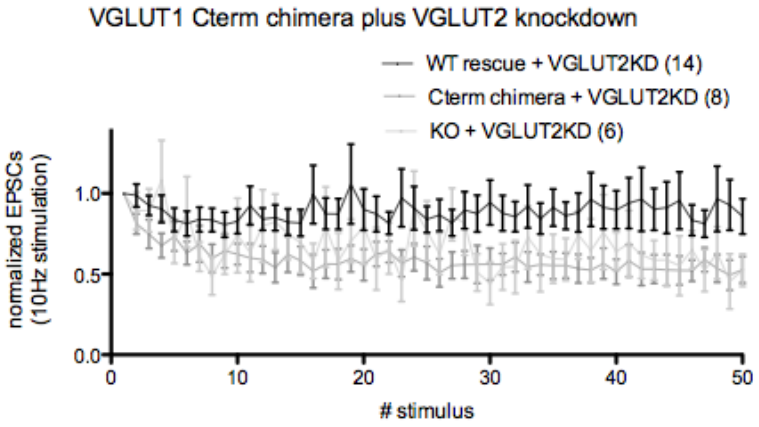

F: spontaneous activity
(mEPSC amplitude)

G: spontaneous activity
(mEPSC frequency)

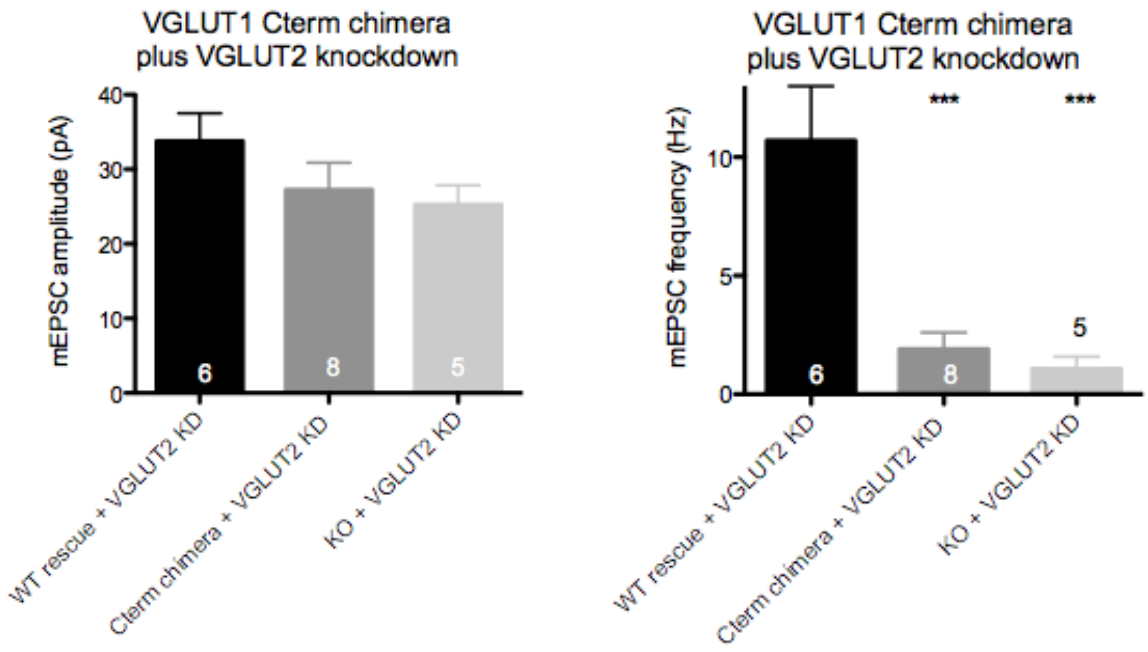

Fig. 21 (A-G): **Electrophysiological analysis of the VGLUT1 C-terminus chimera with additional VGLUT2 KD in comparison with WT rescue and VGLUT1 KO neurons:** usually about 12% of the hippocampal neurons express VGLUT2 (Wojcik et al., 2004). To investigate the influence of the remaining VGLUT2 expression in the hippocampal VGLUT1 KO neuron culture on the detected small postsynaptic responses of the VGLUT1 C-terminus chimera construct, a VGLUT2 KD by a shRNA-expressing construct was used. Therefore, VGLUT1 KO neurons were co-infected with different VGLUT1 rescue constructs and in addition with VGLUT2 shRNA. EPSCs (A) and the RRPs (B) are still significantly reduced in VGLUT1 C-terminus chimera (dark grey) and VGLUT1 KO neurons co-infected with VGLUT2 shRNA (light grey) compared to WT rescued shRNA co-infected neurons (black). However, the EPSC amplitude and RRP sizes of the VGLUT1 chimera are slightly larger than in the KO group (A and B). The calculated Pvr (C) and measured PP ratio (D) are not different in the VGLUT2 shRNA co-infected VGLUT1 chimera or VGLUT1 KO neurons compared to shRNA co-infected WT rescue. The 10 Hz train stimulation (E) shows small changes in the co-infected VGLUT1 chimera and KO neurons apparent by a little higher depression compared to the WT rescue. mEPSC amplitudes (F) show no differences between the shRNA co-infected recorded groups, whereas the mEPSC frequencies (G) are significantly reduced in the VGLUT1 chimera and even further reduced in KO neurons (n numbers correspond to 1 cell culture, bars indicate mean±SEM, One way ANOVA with tukey`s multiple comparison test: *$p<0.05$, ***$p<0.0001$).

3.2.6 A shorter VGLUT1 C-terminus truncation version with an additional WAEPE motif sequence can rescue defects in neurotransmission to wildtype rescue levels

Neurons expressing the full C-terminus truncation construct VGLUT1Δ496-560 show impaired NT release to almost VGLUT1 KO levels (fig.18).

There are characteristic amino acids located after the 12th VGLUT1 transmembrane domain with the sequence: WAEPE. In comparison to the other two mammalian VGLUT isoforms (cf. fig.4 and 5) as well as the invertebrate *Drosophila melanogaster* version of VGLUT this motif sequence is very conserved (WA(X)P(X)).

Foss et al., 2013 used, to monitor the VGLUT1 recycling during endocytosis, a pHluorin-based VGLUT1 C-terminus truncation construct with a few additional amino acids after the last transmembrane domain including this VGLUT1 WAEPE motif sequence (PWAEPEEM). They could show normal synaptic protein expression of the VGLUT1-pHluorin C-terminus truncation construct compared to the corresponding VGLUT1-pHluorin full-length construct (Foss et al., 2013).

Therefore, it can be hypothesized that these additional C-terminal amino acids including the WAEPE motif sequence might be sufficient for a correct located VGLUT1 protein and consequently to restore postsynaptic responses of VGLUT1 KO neurons to WT rescue levels. To study this, electrophysiological analyses in hippocampal VGLUT1 KO background were performed by using a by lentivirus expressed VGLUT1 rescue construct similar to Foss et al., 2013. This shorter VGLUT1 C-terminus truncation construct until aa504 (VGLUT1Δ504-560) includes the VGLUT1 WAEPE motif sequence.

This shorter C-terminus truncation construct VGLUT1Δ504-560 can indeed restore the EPSCs to WT rescue levels (4.4± 0.5nA in WT resc., 4.1± 0.7nA in C-term trunc., 0.4± 0.1nA in KO, fig.22A). The RRP of the truncated version VGLUT1Δ504-560 is not different to the WT rescue as well (666.8± 83.7pC in WT resc., 624.3± 79.9pC in C-term trunc., 0.4± 0.1pC in KO, fig.22B). The release property and short term plasticity of this shorter VGLUT1 C-terminus truncation construct are also not different to WT rescue levels (Pvr: 5.2± 0.4% in WT resc., 5.1± 0.7% in C-term trunc., 3.9± 0.8% in KO; PP ratio: 1.2± 0.1 in WT resc., 1.2± 0.04 in C-term trunc., 1.6± 0.1 in KO, fig.22C and D). mEPSC amplitudes are similar between the recorded groups as well (20.1± 2pA in WT resc., 21.1± 2.3pA in C-term trunc., 17.3± 2.8pA in KO, fig.22F). mEPSC frequencies only differ, as expected, in KO neurons (fig.22G). The mEPSC frequency of the C-terminus truncation version VGLUT1Δ504-560 is

not different to WT rescue levels (13.9± 1.8Hz in WT resc., 12.8± 1.7Hz in C-term trunc., 6.8± 2.8Hz in KO, fig.22G). The 10 Hz train stimulation data of the C-terminus truncation construct VGLUT1Δ504-560 also reveal no differences to the WT rescue (fig.22E). Unexpected, ICC quantifications show a significantly reduced protein expression of VGLUT1Δ504-560 compared to the WT rescue levels, even though the NT release is not affected (1± 0.09 in WT resc., 0.33± 0.06 in C-term trunc., 0.24± 0.02 in KO, fig.37B, appendix). This might be due to a low number of analyzed samples in this experiment.

Altogether, the data with the shorter VGLUT1 C-terminus truncation until aa504 including a WAEPE motif sequence illustrate the importance of these additional amino acids after the 12th transmembrane domain for VGLUT1 function in regular neurotransmission. The C-terminus truncation version VGLUT1Δ504-560 can rescue the VGLUT1 KO phenotype of significantly decreased postsynaptic responses to WT rescue levels. It can be assumed that in general the conserved VGLUT WA(X)P(X) motif sequence seems to be essential for a proper VGLUT performance in synaptic transmission.

A: Evoked postsynaptic responses

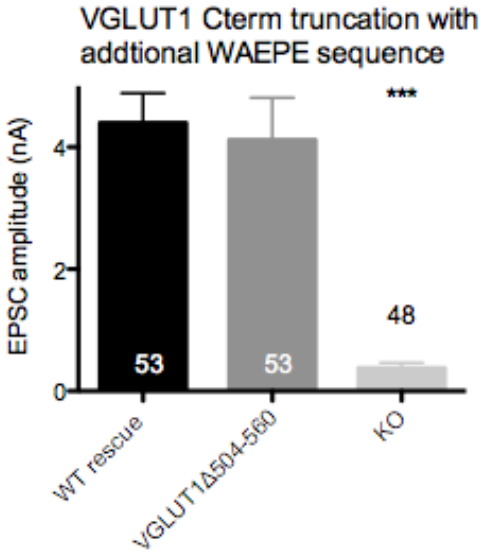

B: Readily releasable pool

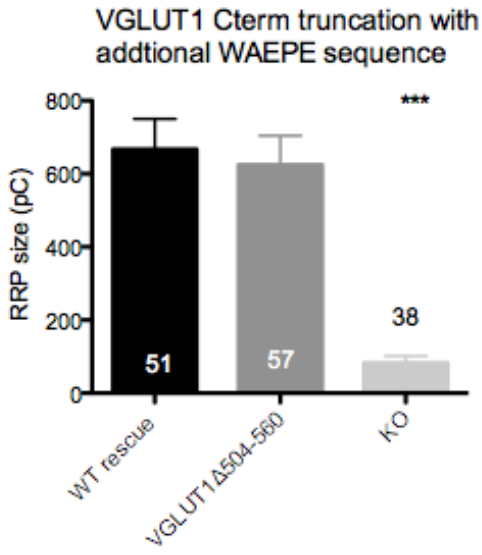

C: Vesicular release probability

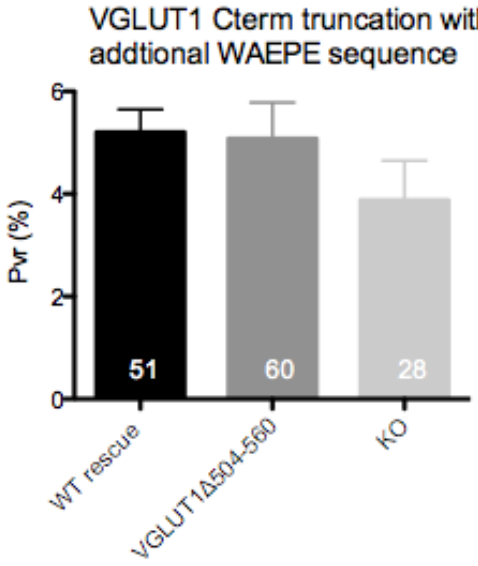

D: Paired pulse ratio

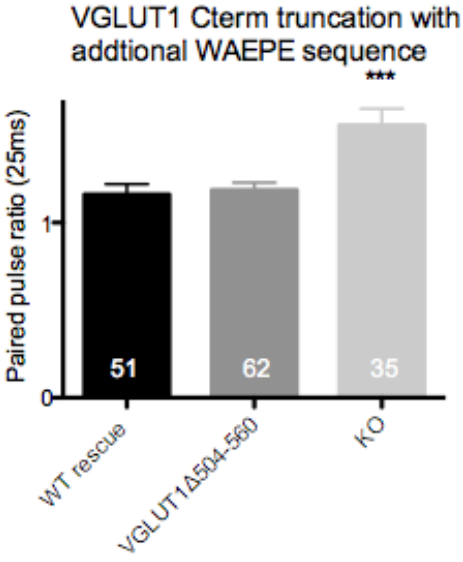

E: 10 Hz train stimulation

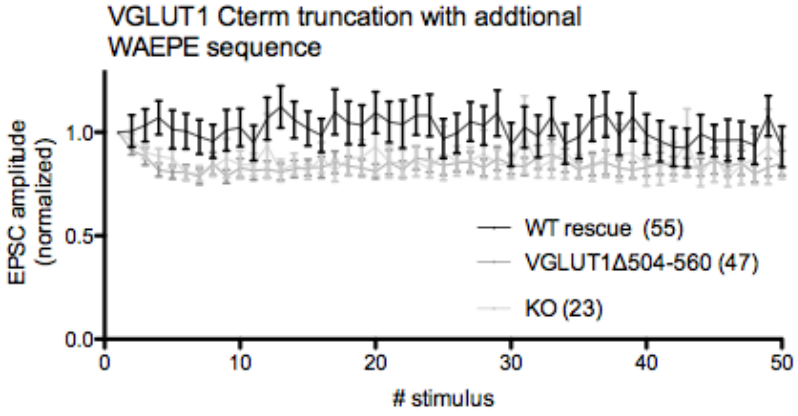

F: spontaneous activity (mEPSC amplitude)

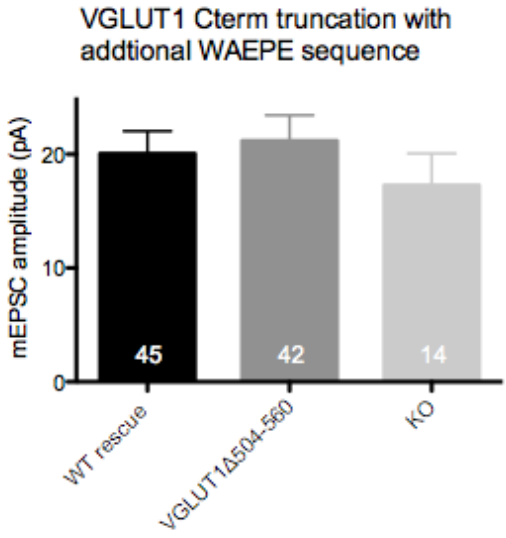

G: spontaneous activity (mEPSC frequency)

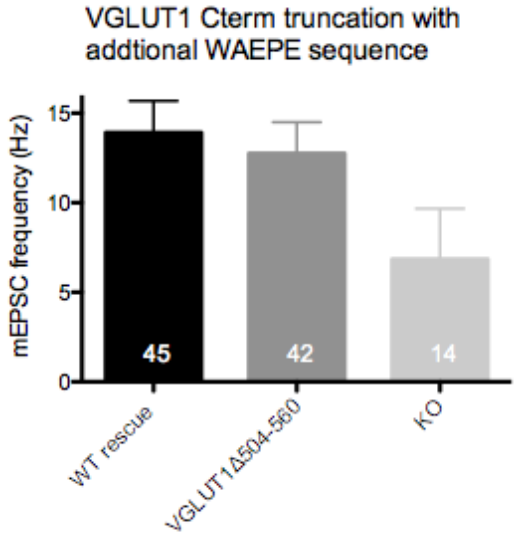

Fig. 22 (A-G): **Electrophysiological analysis of a shorter C-terminus truncation VGLUT1Δ504-560 in comparison with WT rescue and VGLUT1 KO neurons:** to investigate the neurotransmission hippocampal VGLUT1 KO neurons were used for lentivirus indcued rescue experiments with the C-terminus truncation construct VGLUT1Δ504-560 in comparison to the WT rescue and VGLUT1 KO neurons. This shorter C-terminus truncation construct contains eight more amino acids with a WAEPE motif sequence compared to the full C-terminus truncation contruct VGLUT1Δ496-560. EPSCs (A) and RRP (B) of the C-terminus truncation VGLUT1Δ504-560 (dark grey) are similar to WT rescue levels (black). Only KO neurons (light grey) show a reduction of the EPSCs and RRP (A and B). The calculated Pvr (C) and measured PP ratio (D) are not different in the C-terminus truncation VGLUT1Δ504-560 or VGLUT1 KO neurons compared to the WT rescue. The 10 Hz train stimulation data (E) also show no alteration in the C-terminus truncation VGLUT1Δ504-560 compared to the WT rescue and VGLUT1 KO neurons. mEPSC amplitudes (F) show no differences between the measured groups as well, whereas the mEPSC frequencies (G) are, as expected, reduced in VGLUT1 KO neurons, but not in VGLUT1Δ504-560 (n numbers correspond to 3 independent cell culture, bars indicate mean±SEM, One way ANOVA with tukey`s multiple comparison test: ***p<0.0001).

3.2.7 Further synaptic vesicle pool depletion experiments also reveal no differences between the shorter VGLUT1 C-terminus truncation and the wildtype rescue

The shorter C-terminus truncation VGLUT1Δ504-560 can rescue the KO phenotype of significantly reduced NT release to WT rescue levels, which was observed in the full C-terminus truncation VGLUT1Δ496-560. The shorter C-terminus truncation VGLUT1Δ504-560 show no changes in AP-evoked or spontaneous EPSCs. Similarly, the probability of vesicles to release during electrical stimulation (Pvr) and the comparison of 10 Hz train stimulation (50AP) reveal no differences of VGLUT1Δ504-560 compared to the WT rescue. However, a 10 Hz train stimulation (50AP) does not deplete the SV pool. Whether the shorter C-terminus truncation VGLUT1Δ504-560 might influence the neurotransmission during very high frequency stimulation, is not investigated yet. Therefore, a 1,000AP-train stimulation protocol (20 Hz, fig.23A) was used to deplete the SVs per synapse. To also investigate the subsequent recovery phase after the depletion the first 24AP-induced EPSCs (0.2 Hz, fig.23B) were analyzed as well. For this, the C-terminus truncation construct VGLUT1Δ504-560 as well as a VGLUT1 WT full-length construct were lentiviral rescued in hippocampal VGLUT1 KO neurons.

No changes could be detected between neurons expressing either the VGLUT1 WT or the C-terminus truncation rescue construct. VGLUT1Δ504-560 and the WT rescue show a similar depression curve of the plotted EPSC amplitudes (fig.23A). The subsequent EPSC amplitude recovery is also similar between the VGLUT1 truncation construct and the WT rescue (fig.23B).

However, none of the recorded groups seems to deplete the entire SV pool, because there are remaining small postsynaptic responses in the end of the stimulation trains (fig.23A). Therefore, it can be concluded that a higher electrical stimulation would be necessary for an absolute SV pool depletion.

In this experiment, data from VGLUT1 KO neurons, where a postsynaptic response was detectable, were also included. In comparison to the WT rescue and the C-terminus truncation construct VGLUT1Δ504-560, the KO neurons show a slightly less depression in the depletion experiment and a slower recovery of the subsequent EPSC amplitudes (fig.23A and B).

A: pool depletion by high frequency

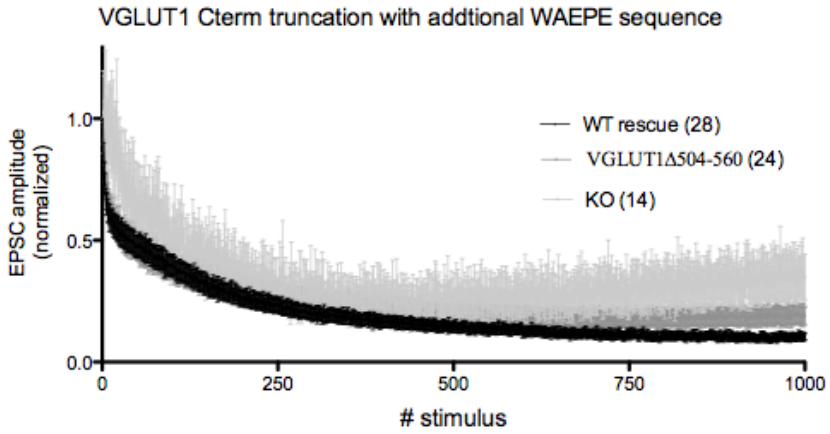

stimulation

A: recovery after high frequency stimulation

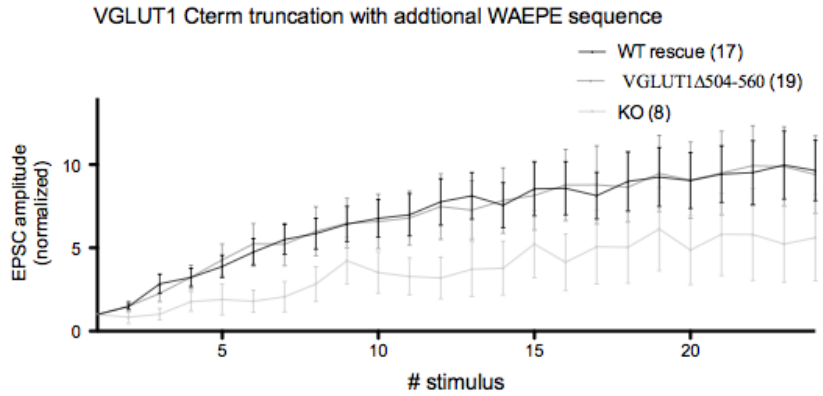

Fig. 23 (A and B): **SV depletion and recovery of the shorter C-terminus truncation VGLUT1Δ504-560 in comparison with WT rescue and VGLUT1 KO neurons:** high frequent electrical stimulation were investigated in lentiviral infected hippocampal VGLUT1 KO neurons, which express the VGLUT1Δ504-560 construct (dark grey) or WT rescue (black) in comparison with VGLUT1 KO neurons (light grey). To deplete the entire SV pool a high frequency train stimulation of 1,000AP (20 Hz) was applied (A). The subsequent recovery of the postsynaptic responses was measured by recording the first 24AP-induced EPSCs (0.2 Hz) after the high frequent stimulation (B). No changes were detected between the WT rescue and the C-terminus truncation VGLUT1Δ504-560, whereas the EPSCs from VGLUT1 KO cells tend to deplete and recover slower (n numbers correspond to 2 independent cell cultures, bars indicate mean±SEM).

3.2.8 pHluorin experiments demonstrate a drastic impaired VGLUT1 recycling of the shorter C-terminus truncation

VGLUT1 KO neurons expressing the shorter truncation rescue construct VGLUT1Δ504-560 show no differences in neurotransmission compared with those expressing a WT VGLUT1 construct. However, with electrophysiological measurements alone the VGLUT1 cycling during exo- and endocytosis cannot be investigated, especially not in single boutons. Therefore, to also monitor the VGLUT1 cycling of VGLUT1Δ504-560, in this experiment

electrophysiology was again combined with pHluorin-based imaging (cf. paragraph 2B, fig.7). The combination of both techniques allows to gain insights into the VGLUT1Δ504-560 release during electrical stimulation (also here 5 Hz stimulation for one minute (300AP), similar to Voglmaier et al., 2006) and to observe the VGLUT1Δ504-560 recycling (cf. paragraph 2B "pH-sensitive green fluorescent protein (pHluorin)-based live cell imaging to monitor synaptic vesicle cycling").

For that, the pHluorin molecule is again directly attached to the VGLUT1 mutant construct and hippocampal VGLUT1 KO neurons were infected with lentivirus to express VGLUT1Δ504-560-pHluorin, but also to test a VGLUT1 C-terminus chimera-pHluorin construct in comparison to the VGLUT1 full lenght (WT)-pHluorin, similar to the experiments as described before.

By applying NH_4Cl- or pH5.5-containing solutions the total amount of VGLUT1Δ504-560-pHluorin molecules expressed in a synapses as well as all the VGLUT1Δ504-560-pHluorin molecules on the synapse surface could be determined as well (cf. paragraph 2B). With these information it is possible to also calculate the surface expression in percentage (%) as a fraction of VGLUT1Δ504-560-pHluorin molecules on the surface to the total amount of pHluorin molecules. For control, the C-terminal VGLUT1 FV510/511AA mutant was also used again.

The pHluorin-tagged VGLUT1 C-terminus chimera construct fails to generate a sufficient pHluorin expression in synapses to perform pHluorin-based imaging (fig.24B). There is no punctate (synaptic) expression pattern (baseline fluorescence, data not shown), but also no increase in fluorescence apparent during the application of NH_4Cl-containing solution (fig.24B), where the pH inside the SVs becomes neutralized and thereby the pHluorin fluorescence normally raises (cf. fig.7). In contrast, neurons infected with the WT rescue version of VGLUT1-pHluorin show, as expected, a punctate (synaptic) expression pattern, also after NH_4Cl-containing solution application, which indicates a normal synaptic expression pattern (fig.24A). The shorter C-terminus truncation pHluorin version VGLUT1Δ504-560 including the WAEPE motif is also well enough expressed in synapses (fig.24C) to be used for pHluorin-based imaging experiments.

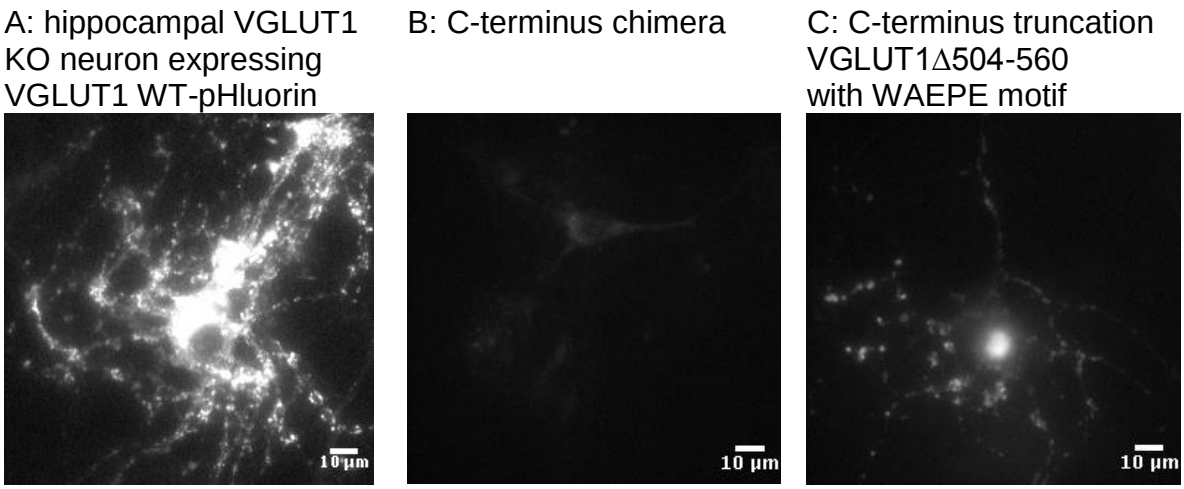

Fig. 24 (A-C): **Example images of WT and mutant VGLUT1-pHluorin constructs in hippocampal VGLUT1 KO neurons:** for pHluorin-based imaging experiments hippocampal VGLUT1 KO neurons were lentiviral infected to express different mutated VGLUT1-pHluorin constructs in comparison with a WT rescue-pHluorin construct. By application of NH_4Cl-containing solution the acidic pH inside SVs becomes neutralized and thereby the fluorescence of pHluorin molecues increases. This change in expression of pHluorin-tagged VGLUT1 constructs can be detected. In the WT rescue-pHluorin construct (A) a bright punctate (synaptic) fluorescence signal is detectable. Instead, the VGLUT1 C-terminus chimera-pHluorin construct (B) shows no fluorescence increase by application of NH_4Cl-containing solution indicating an impaired protein expression of the construct. The shorter C-terminus truncation VGLUT1Δ504-560-pHluorin construct with a WAEPE motif sequence (C) is well expressed and shows a fluorescence pattern similar to WT rescue levels (neurons with 60x magnification).

The pHluorin-based imaging experiments show that the SV endocytosis phase with VGLUT1 retrieval for SV refilling and re-acidification, which starts during 300AP stimulation, is severely impaired in neurons expressing the C-terminus truncation construct VGLUT1Δ504-560 compared to those expressing the WT rescue. This is shown in fig.25A, where the normalized fluorescence change (ΔF) of the pHluorin molecules is plotted over time and normalized to the peak fluorescence during 300AP stimulation. The control group, FV510/511AA, causes as expected a slower VGLUT1 recycling as well.

The slower endocytic phase of VGLUT1Δ504-560-pHluorin compared to WT rescue-pHluorin is reflected by single exponential fit of the pHluorin fluorescence decline and also apparent in differences of the fluorescence values 125 s post stimulus (exponential fit (τ): 11.9± 0.2s in WT resc., 13.1± 0.6s in C-term trunc., 15± 0.3s in FV510/511AA; t_{150s} $\Delta F/F_0$: 0.2 in WT resc., 0.6 in C-term trunc., 0.3 in FV510/511AA, fig.25A). The rise phase of the pHluorin fluorescence during the electrical stimulation differs between the analyzed groups as well. In both cases, the FV510/511AA-pHluorin and the VGLUT1Δ504-560-pHluorin, the rise time is much slower than in the WT rescue-pHluorin, which is also apparent in different pHluorin fluorescence values 25 s post stimulus (exponential fit (τ): 5.9± 1s in WT

resc., 27± 1s in C-term trunc., 13.6± 1s in FV510/511AA; t_{50s} $\Delta F/F_0$: 1 in WT resc., 0.6 in C-term trunc., 0.8. in FV510/511AA, fig.25A). The surface expression is altered in the shorter C-terminus truncation VGLUT1Δ504-560 as well (fig.25C). The surface expression is higher in VGLUT1Δ504-560-pHluorin-expressing neurons similar to FV510/511AA-pHluorin-expressing neurons (1± 0.1% in WT resc., 1.49± 0.13% in C-term trunc., 1.61± 0.19% in FV510/511AA, fig.25C). Statistical significant differences between VGLUT1Δ504-560-pHluorin and the WT rescue-pHluorin might be detectable with an increased sample number.
The total amount of pHluorin molecules in the synapses, reflected in their fluorescence after NH_4Cl-containing solution application, is drastically reduced in both groups, FV510/511AA-pHluorin and VGLUT1Δ504-560-pHluorin in comparison to the WT rescue-pHluorin (1.1± 0.1 in WT resc., 0.27± 0.03 in C-term trunc., 0.41± 0.05 in FV510/511AA, fig.25D). ICC analyses of neurons expressing the VGLUT1Δ504-560 construct, which were used in pure electrophysiology investigations also show differences in protein expression levels compared to WT rescued neurons (fig.37B, appendix), whereas the neurotransmission of VGLUT1Δ504-560 is unaffected (fig.22).
Similarly, the recorded EPSC amplitudes during 5 Hz, 300AP train stimulation of the pHluorin-based imaging experiments of neurons expressing the C-terminus truncation construct VGLUT1Δ504-560 are similar to the EPSCs of WT rescued cells (1±0.1 in WT resc., 0.7± 0.1 in C-term trunc., 1.1± 0.1 in FV510/511AA, fig.25G). Analyzing the EPSC amplitudes before starting the pHluorin-based imaging protocol, to also test by the EPSC kinetics, whether the recorded neuron is glutamatergic or gabaergic, show that VGLUT1 KO neurons rescued with VGLUT1Δ504-560-pHluorin have almost same EPSC sizes than those rescued with VGLUT1 WT-pHluorin (1± 0.08 in WT resc., 0.71± 0.13 in C-term trunc., 1.06± 0.1 in FV510/511AA, fig.25E). The PP ratio of the recorded groups was also measured and is unexpected higher in VGLUT1Δ504-560-pHluorin (1.16± 0.04 in WT resc., 1.37± 0.04 in C-term trunc., 1.21± 0.03 in FV510/511AA, fig.25F).

Altogether, the data show a very decelerated VGLUT1 retrieval and higher surface expression of VGLUT1Δ504-560-pHluorin compared to the WT rescue-pHluorin indicating an important role of the VGLUT1 C-terminus for its recycling. However, the neurotransmission of VGLUT1Δ504-560-pHluorin is, similar to the electropgysiology data before, not affected even the overall pHluorin expression in the synaptic boutons seems to be also lower.

A: Fluorescence changes normalized to the peak of 300AP

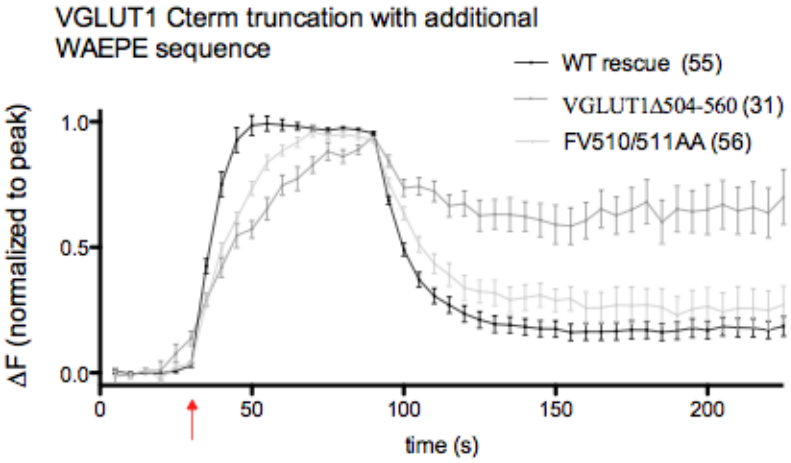

stimulation

B: Fluorescence changes normalized to the peak of NH_4Cl-induced fluorescence

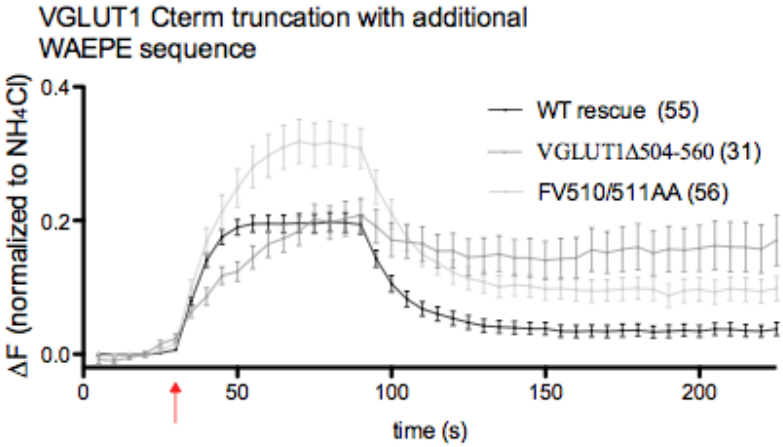

C: Surface expression

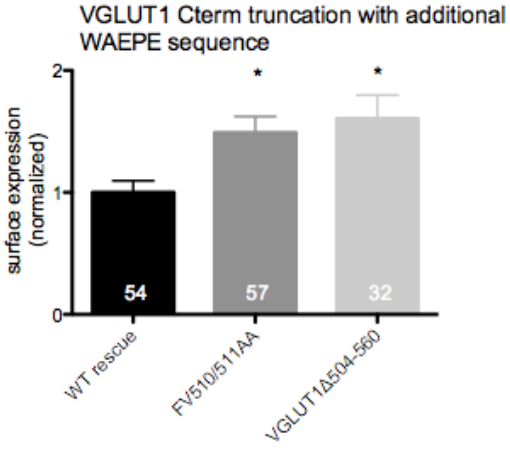

D: Total pHluorin expression

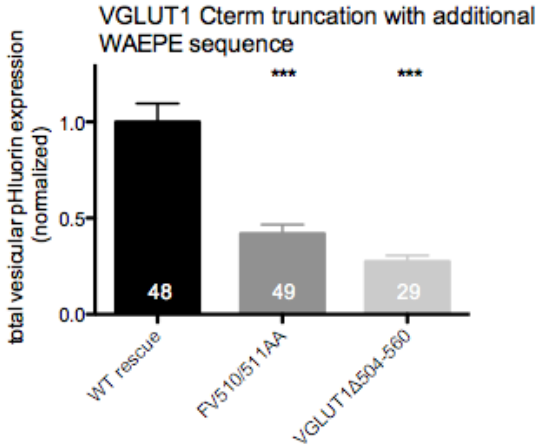

E: Evoked postsynaptic responses

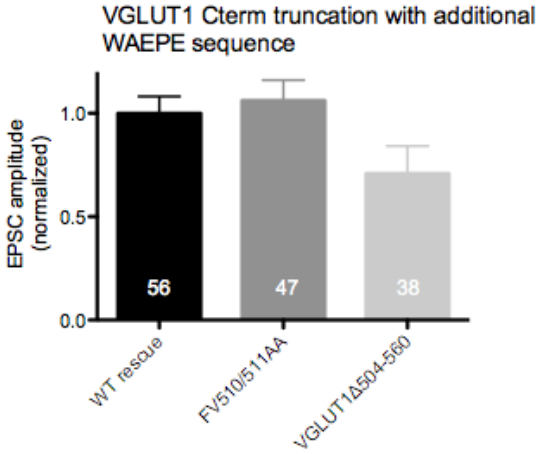

F: Paired pulse ratio

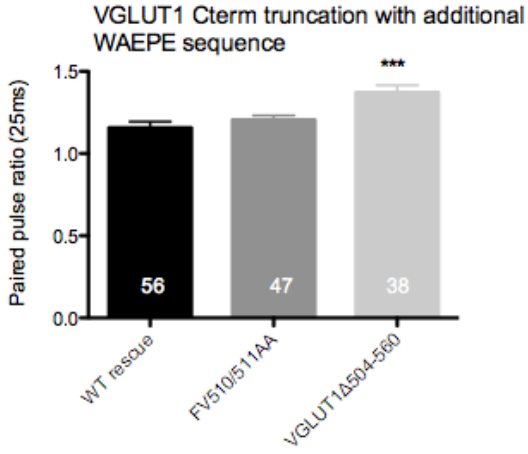

G: EPSCs during 5 Hz, 300AP train stimulation

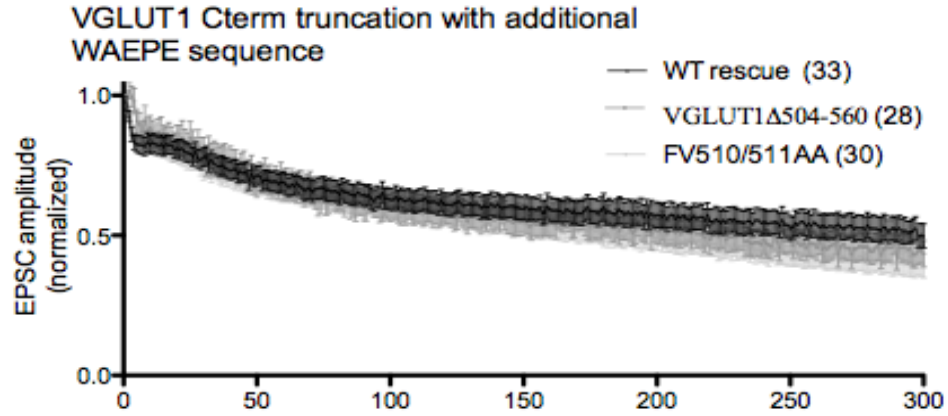

Fig. 25 (A-G): **pHluorin-based VGLUT1 cycling and electrophysiology analyses of the shorter C-terminus truncation VGLUT1Δ504-560:** to investigate VGLUT1 cycling hippocampal VGLUT1 KO neurons were lentiviral infected to express different VGLUT1 C-terminus mutant pHluorin-constructs (FV510/511AA (dark grey) and the shorter C-terminus truncation VGLUT1Δ504-560 with a WAEPE motif (light grey)) in comparison with a WT rescue-pHluorin construct (black). The plotted pHluorin fluorescence traces were normalized to either the peak fluorescence during 300AP stimulation (A) or the peak fluorescence during NH_4Cl-containing solution application (B). The comparison of the recorded groups illustrate that the C-terminus truncation causes a severely impaired VGLUT1 retrieval after 5 Hz, 300AP stimulation (start red arrow) (A). FV510/511AA-pHluorin also shows a slowed VGLUT1 retrieval (A). Additionally, the surface expression is higher in VGLUT1Δ504-560-pHluorin and FV510/511AA-pHluorin (C). The surface expression is calculated as the ratio of the pHluorin peak fluorescence during 300AP train stimulation to the peak fluorescence during NH_4Cl-containing solution application. The total expression of pHluorin molecules (measured by application of NH_4Cl-containing solution) is reduced in FV510/511AA-pHluorin and VGLUT1Δ504-560-pHluorin (D). However, additional electrophysiological investigations before the imaging protocol started show that the EPSC amplitudes are not changed between the recorded groups (E), whereas the PP ratio is increased in VGLUT1Δ504-560-pHluorin, but not in FV510/511AA-pHluorin (F). The plot of the EPSCs during 5 Hz, 300AP train stimulation also reveals no changes between the recorded groups (G) (n numbers correspond to 3 independent cell cultures, bars indicate mean±SEM, in parts normalized to WT=1, One way ANOVA with tukey`s multiple comparison test: * $p<0.05$, *** $p<0.0001$).

3.2.9 Synaptophysin-pHluorin experiments reveal only slight changes in the general synaptic vesicle cycle of the shorter VGLUT1 C-terminus truncation

The severely slower VGLUT1 retrieval of VGLUT1Δ504-560 during SV endocytosis (fig.25A) might additionally affect the overall SV recycling. To test that possibilitiy the pHluorin experiments were repeated using a synaptophysin-pHluorin instead of a VGLUT1-pHluorin. Synaptophysin is a common SV marker and generally used in pHluorin experiments. Therefore, VGLUT1 KO neurons were lentiviral co-infected to express the VGLUT1 WT rescue construct or the shorter C-terminus truncation version VGLUT1Δ504-560 (including the WAEPE sequence) together with synaptophysin-pHluorin. In this experiment, also KO neurons were used and lentiviral infected to express synaptophysin-pHluorin.

The results show no differences of the SV recycling of the truncated C-terminus construct VGLUT1Δ504-560 in comparison with the WT rescue. The decline of the pHluorin fluorescence after 5 Hz, 300AP stimulation between the WT rescue and VGLUT1Δ504-560 is not different. SVs from the KO group sems to recycle a little bit slower after electrical stimulation (exponential fit (τ): 17.54± 0.2s in WT resc., 19.42± 0.25s in C-term trunc., 22.61± 0.25s in KO, t_{150s} $\Delta F/F_0$: 0.25 in WT resc., 0.3 in C-term trunc., 0.3 in KO, fig.26). In contrast, neurons expressing the truncated C-terminus version VGLUT1Δ504-560 and neurons from the KO group show a slower increase in pHluorin fluorescence during 300AP stimulation compared to cells from the WT rescue group (fig.26). The analyzed rise time of the KO neurons is even significantly slower (exponential fit (τ): 11.3± 1.04s in WT resc., 15.73± 1.04s in C-term trunc., 24.94± 1.13s in KO, fig.26). The results of a lower rise time can be confirmed by the analysis of the pHluorin fluorescence values of the different groups 50 s post stimulus (t_{50s} $\Delta F/F_0$: 0.86 in WT resc., 0.75 in C-term trunc., 0.6 in KO, fig. 26).

Altogether, these data illustrate that the substantially impaired VGLUT1 retrieval of the C-terminus truncation, shown in fig. 25A, does not affect the synaptophysin recycling, which in turn indicates that the general SV recycling is not impaired by VGLUT1Δ504-560. Both, the VGLUT1 recycling and the synaptophysin recycling, seem to be independent from each other.

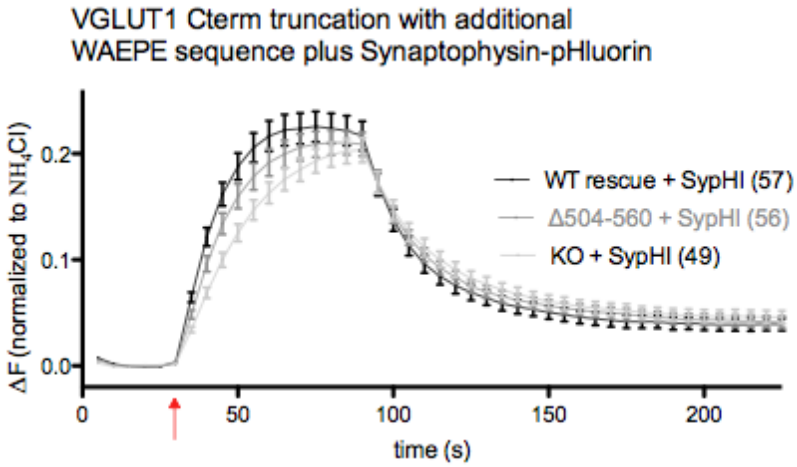

Fig. 26: **Synaptophysin-pHluorin-based analysis of the shorter C-terminus truncation VGLUT1Δ504-560 to investigate the general SV cycling:** to investigate the general SV cycling synaptophysin-pHluorin (SypHl) was used as a common SV marker to monitor potential pHluorin fluorescence changes after high frequency stimulation (5 Hz, 300AP; start red arrow). A double lentiviral infection of hippocampal neurons to express synaptophysin-pHluorin plus different VGLUT1 constructs (WT rescue, C-terminus truncation VGLUT1Δ504-560 or in case of the KO group a vehicle (empty vector)) was done in VGLUT1 KO background. The endocytosis phase is not slower in VGLUT1Δ504-560 (dark grey) compared to the WT rescue (black) and KO neurons (light grey). Instead, the rise time during electrical stimulation is slower in VGLUT1Δ504-560 and KO neurons (n numbers correspond to 1 cell culture, bars indicate mean±SEM).

3.2.10 Morphological synaptic vesicle analyses reveal a KO-like phenotype of the VGLUT1 full C-terminus truncation, which can be rescued with the shorter truncation

The physiology of the full C-terminus truncation VGLUT1Δ496-560 is impaired, but not of the shorter C-terminus truncation VGLUT1Δ504-560 including the WAEPE motif sequence. pHluorin-based imaging experiments illustrate substantially impaired VGLUT1 retrieval of the shorter C-terminus truncation construct VGLUT1Δ504-560. To test, whether the SV morphology of a VGLUT1 C-terminus truncation construct is potentially affected as well or, whether abnormal structures occur in the synapses, EM analyses were performed. The SV morphology of neurons expressing the VGLUT1 C-terminus truncated versions was compared with those expressing the VGLUT1 WT rescue and KO neurons.

As expected from previous data (Fremeau et al., 2004; Siksou et al., 2013), the SVs from VGLUT1 KO neurons are significantly smaller compared to vesicles from WT rescued neurons (area: 1± 0.03 in WT resc., 0.86± 0.03 in KO; perimeter: 1± 0.01 in WT rescue, 0.93± 0.01 in KO, fig.27 A, B1 and 28A, B, E). Also the shape of SVs from KO neurons is different. They are less round and look more deformed than VGLUT1 WT rescued vesicles (KO phenotype) (roundness: 1± 0.01 in WT resc., 0.85± 0.01 in KO, fig.27A, B and 28C). Similarly, the SVs from neurons rescued with VGLUT1Δ496-560 are less round compared to vesicles from WT rescued neurons as well (0.91± 0.01 in full C-term trunc., fig.27C and 28C). Instead, the SVs from neurons rescued with the shorter C-terminus truncation version VGLUT1Δ504-560 exhibit a normal WT rescue-like SV shape (area: 1± 0.03 in WT resc, 0.98± 0.04 in shorter C-term trunc.; perimeter: 1± 0.01 in WT resc., 1± 0.02 in shorter C-term trunc.; roundness: 1± 0.01 in WT resc., 0.95± 0.02 in shorter C-term trunc., fig.27D and 28A-C). It can be concluded that the VGLUT1Δ504-560 construct can rescue the VGLUT1 KO phenotype.

A: synapse of a hippocampal VGLUT1 KO neuron expressing VGLUT1 WT rescue

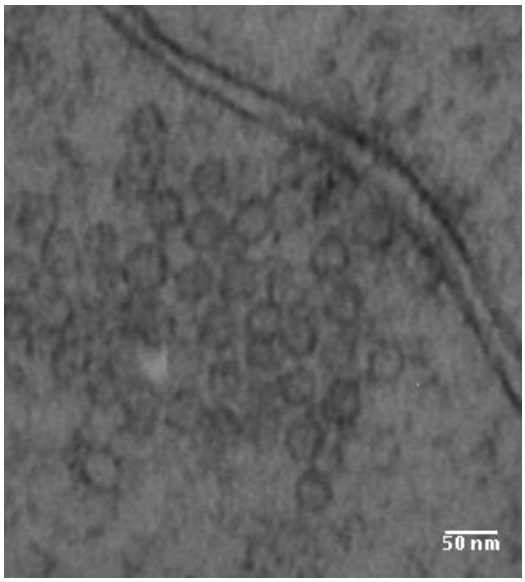

B1: VGLUT1 KO synapse

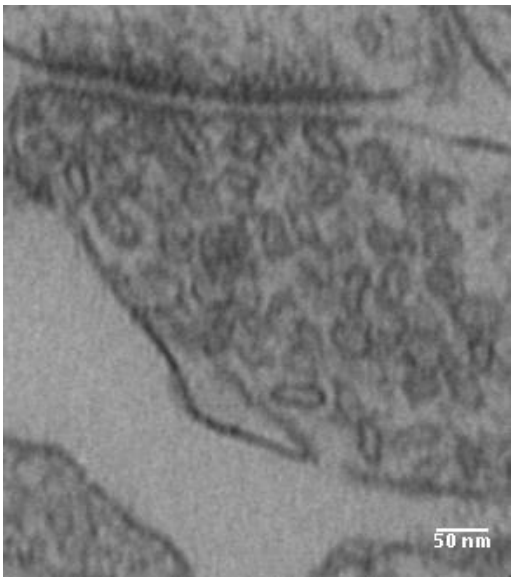

B2: KO synapse with enlarged vesicular structures

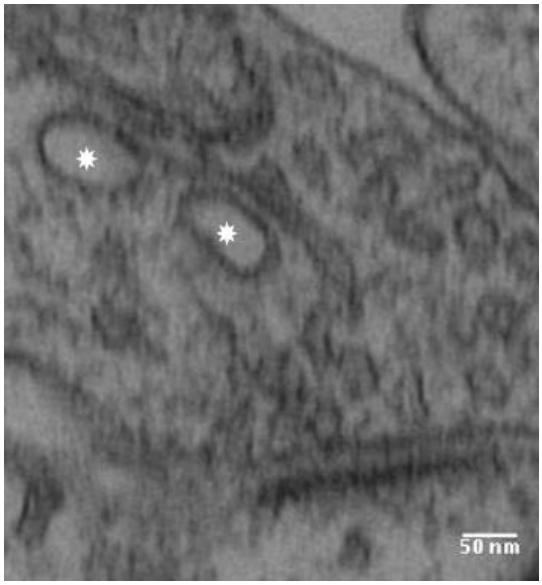

B3: KO synapse with multivesicular bodies

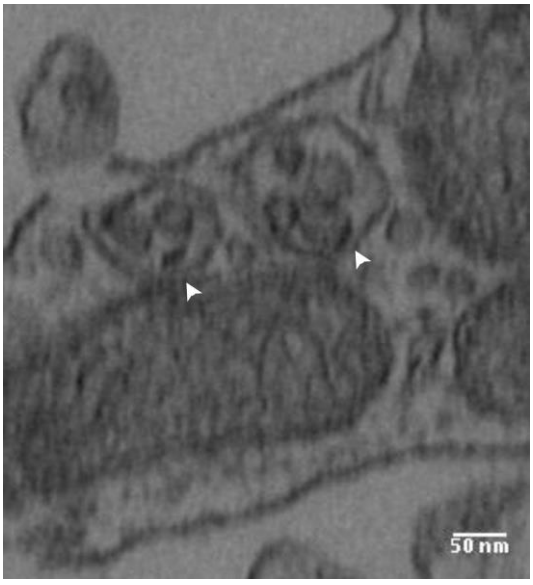

C: synapse of VGLUT1Δ496-560

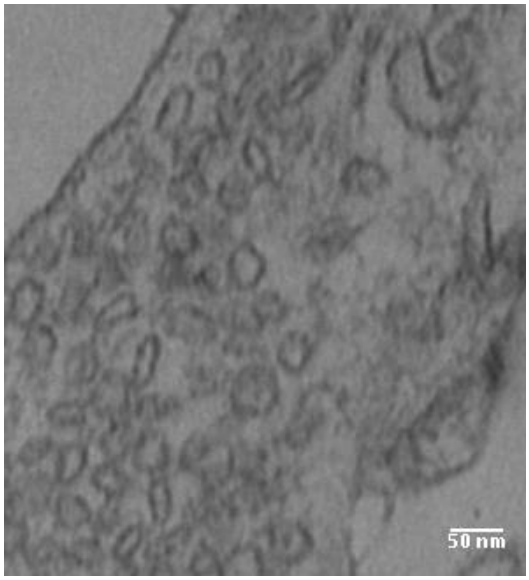

D: synapse of VGLUT1Δ504-560

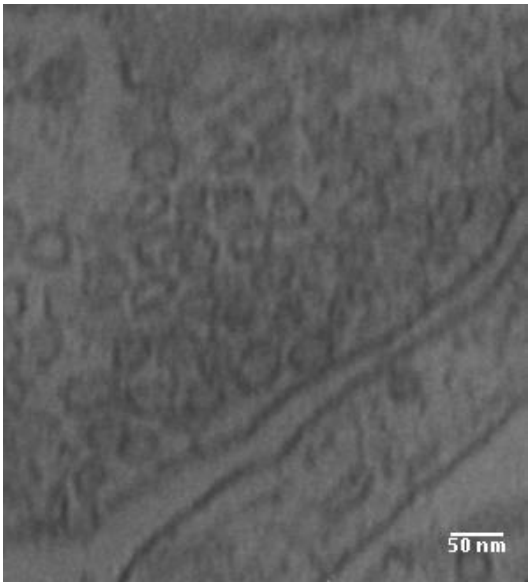

Fig. 27 (A-D): **Example EM images of the SV morphology of different VGLUT1 variants**: for EM analyses hippocampal VGLUT1 KO neurons were lentiviral infected to express different VGLUT1 mutant constructs in comparison with the WT rescue and VGLUT1 KO neurons. Analyses of the shape and number of SVs reveal differences between the WT rescue (A) and VGLUT1 KO (B). SVs from VGLUT1 KO neurons are less round (deformed). Also accumulation of enlarged vesicular structures (white asterisk) and MVB (white arrow) were detected in VGLUT1 KO compared to the WT rescue (B2 and B3). The full C-terminus truncation VGLUT1Δ496-560 shows a KO-like phenotype with less round SVs, whereas the shorter C-terminus truncation VGLUT1Δ504-560 including a WAEPE sequence can rescue the KO phenotype and shows normal round vesicles (magnification about 30,000x).

To investigate the SV density, their number was analyzed in a defined area of a box according to the length of the dark appearing electron dense active zone (cf. fig.9), which includes most likely readily releasable and docked SVs. However, the active zone was sometimes not distinctly visible. Therefore, these images were excluded from the analysis resulting in a smaller sample number of the SV density data compared to the sample number of the other analyzed morphological parameters.

The SV density in the defined area above the active zone is not changed in one of the VGLUT1 C-terminus truncation constructs compared to the WT rescue and VGLUT1 KO neurons (#SV/area above active zone: 1± 0.06 in WT resc., 1.5± 0.12 in shorter C-term trunc., 0.8± 0.05 in full C-term trunc., 1.2± 0.11 in KO, fig.28D). In contrast and similar to previous data (e.g. from Siksou et al., 2013), which reported a significantly decreased number of SVs per entire synapse in VGLUT1 KO neurons, a decrease in the SV density per synapse in KO

neurons is observed in this present study as well (fig.28E). However, the SV density per synapse is not different in the VGLUT1 C-terminus truncation constructs (fig.22E).

The size of vesicular structures in a synapse was quantified as well by classifying them into three groups: diameter <30 nm, 30-50 nm and >50 nm. Apparently, fewer VGLUT1 KO vesicles have a diameter about 30-50 nm and more vesicular structures have a diameter >50 nm compared to the WT rescue (diameter 30-50nm: 84.4± 2.38% in WT resc., 75.2± 4.73% in KO, diameter >50nm: 14.4± 2.1% in WT resc, 20.2± 1.41% in full C-term trunc., fig.28E). There were no changes observed in the diameter of SVs from neurons expressing a VGLUT1 C-terminus truncation construct (fig.28E).

The occurrence of abnormal structures was also investigated in the analyzed groups. There are an increased number of enlarged vesicular structures and supposedly MVBs in the VGLUT1 KO and C-terminus truncation VGLUT1Δ496-560 group, apparent in numerous images (example images, fig.27B2, B3, C). These enlarged vesicular compartments in KO neurons accumulate occasionally in clusters (fig.27B). However, abnormal structures are not detected in VGLUT1Δ504-560-expressing neurons (fig.27D).

In summary, these data also confirm that KO neurons fixed and embedded for EM by the classical protocol have smaller and less round (deformed) SVs with lower density (Fremeau et al., 2004; Siksou et al., 2013). The EM results also reveal a KO-like phenotype of the C-terminus truncation version VGLUT1Δ496-560, where the shape of the SVs looks deformed as well. In contrast, the number and morphology of the SVs of the C-terminus truncation VGLUT1Δ504-560 are not altered, indicating that a few more amino acids including the WAEPE motif sequence can rescue the KO-phenotype to WT rescue levels.

A: vesicle area

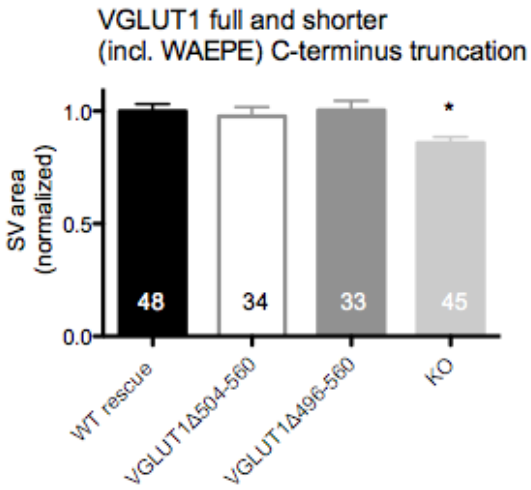

B: vesicle perimeter

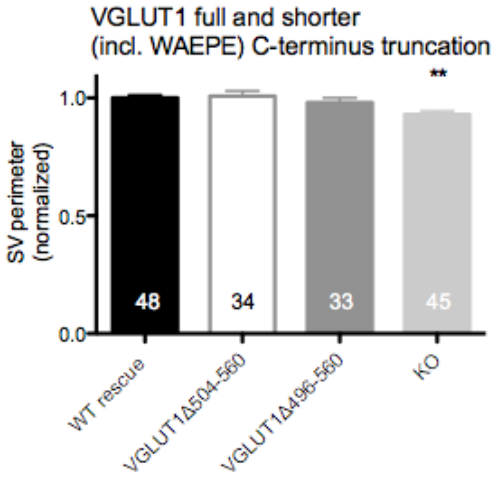

C: vesicle roundness

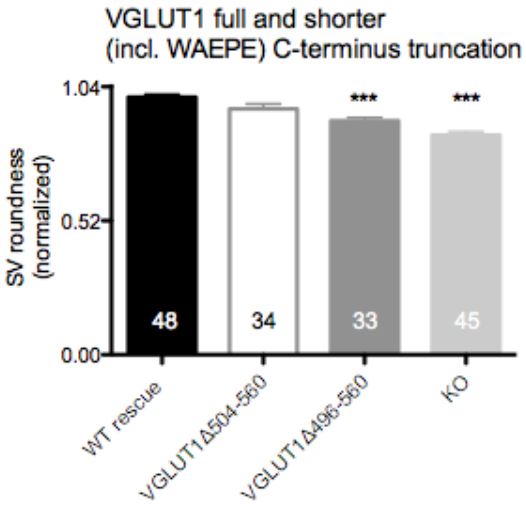

D: vesicle density

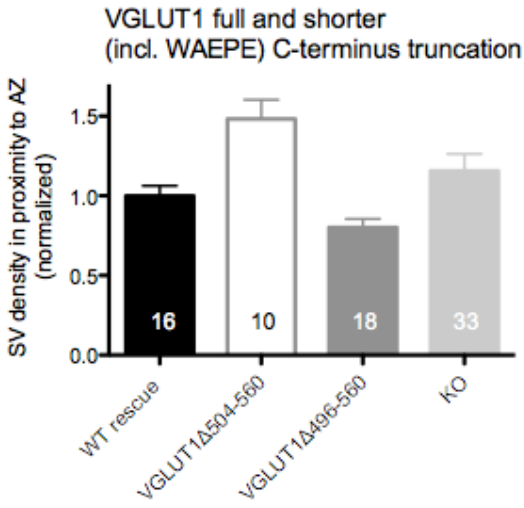

E: grouped vesicle size

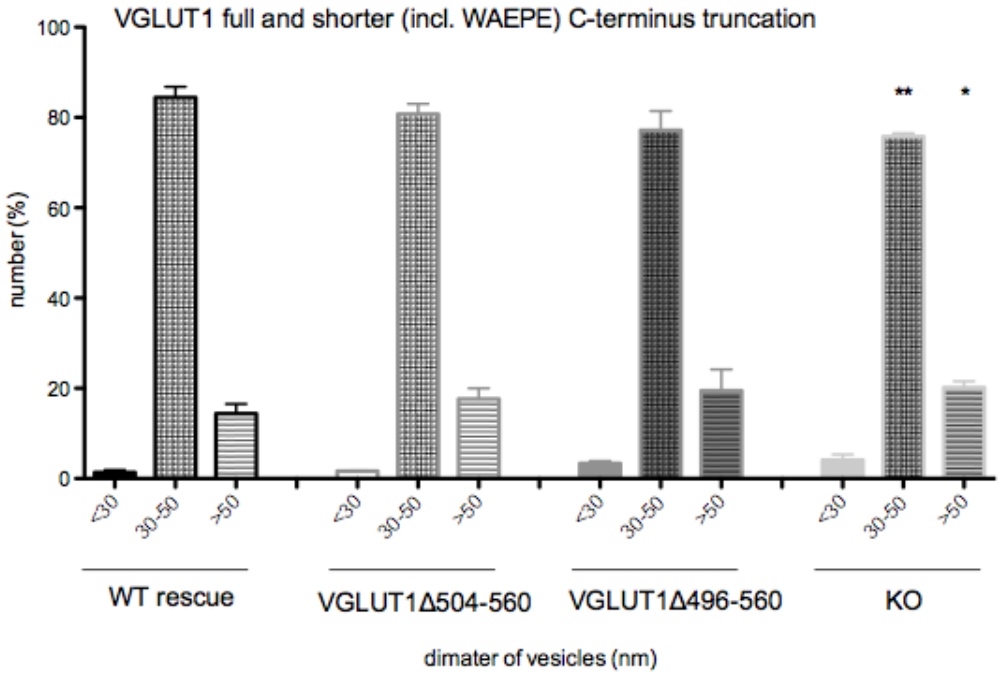

Fig. 28 (A-E): **Morphological quantifications of SVs from VGLUT1 C-terminal truncation constructs by EM in comparison to WT rescue and KO**: for EM image analyses hippocampal VGLUT1 KO neurons were lentiviral infected to express different mutated VGLUT1 constructs. Investigations of the SV shape (area, perimeter, Feret`s diameter, roundness) were done as well as the calculation of the SV density in proximity to the active zone (AZ). The data reveal significant alterations in VGLUT1 KO (light grey) compared to the WT rescue (black). Their SVs are less round (C) and smaller (A and B) similar to results already shown in fig.14. The number of normal sized vesicles (30-50 nm diameter) is also reduced in KO neurons and the number of enlarged vesicular structures (>50 nm) is increased (E). The full C-terminus truncation VGLUT1Δ496-560 (dark grey) shows similar results to the KO. Their SVs have the tendency to be smaller (B), less round (C) and with lower density (D). In contrast, the shorter C-terminus truncation VGLUT1Δ504-560 (dark grey, not filled) including a WAEPE motif does not show differences in the SV shape or number (n number mentioned in the bar graphs, bars indicate mean±SEM, for A-D: One way ANOVA with tukey`s multiple comparison test: * $p<0.05$, ** $p<0.01$, *** $p<0.0001$; fro E: Student`s t-test: * $p<0.05$, ** $p<0.01$).

3.3 Investigations of putative VGLUT1 C-terminal serine phosphorylation sites suggest a modulatory role of S504 in synaptic transmission

For the mouse VGLUT1 C-terminus different phosphorylation sites are predicted by computer software based on its amino acid sequence. There are five serine (S) sites (S504, S519, S522, S540 and S546), two threonine (T) sites (T544 and T547), one tyrosine (Y) site (Y541) and one histidine (H) site (H545) proposed (http://kinasephos2. mbc.nctu.edu.tw), but their relevance for VGLUT1 function in neurotransmission or SV cycling is unknown. Therefore, the focus in the third part of this study is set on the investigation of the four putative serine phosphorylation sites: S504, S519, S522 and S540 (cf. fig.5).

S504 flanks the VGLUT1 C-terminal dileucine-like motif sequence upstream and exists in all three mammalian VGLUTs. S519 and S522 are located in front of the VGLUT1 specific PRD1. A very recent study confirmed VGLUT1 S519 and S522 as phosphorylation sites (Santos et al., 2014). S540 belongs to a VGLUT1 unique SYGAT motif sequence between PRD1 and PRD2.
A previous study has shown that the phosphorylation site D38 in front of the dileucine-like trafficking motif sequence of VGAT plays a role in neurotransmission. A D38A mutation causes higher NT release (Santos et al., 2013). If mutations of putative VGLUT1 phosphorylation sites also cause changes in neurotransmission has not been investigated yet. To study phosphorylation sites it is common to create mutants. Mutating the serine sites to alanine (A), which was done in this research project, prevents potential phosphorylation and consequently mimics permanent dephosphorylation (phosphodeficient mutants). Another option is to mimic permant protein phopshorylation (phosphomimetic mutants).
A complication to study phosphorylation sites is that phosphorylation *in vivo* is a dynamic process and often variable in responses to electrical stimulation or other cellular events. Therefore, phosphorylation site mutants and investigations *in vitro* may or may not be informative about their actual functional role for a certain protein.

Here, the putative VGLUT1 C-terminal serine phosphorylation sites were mutated to alanine and analyzed using whole-cell voltage clamp recordings and phluorin-based imaging as well as EM. Rescue experiments of hippocampal VGLUT1 KO Neurons by lentiviral infection were also performed again. Therefore, constructs of the different putative VGLUT1

C-terminal phosphorylation site mutants were in parallel expressed with a GFP-containing nuclear localization signal (NLS-GFP). The reason was to be able to distinguish virus infected and non infected neurons. The electrophysiological measurements of the VGLUT1 mutants were recorded in different cultures, but always compared to the WT rescue. To combine the data and test them for statistical significance each group per culture was normalized to the respective mean WT rescue values.

3.3.1 The VGLUT1 mutant S504A shows evidence of higher neurotransmitter release

To investigate the physiology of putative VGLUT1 serine phosphorylation site mutants whole-cell voltage clamp recordings were performed.
The VGLUT1 S504A mutant shows higher evoked postsynaptic responses compared to the WT rescue apparent in increased EPSC amplitudes (1± 0.06nA in WT resc., 1.31± 0.1nA in S504A, fig.29A). The RRP of S504A is unchanged (1± 0.05pC in WT resc., 1.05± 0.08pC in S504A, fig.29B), but the calculation of the Pvr illustrates a considerably increase (1± 0.05% in WT resc., 1.25± 0.07% in S504A, fig.29C) according to the increased EPSC results. The PP ratio of S504A is also, as expected, decreased (1± 0.03 in WT resc., 0.93± 0.03 in S504A, fig.29D). Usually an increase in Pvr accompanies with a decrease in PP ratio. A higher NT release is also suggested by analyses of the mEPSC frequencies of S504A, which are in S504A higher than in the WT rescue (1± 0.07Hz in WT resc., 1.29± 0.1Hz in S504A, fig.29I). However, the mEPSC amplitudes of S504A are not changed (1± 0.03pA in WT resc., 1.04± 0.03pA in S504A, fig.29H). The 10 Hz train stimulation data also does not show any differences between S504A and the WT rescue (fig.29E).

In contrast, the VGLUT1 S519A/S522A mutant does not reveal changes in EPSC amplitudes compared to the WT rescue (1± 0.08nA in WT resc., 1.14± 0.12nA in S519A/S522A, fig.29A). The RRP is unchanged as well (1± 0.08pC in WT resc., 0.9± 0.08pC in S519A/S522A, fig.23B). However, the Pvr of S519A/S522A is significantly increased (1± 0.08% in WT resc., 1.25± 0.08% in S519A/S522A, fig.29C), which fits with the finding of a decreased PP ratio of S519A/S522A (1± 0.03 in WT resc., 0.87± 0.03 in S519A/S522A, fig.29D). These data indicate a higher NT release probability, but no confirming changes are found for example in 10 Hz train stimulation data (fig.29F). Furthermore, the mean mEPSC frequency of S519A/S522A (1± 0.12Hz in WT resc., 1.09± 0.15Hz in S519A/S522A, fig.29I)

as well as the mean mEPSC amplitude of S519A/S522A (1± 0.07pA in WT resc., 0.94± 0.06pA in S519A/S522A, fig.23H) show no differences compared to the WT rescue.
Likewise, the VGLUT1 S540A mutant shows no changes in EPSC amplitudes or in the RRP (EPSC amplitude: 1± 0.1nA in WT resc., 1.1± 0.12nA in S540A; RRP: 1± 0.1pC in WT resc., 0.84± 0.2pC in S540A, fig.29A and B). The Pvr of S540A is significantly increased similar to S519A/S522A and the PP ratio also shows a trend towards a lower ratio (Pvr: 1± 0.09% in WT resc., 1.35± 0.11% in S540A; PP ratio: 1± 0.03 in WT resc., 0.89± 0.05 in S540A, fig.29C, D). Different to S519A/S522A, S540A shows a higher depression in the 10 Hz train stimulation (fig.29G), which indicates a higher NT release probability according to the Pvr and PP ratio data. However, the mean mEPSC frequency and amplitude of S540A are not altered (mEPSC frequency: 1± 0.13Hz in WT resc., 0.96± 0.18Hz in S540A; mEPSC amplitude: 1± 0.08pA in WT resc., 0.94± 0.07pA in S540A, fig.29I, H).
Altogether, most consistent changes are seen in VGLUT1 S504A, whereas S519A/S522A and S540A show alterations only in a few analyzed electrophysiological parameters. Therefore, their results are not clear to interpret.

Analyses of ICC data show no differences in protein expression levels of the recorded putative VGLUT1 serine phosphorylation site constructs in comparison to the WT rescue (1± 0.05 in WT resc., 0.96± 0.08 in S504A, 0.87± 0.11 in S519A/S522A, 0.78± 0.09 in S540A, fig.37C, appendix).

A: Evoked postsynaptic responses

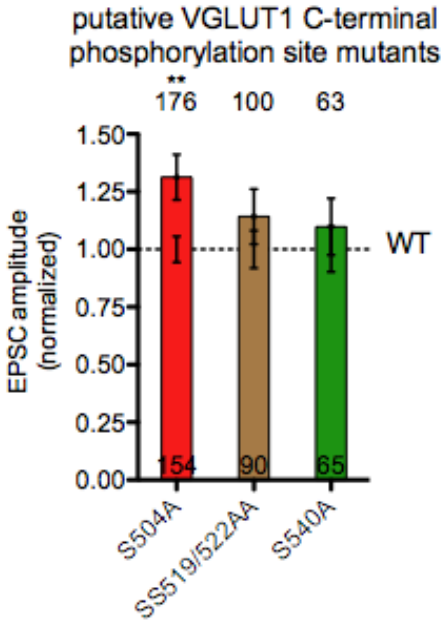

B: Readily releasable pool

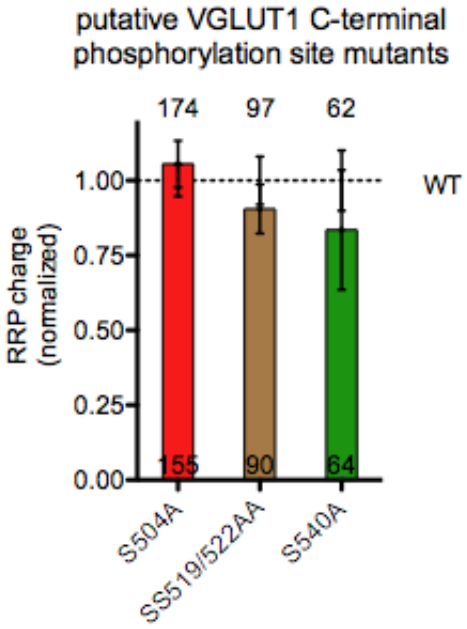

C: Vesicular release probability

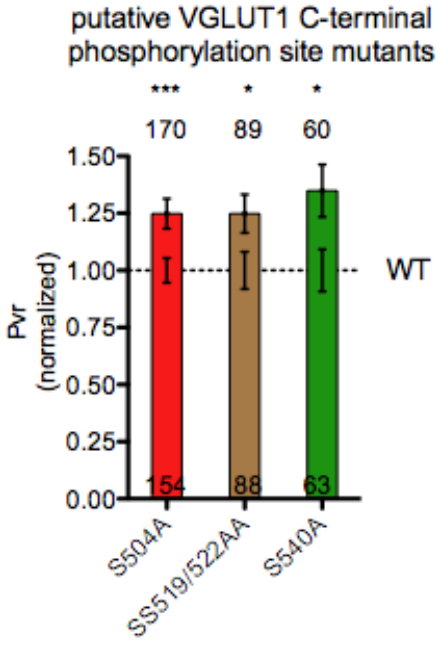

D: Paired pulse ratio

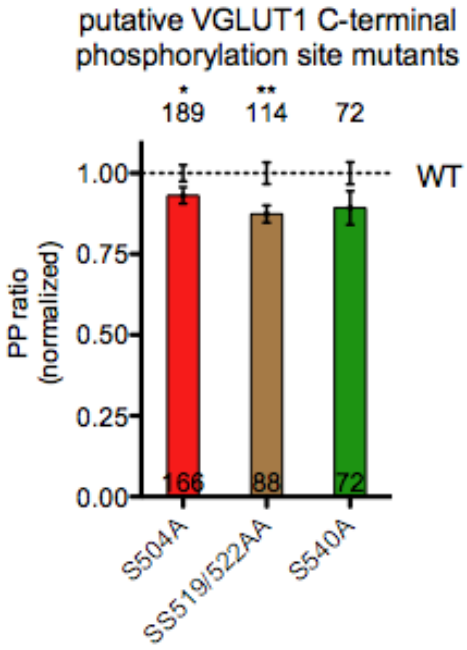

E: 10 Hz train stimulation

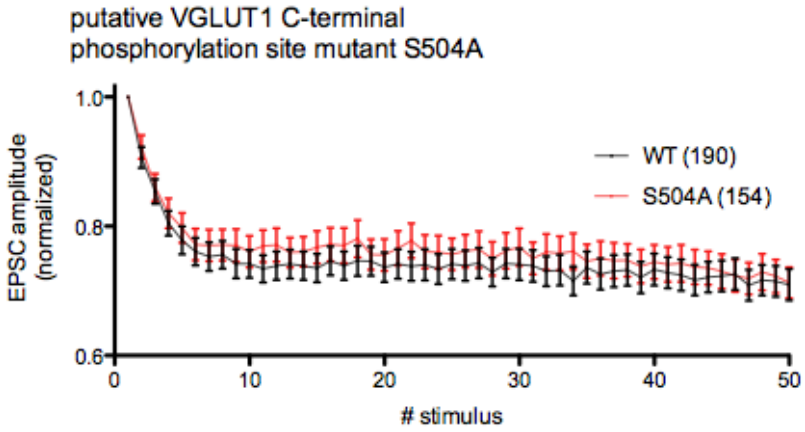

F: 10 Hz train stimulation

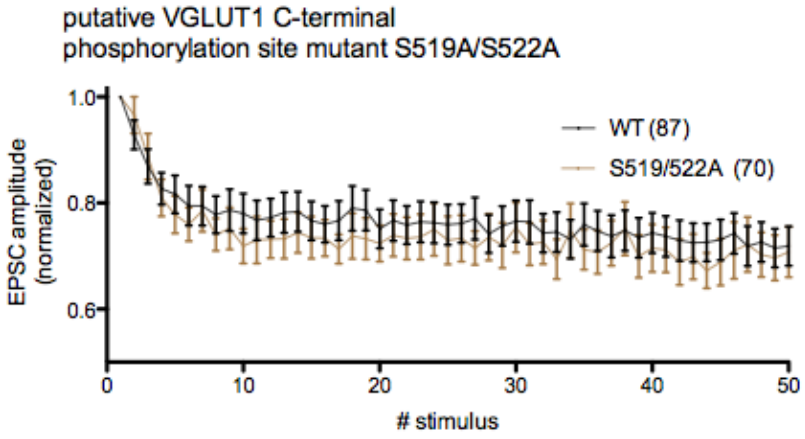

G: 10 Hz train stimulation

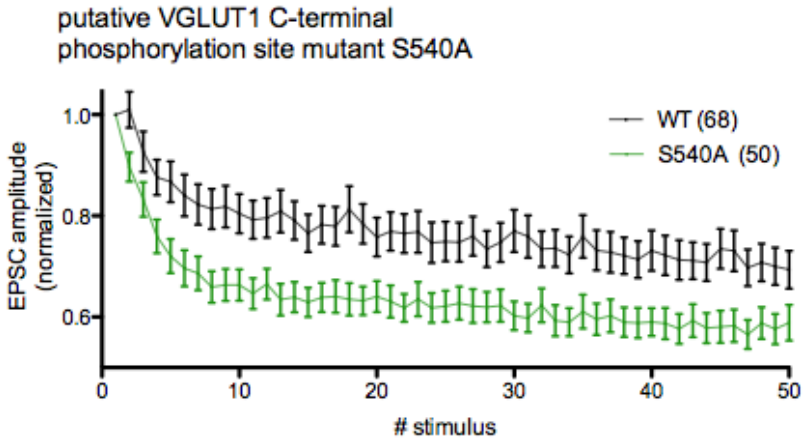

H: spontaneous activity
(mEPSC amplitude)

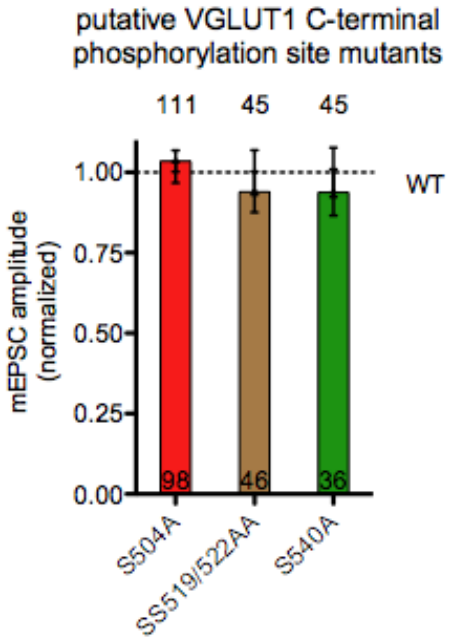

I: spontaneous activity
(mEPSC frequency)

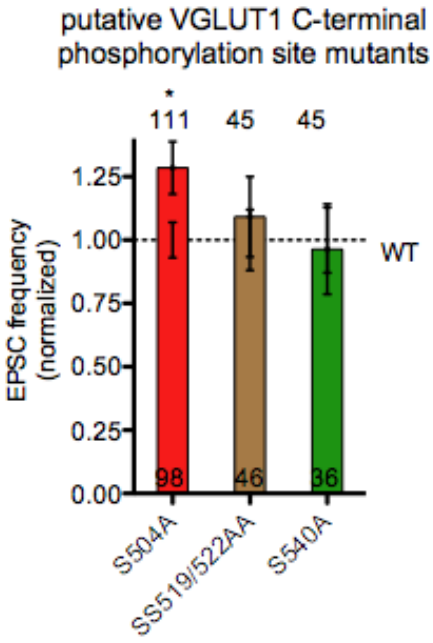

Fig. 29 (A-I): **Electrophysiological characterization of putative C-terminal VGLUT1 serine phosphorylation site mutants:** to investigate the neurotransmission hippocampal VGLUT1 KO neurons were lentiviral infected to express different mutated VGLUT1 constructs. The putative serine phosphorylatione sites mutants S504A (red), S519A/S522A (brown), S540A (green) were compared to the corresponding WT rescue recorded in the same culture. S504A shows significantly increased EPSC amplitudes (A). The RRP is changed in none of the recorded groups (B), but the Pvr is higher in all the recorded groups (C). The PP ratio is also decreased in all groups, whereat not significantly in S540A (D). The 10 Hz train stimulation data of S504A and S519A/S522A show no differences to the WT rescue (E and F). In S540A the 10 Hz train stimulation data results in a higher depression than the WT rescue (G). The mean mEPSC amplitudes show no changes in any of the recorded groups (H). The mean mEPSC frequency is increased in S504A, but not changes in S519A/S522A and S540A (I) (normalized to WT rescue=1, n number marked in the bargraphs, bars indicate mean±SEM, Student`s t test: *<0.05, ** p<0.001, ***p<0.0001).

3.3.2 Different to S504A a VGLUT1 S504E mutation does not lead to changes in neurotransmitter release

Most changes are seen in the VGLUT1 S504A mutant by analyzing electrophysiological parameters in comparison to the WT rescue. The EPSC amplitude, mEPSC frequency and Pvr of S504A are increased. The PP ratio of S504A is reduced. Altogether, the results suggest an increased NT release. Therefore, to determine, whether a phosphomimic form of VGLUT1 S504 might lead to an opposite effect of a higher NT release seen in the S504A mutant, a S504E mutation was also investigated. For this, the VGLUT1 S504E mutant was directly compared to the VGLUT1 S504A mutant and the VGLUT1 WT rescue control group.

The S504E mutant does not show clear differences to the WT rescue in any investigated parameter (fig.30). The EPSC amplitudes of S504E are slightly increased, but not significantly different in comparison with S504A and the WT rescue (3.8± 0.4nA in WT resc., 3.8± 0.6nA in S504A, 5± 0.9nA in S504E, fig.30A). The RRP of S504E is not different as well (751.4± 99.3pC in WT resc., 661.5± 184.8pC in S504A, 749.8± 147.8pC in S504E, fig.30B). The Pvr of S504E shows no changes compared to the WT rescue, whereas the Pvr of S504A is slightly increased similar to the results as described before (fig.29C) (4.6± 0.7% in WT resc., 6± 0.9% in S504A, 4.6± 0.4% in S504E, fig.30C). The PP ratio is by trend smaller in both recorded groups, S504A and S504E (1.34± 0.06 in WT resc., 1.24± 0.08 in S504A, 1.24± 0.05 in S504E, fig.30D). The mEPSC amplitude and frequency are also not significantly different in S504E compared to the WT rescue (fig.30F, G). The mEPSC frequency of S504A is, as expected, slightly increased compared to the WT rescue. The mEPSC amplitude of S504A is unchanged (mEPSC amplitude: 26.8± 1.5pA in WT resc., 27.8± 3pA in S504A, 31.3± 3.4pA in S504E; mEPSC frequency: 3.4± 0.5Hz in WT resc., 6± 1.4Hz in S504A, 4.6± 1Hz in S504E, fig.30F, G). The differences in the Pvr and mEPSC frequency of S504A compared to the WT rescue are not significant in this experiment as described before (fig.29), which might be due the lower sample number in this experiment. Small effects of changes in NT release are easier to detect with an increased sample number.
ICC data of S504A and S504E show no changes in protein expression levels in comparison to the WT rescue (fig.37D, appendix).
Altogether, a VGLUT1 S504 mutation to S504E does not lead to changes in NT release. However, no alterations of the investigated electrophysiological parameters of S504E in comparison to S504A and the WT recue *in vitro* do not mean that there might be no effects

in vivo as well. The influence, for instance of electrical stimulation on protein phosphorylation or by other cellular events was not investigated in this study. Therefore, to draw conclusions about a potential functional role of mutated VGLUT1 S504 by mimicking different phosphorylation states is difficult.

For the other proposed VGLUT1 serine phosphorylation sites S519/S522 and S540 no phosphomimetic analyses, mutating the S to E, were performed.

In summary, the results of both experiments (fig.29 and 30) suggest that dephosphorylation of VGLUT1 S504, mimict by a S504A mutation, seems to play a role in regulating NT release. However, permanent phosphorylation of S504, mimict by a S504E mutation, seems to have no effect on the neurotransmission.
VGLUT1 S519A/S522A as well as S540A show only inconsistent effects on neurotransmission and seem to be not primarily relevant for VGLUT1 protein function.

A: Evoked postsynaptic responses

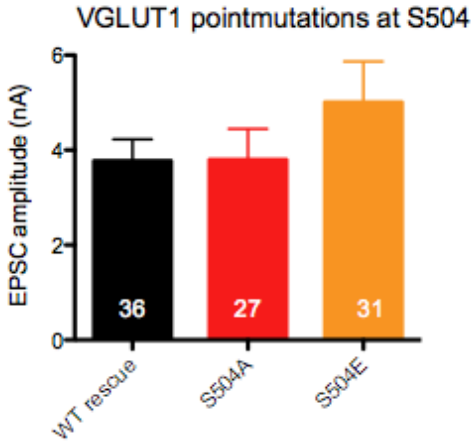

B: Readily releasable pool

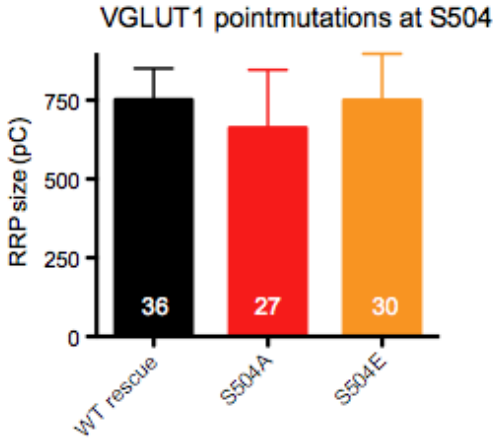

C: Vesicular release probability

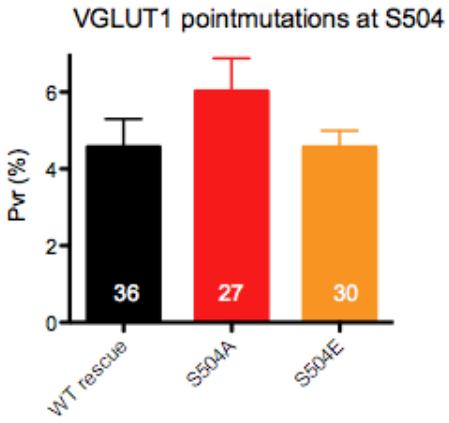

D: Paired pulse ratio

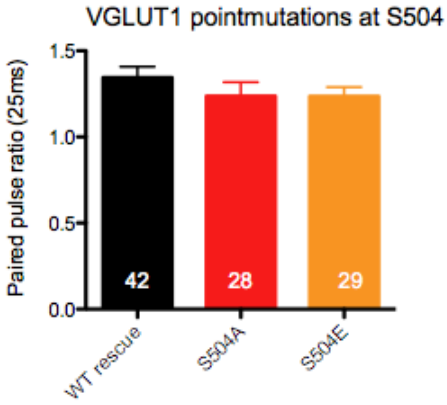

E: 10 Hz train stimulation

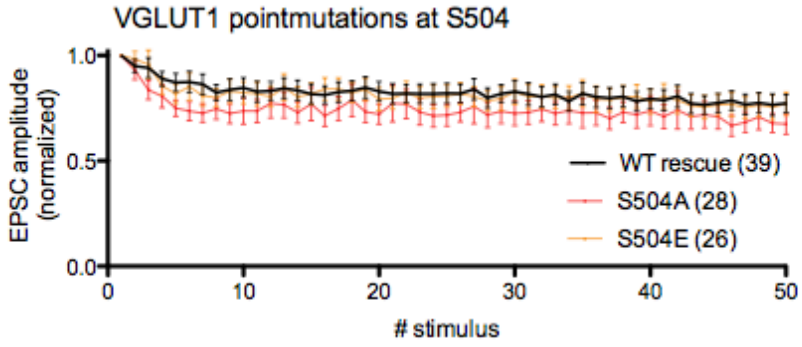

F: spontaneous activity (mEPSC amplitude)

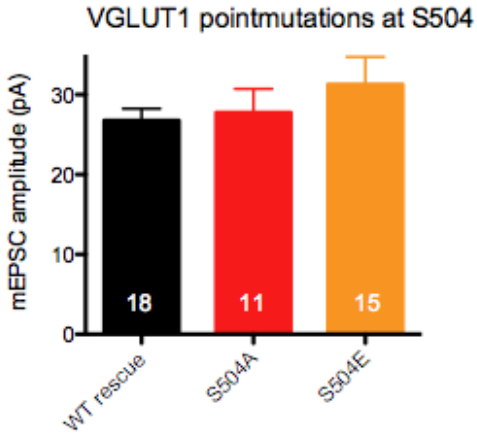

G: spontaneous activity (mEPSC frequency)

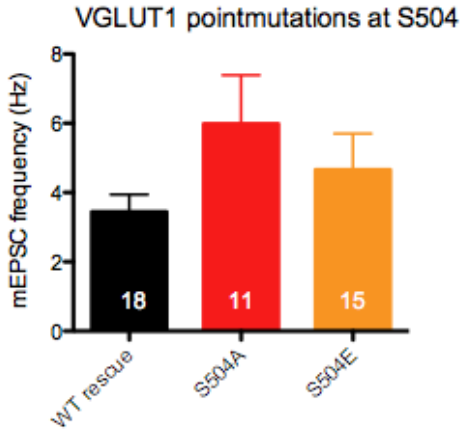

Fig. 30 (A-E): **Direct comparison of the C-terminal VGLUT1 mutants S504A and S504E with WT rescue:** the putative VGLUT1 serine phosphorylation site S504 was in more detail investigated. Therefore, phosphorylation site mutants of S504 were generated by replacing S with A and S with E to mimic permanent dephosphorylation or phosphorylation. No significantly different effects on neurotransmission could be detected between S504A (red) and S504E (orange) in comparison to the WT rescue (black). The EPSC amplitudes (A) as well as the RRP (B) of S504A and S504E are not changed. The Pvr of S504A is by trend increased, which was already described in fig.29C. In contrast, the Pvr of S504E is not different (C) compared to the WT rescue. The PP ratio of both, S504A and S504E, show only a slight decrease (D). The 10 Hz train stimulation data reveal no differences between the recorded groups (E). The mEPSC amplitude is also not changed (F), whereas the mEPSC frequency of S504A shows the tendency to be increased (cf. fig. 29H). The mEPSC frequency of S504E is not different to the WT rescue (G) (n numbers correspond to 2 cell cultures, bars indicate mean±SEM, One way ANOVA with tukey`s multiple comparison test).

3.3.3 Putative C-terminal VGLUT1 serine phosphorylation site mutants show no changes in synaptic vesicle cycling

To further study the properties of the putative VGLUT1 C-terminal phosphorylation site mutants S504A, S519A/522A and S540A pHluorin-based imaging experiments were performed again to monitor potential changes in VGLUT1 cycling. Therefore, pHluorin-tagged constructs of those putative VGLUT1 phosphorylation site mutants were created and expressed in lentiviral infected hippocampal VGLUT1 KO neurons. For control, the different putative phosphorylation site mutants were compared with a VGLUT1 WT rescue and FV510/511AA-pHluorin construct similar to the pHluorin-based experiments before. The same stimulation protocol with 5 Hz, 300AP train stimulation was also used.

None of the putative VGLUT1 C-terminal phosphorylation site mutants show changes in VGLUT1 recycling, analyzing the pHluorin fluorescence decline after 300AP train stimulation (fig.31A). As illustrated before, FV510/511AA shows a slower fluorescence decline compared to WT rescue apparent in the investigated decay time by single exponential fit and the pHluorin fluorescence values 125 s post stimulus (exponential fit (τ): 16.38± 0.07s in WT resc., 11± 0.16s in S504A, 22.47± 0.07s in S519A/S522A, 17.85± 0.002s in S540A; t_{150s} $\Delta F/F_0$: 0.15 in WT resc., 0.2 in S504A, 0.1 in S519A/S522A, 0.1 in S540A, 0.35 in FV510/511AA, fig.31A). The rise time of the to the pHluorin fluorescence peak normalized traces was also investigated by a single exponential fit. The rise time is slower in S519A/S522A compared to WT rescue and even slower in FV510/511AA, but not different in the other investigated putative C-terminal VGLUT1 serine phosphorylation sites (exponential fit (τ): 9.34± 0.99s in WT resc., 7.91± 0.97s in S504A, 13.32± 0.97s in S519A/S522A,

8.62± 0.98s in S540A, 18.89± 1.03s in FV510/511AA; t_{50s} $\Delta F/F_0$: 0.6 in WT resc., 0.6 in S504A, 0.7 in S519A/S522A, 0.6 in S540A, 0.9 in FV510/511AA, fig.31A).

Observing the pHluorin fluorescence increase after 300AP stimulation normalized to the fluorescence maximum after NH_4Cl-containing solution application reveals a trend towards a higher peak fluorescence for the FV510/511AA mutant compared to the WT rescue (0.18a.u. in WT resc., 0.2a.u. in S504A, 0.16a.u. in S519A/S522A, 0.15a.u. in S540A, 0.21a.u. in FV510/511AA, fig.31B). This might reflect a difference in the balance of VGLUT1 exo- and endocytosis, meaning that more VGLUT1 pHluorin-tagged SVs are released during electrical stimulation. The S504A mutant also shows a by trend higher peak fluorescence (fig.31B). A change in neurotransmission was already clear after investigating the electrophysiology of the S504A mutant by whole-cell voltage clamp, where the NT release is significantly higher (fig.29A, C, I). The mutants SS519/522AA and S540A show a by trend little lower pHluorin peak fluorescence (fig.31B).

The calculated surface expression is only higher in the FV510/511AA mutant, as expected from previous data (fig.10D and 25C and Voglmaier et al., 2006; Foss et al., 2013). The putative VGLUT1 C-terminal serine phosphorylation site mutants show no changes in their surface expression (1± 0.1% in WT resc., 1.26± 0.16% in S504A, 1.24± 0.11% in S519A/S522A, 1.1± 0.19% in S540A, 1.51± 0.12% in FV510/511AA, fig.31C). The total amount of pHluorin molecules in the synapses of S504A is slightly, but not significantly lower compared to WT rescue, but not different in FV510/511AA or the other phosphorylation site mutants (1± 0.08 in WT resc., 0.61± 0.06 in S504A, 1.11± 0.21 in S519A/S522A, 1.2± 0.15 in S540A, 1.03± 0.17 in FV510/511AA, fig.31D). However, this lower pHluorin expression in S504A does not lead to changes in VGLUT1 retrieval.

A: Fluorescence changes normalized to the peak of 300AP stimulation

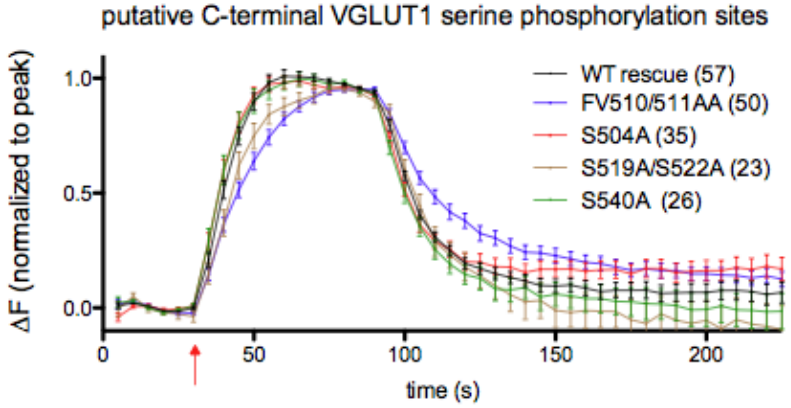

B: Fluorescence changes normalized to the peak of NH_4Cl-induced fluorescence

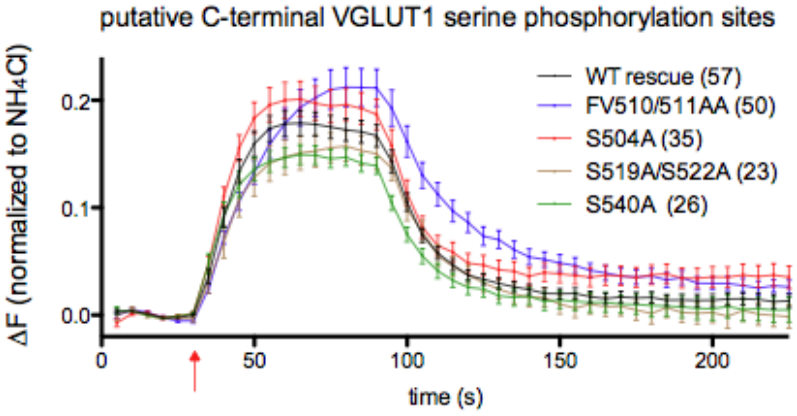

C: Surface expression

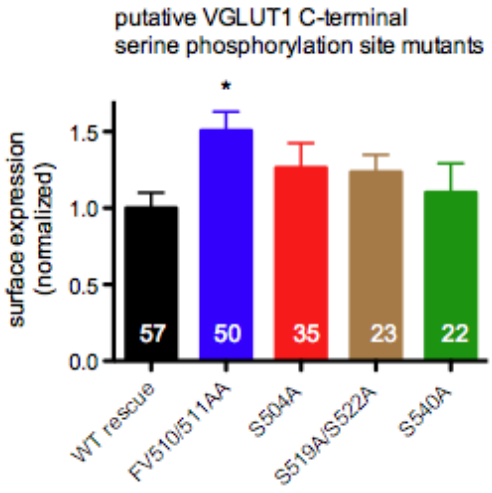

D: Total pHluorin expression

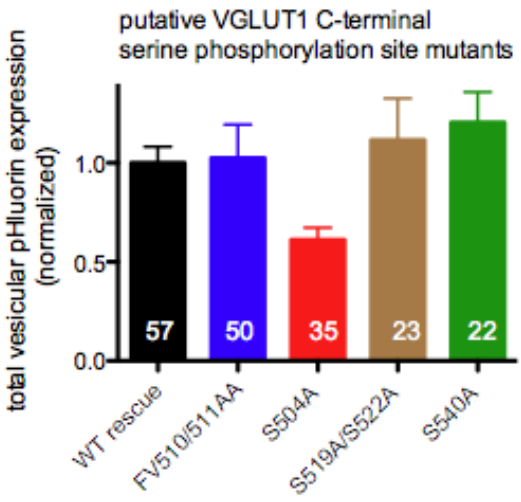

Fig. 31 (A-D): **pHluorin-based VGLUT1 cycling analysis of putative C-terminal VGLUT1 serine phosphorylation site mutants:** to monitor pHluroin fluorescence changes after electrical stimulation (5 Hz, 300AP, start red arrow) of the putative serine phosphorylation site mutants S504A (red), S519A/S522A (brown) and S540A (brown) hippocampal VGLUT1 KO neurons were lentiviral infected to express different pHluorin-based VGLUT1 mutant constructs. The data were normalized to either the pHluorin peak fluorescence during the 300AP train stimulation (A) or the peak fluorescence during application of NH_4Cl-containing solution, which reflects the total amount of VGLUT1 pHluorin-tagged molecules (B). The endocytosis phase with VGLUT1 retrieval is not different in any of the recorded putative VGLUT1 C-terminal serine phosphorylation site mutants compared to the WT rescue (black) and FV510/511AA mutant (blue). FV510/511AA shows, as expected, a slower VGLUT1 recycling. (A). The rise time during 300AP stimulation is slower in FV510/511AA as well as in S519A/S522A (A). S504A and FV510/511AA show a by trend higher NT release apparent in a higher peak fluorescence in the traces normalized to the peak fluorescence during NH_4Cl-containing solution application (B). This peak fluorescence is by trend lower in S519A/S522A and S540A (B). FV510/511AA has a higher surface expression, whereas the putative VGLUT1 serine phosphorylation site mutants show no differences in their surface expression (C). The total expression of pHluorin molecules is lower in S504A compared to the WT rescue, but not different in the other mutants (D) (n numbers marked in the figure legend/bar graphs, bars indicate mean±SEM, One way ANOVA with tukey`s multiple comparison test: * $p<0.05$).

The EPSC amplitudes during 5 Hz, 300AP train stimulation of the pHluorin-based imaging experiment were also analyzed. There are no differences between the recorded groups during the train stimulation compared to WT rescue (fig.32A). The traces illustrate again that small EPSCs are still detectable after 300AP stimulation in all of the recorded groups, which means that the SV pool is not completely depleted during the 300AP stimulation. Before starting the pHluorin-based imaging protocol postsynaptic currents were recorded. Thereby, the AP-evoked EPSCs and the PP ratio could be determined. The EPSC amplitudes of S519A/S522A and S540A, normalized per cell culture, are not significantly different compared to the WT rescue and FV510/511AA mutant, whereas the normalized EPSCs of S504A are by trend higher as reported before (1± 0.08 in WT resc., 1.3± 0.13 in S504A, 0.93± 0.16 in S519A/S522A, 1.1± 0.24 in S540A, 1.12± 0.09 in FV510/511AA, fig.32B and cf. 29A). The analyzed PP ratio of the putative VGLUT1 serine phosphorylation site mutants are also not significantly different. Only the PP ratio of S504A is again slightly decreased compared to the WT rescue (1.19± 0.03 in WT resc., 1.14± 0.03 in S504A, 1.28 ± 0.08 in S519A/S522A, 1.23± 0.05 in S540A, 1.13± 0.03 in FV510/511AA, fig.32C).

In summary, the putative VGLUT1 C-terminus serine phosphorylation site mutants do not show alterations in VGLUT1 recycling. The physiology, also tested during the pHluorin-based imaging experiments, is not significantly different in any of the putative serine phosphorylation sites as well. Only S504A shows a by trend higher NT release as already reported before in pure whole-cell voltage-clamp experiments. However, these data

demonstrate again that the VGLUT1 FV510/511AA mutant slows the VGLUT1 recycling compared to the WT rescue, which in turn seems to slow the rise time of the pHluorin fluorescence during 300AP stimulation as well. The surface expression is also increased in FV510/511AA in this experiments.

A: EPSCs during 5 Hz, 300AP train stimulation

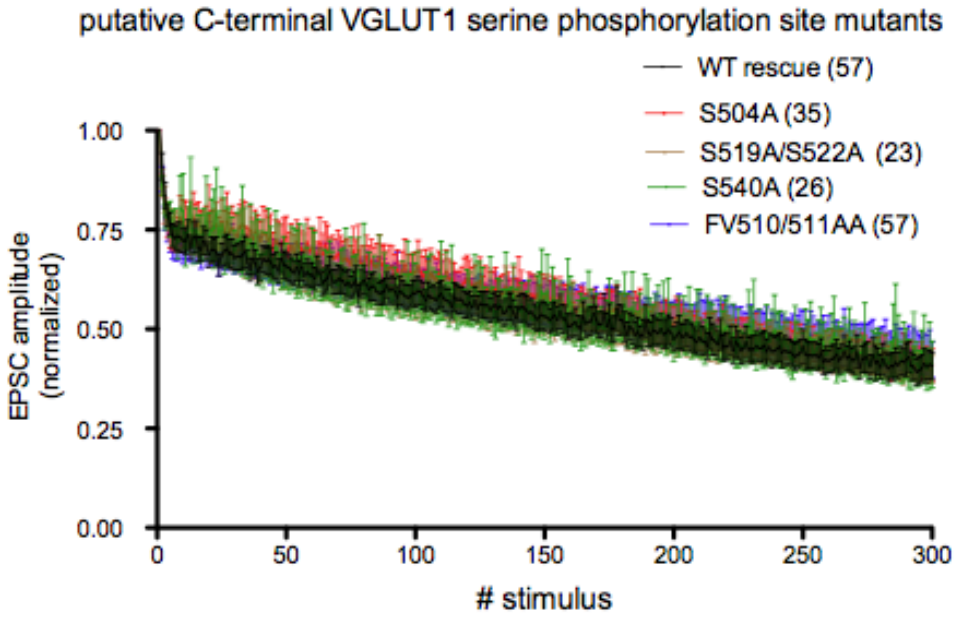

B: Evoked postsynaptic Responses

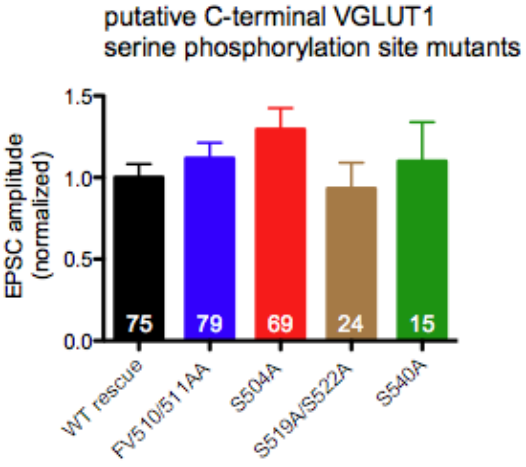

C: Paired pulse ratio

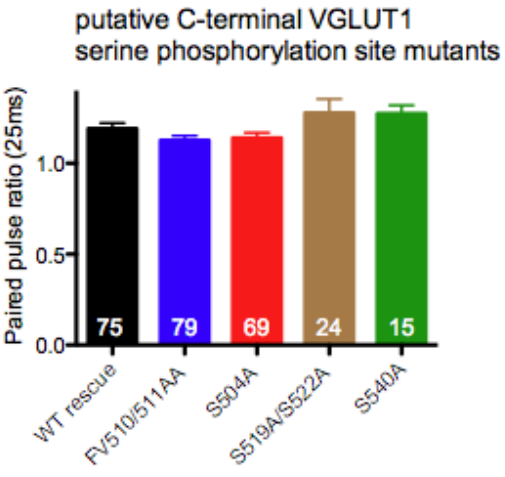

Fig. 32 (A-C): **Analysis of NT release parameters of putative VGLUT1 C-terminal serine phosphorylation site mutants during pHluorin-based imaging experiments in comparison to WT rescue and FV510/511AA mutant:** before and during pHluorin-based imaging experiments the neurotransmission of the putative VGLUT1 serine phosphorylation site mutants was investigated as well. Therefore, hippocampal VGLUT1 KO neurons were lentiviral infected to express different putative VGLUT1 serine phosphorylation site mutant constructs in comparison with the WT rescue and FV510/511AA. EPSC amplitudes recorded during the 5 Hz, 300AP stimulation were displayed normalized to the first EPSC (A). Between the putative serine phosphorylation site mutants S504A (red), S519A/S522A (brown), S540A (green) and the WT rescue (black) as well as the FV510/511AA mutant (blue) no differences in NT release were detected (A). Before the imaging protocol started the EPSC amplitudes and PP ratio of each recoeded group was analyzed as well (B and C). There are no significant changes between the putative phosphorylation site mutants, the WT rescue and FV510/511AA. S504A shows, as expected, the tendency towards a higher NT release, reflected in higher EPSC amplitudes, and a lower PP ratio (B and C) (n numbers marked in the traces/bargraphs, bars indicate mean±SEM, One way ANOVA with tukey`s multiple comparison test).

3.3.4 The putative C-terminal VGLUT1 serine phosphorylation site mutants show no changes in synaptic vesicle morphology and density

EM images were quantified to examine, whether mutations of the putative VGLUT1 serine phosphorylation site mutants from S to A cause changes in the SV appearance.

The quantifications show no differences between VGLUT1 S504A, SS519/522AA or S540A mutants in comparison to the WT rescue. Analyzed was the SV area, roundness and density (area: 1± 0.04 in WT resc., 1.14± 0.03 in S504A; 0.98± 0.03 in S519A/S522A, 0.96± 0.03 in S540A, 0.85± 0.02 in KO; perimeter: 1± 0.03 in WT resc.,1.07± 0.01 in S504A, 1.06± 0.02 in S519A/S522A, 1.01± 0.02 in S540A, 0.96± 0.01 in KO; roundness: 1± 0.01 in WT resc., 1± 0.01 in S504A, 0.97± 0.02 in S519A/S522A, 0.98± 0.01 in S540A, 0.85± 0.01 in KO; density (#SV/area above active zone): 1± 0.04 in WT resc., 1.08± 0.08 in S504A, 0.93 in S519A/S522A, 1.09± 0.09 in S540A, 1.05± 0.09 in KO, fig.33A-C). Synapses from the VGLUT1 KO group show as described before (cf. fig.14, 27 and 28) smaller sizes and less round SVs (fig.33C, E). The number of SV with a diameter of 30-50nm from KO neurons is reduced as well (84.5± 2.38% in WT, 75.8± 0.08% in KO fig.33E). The number of larger vesicular structures (>50nm) are increased in KO neurons (14.4± 2.1% in WT, 20.2± 1.42% in KO, fig.33E). The putative VGLUT1 phosphorylation site mutants show no differences in the analyzed SV diameters compared to WT rescue (fig.33E).

Altogether, the data suggest that phosphodeficient putative VGLUT1 C-terminus serine sites have no effect on SV morphology and density.

A: vesicle area

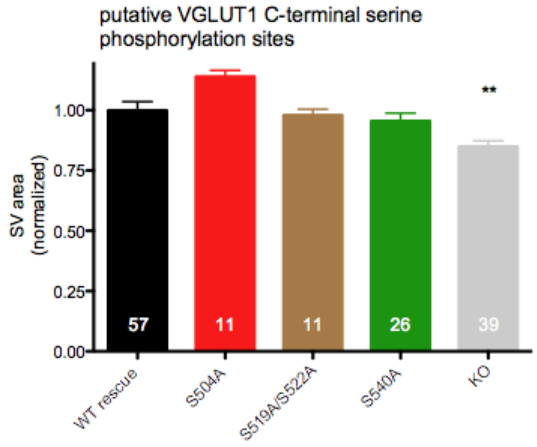

B: vesicle perimeter

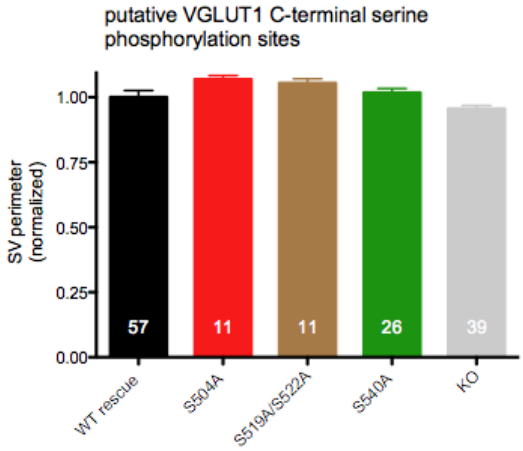

C: vesicle roundness

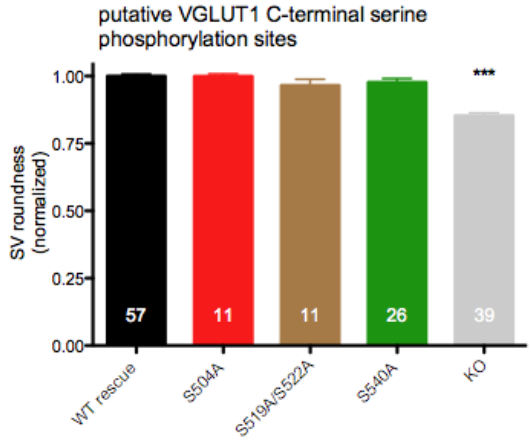

D: vesicle density

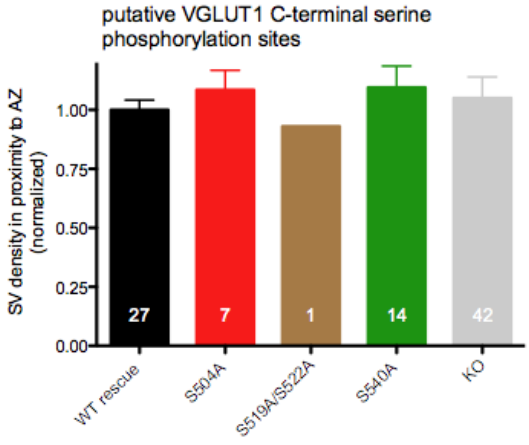

E: grouped vesicle size

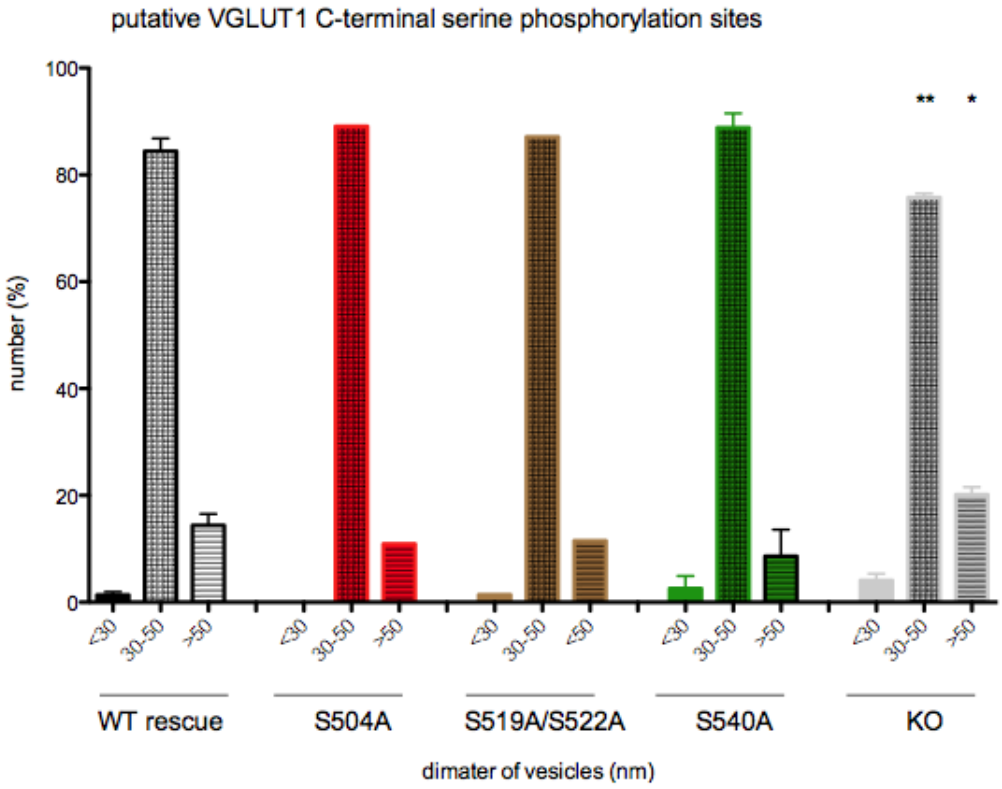

Fig. 33 (A-E): **Morphological quantification of SVs from putative VGLUT1 C-terminal serine phosphorylation sites by EM**: for EM analyses VGLUT1 KO neurons were lentiviral infected to express different putative VGLUT1 serine phosphorylation site constructs (S504A (red), S519A/S522A (brown) and S540A (green)). Quantifications of the SV shape (area, perimeter, Feret`s diameter, roundness) and vesicle density in proximity to the active zone (AZ) do not show changes in the different putative VGLUT1 serine phosphorylation site mutants compared to WT rescue (black). Significant alterations of the SV morphology are seen, as expected, in VGLUT1 KO (light grey). The SVs of KO neurons are less round (C) and smaller (B). The number of normal sized vesicles (30-50nm diameter) is reduced in KO (E). The number of enlarged vesicular structures (>50nm) is increased in KO (E) (n number mentioned in the bar graphs, bars indicate mean±SEM, for A-D: One way ANOVA with tukey`s multiple comparison test: **p<0.01, ***p>0.001; for E: Student`s t-test: * p<0.05, **p<0.01).

4. Discussion

VGLUTs are essential for the formation of glutamate-filled SVs to maintain their supply for reliable SV exocytosis in excitatory neurons. Therefore, VGLUTs needs to be efficiently and correctly targeted to SVs during vesicle recycling.

Previous studies showed the importance of a C-terminal FV motif for mammalian VGLUT1 trafficking. This VGLUT1 FV motif is part of a conserved C-terminal dileucine-like motif sequence and neurons expressing mutant variants showed significantly slower VGLUT1 recycling (Foss et al., 2013; Voglmaier et al., 2006). However, potential consequences for the neurotransmission of decelerated VGLUT1 retrieval by FV motif mutations were never tested. Therefore, the main focus of attention in the present study was the further investigation of the VGLUT1 C-terminus by studying the effects of mutations in the dileucine-like motif sequence E_{505}EKCGFV_{511}, but also the impact of a complete VGLUT1 C-terminus deletion in synaptic function.

To gain more insights in the functionality of the VGLUT1 C-terminus the software-predicted putative serine phosphorylation sites S504, S519, S522 and S540 were also investigated. A recent study confirmed that S519 and S522 play a role in VGLUT1 phosphorylation (Santos et al., 2014), but their relevance for VGLUT1 function was not investigated.

Therefore, mammalian autaptic VGLUT1 KO neurons were lentiviral infected to express either VGLUT mutant or a WT-restoring construct and whole-cell voltage clamp recordings were performed in combination with pHluorin-based imaging to study electrophysiological properties and VGLUT cycling. To investigate potential changes in the SV morphology of VGLUT1 C-terminus mutants EM was performed as well.

4.1 Slower VGLUT1 recycling by mutated C-terminal dileucine-like motif seuquence does not affect neurotransmission

Whether slower VGLUT1 recycling affects the efficiency of NT release, was investigated by mutating the VGLUT1 C-terminal dileucine-like motif sequence E_{505}EKCGFV_{511}.

First, the VGLUT1 recycling of mutated $F_{510}V_{511}$ was tested. The fluorescence recovery after electrical stimulation of FV510/511AA-pHluorin is slower compared to the WT rescue and results in higher surface expression similar to previous studies (Voglmaier et al., 2006, Foss et al., 2013). However, the VGLUT1 recycling of FV510/511AA is not slowed to the same extent as reported before. An explanation might be the different species and culture system

that was used in this study and the different way to stimulate the neurons. In this study autaptic neurons from mice were used allowing a well controlled, direct whole-cell stimulation, but achieving the synapses from only one single neuron. In contrast, Voglmaier et al., 2006 and Foss et al., 2013 used mass cultured neurons from rats and field stimulation that achieves a stimulation of a big fraction of neurons. Thereby, many SVs from different kinds of neurons, a mixture of excitatory and inhibitory ones, are released at the same time. Furthermore, in this study VGLUT1 KO neurons were used with lentiviral induced protein rescue instead of overexpression of different VGLUT constructs in VGLUT1 WT background (Voglmaier et al., 2006, Foss et al., 2013).

Besides the mutation of the FV motif, a deletion of the $S_{504}EEK_{507}$ motif sequence, which is also part of the VGLUT1 C-terminal dileucine-like motif sequence, was investigated as well. The $S_{504}EEK_{507}$ motif exists with a minor difference in VGLUT3 in all three mammalian VGLUT isoforms (cf. fig.5). The $S_{504}EEK_{507}$ deletion-pHluorin construct does not show changes in the surface expression (fig.30C), but a slightly slower VGLUT1 recycling similar to FV510/511AA-pHluorin (fig.30A). These data suggest that not only the FV motif, but rather the entire VGLUT1 dileucine-like motif sequence is important for VGLUT1 recycling.

Interestingly, further investigations and electrophysiology data show that the neurotransmission is not likewise altered, when the VGLUT1 retrieval is slowed by mutations in the VGLUT1 C-terminal dileucine-like motif sequence. Evoked and spontaneous postsynaptic responses of VGLUT1 C-terminus FV510/511AA and $S_{504}EEK_{507}$ deletion-expressing neurons reveal no changes in comparison to WT rescue-expressing cells. Likewise, the RRP and consequently the Pvr and PP ratio of both VGLUT1 dileucine-like motif sequence mutants are unchanged (fig.28 and 29) illustrating that the SV filling function with glutamate is not impaired by that mutations.
Similar findings are known from other proteins involved in the SV recycling, such as endophilin. Here, the clathrin-mediated SV endocytosis is blocked in endophilin mutants, but the NT release is not altered (Verstreken et al., 2002).
Therefore, it can be concluded that changes in endocytosis do not necessarily affect exocytosis. Presumably, to change the extent of exocytosis a major impairment of endocytosis might be required. Otherwise, the great amount of SVs in the recycling pool seems to be sufficient for an efficient SV release even if the NT transporter recycling is slower (as in the

case of VGLUT1). For instance, a lack of dynamin 1 and 2 in a double KO mouse, which are essential for the clathrin-dependent SV endocytosis, lead to a reduced rate of SV recycling, but also causes a defect in the efficiency of synaptic transmission (Raymond et al., 2011).

Recently, two additional dileucine-like motif sequences in the VGLUT1 N-terminus were described (Foss et al., 2013). Mutations in the N-terminal dileucine-like motif sequences of VGLUT1-pHluorin constructs resulted in higher surface expression similar to the C-terminal FV510/511AA mutation, suggesting that these multiple dileucine-like motif sequences are important for VGLUT1 trafficking. In contrast to the C-terminal FV510/511AA mutation, Foss et al., 2013 also showed that mutating the N-terminal dileucine-like motif sequences do not impair endocytosis. These findings indicate that the dileucine-like motif sequences of distinct parts of VGLUT1 seem to have different relevance for its recycling. An explanation for this could be different regulatory mechanisms, for example by other protein interactions of the VGLUT1 N- and C-terminus dileucine-like motif sequences. It was also published that the VGLUT1 C-terminal part acts via adaptor protein 2, whereas the N-terminal part uses adaptor protein 1 (Foss et al., 2013).

Generally, dileucine-like motif sequences of other NT transporters play functional roles as well. In the case of VMAT2 a dileucine-like motif sequence in the C-terminus is also required for its efficient endocytosis (Tan et al., 1998), but apparently for its sorting to synaptic-like micro-vesicles (SLMVs) as well (Fei et al., 2008). Evidence for a role in endocytosis is that a mutation in VMAT2s dileuine-like motif sequence causes higher cell surface expression similar to VGLUT1 (Li etl al., 2005). In case of the VAChT, mutations of the C-terminal dileucine-like motif sequence are known to inhibit its endocytosis as well (Fei et al., 2008; Tan et al., 1998), but there are indications that the dileucine-like motif sequences of VMAT2 and VAChT contribute to selective interactions with adaptor proteins resulting in differences in their localization (Tan et al., 1998).

Besides the investigation of the neurotransmission and cycling of FV510/511AA and the $S_{504}EEK_{507}$ deletion the SV morphology was analyzed by EM. Similar to the electrophysiology data, the EM results show no differences between the mutant groups and the WT rescue. The SV shape and density per synapse are unaltered by mutations of the VGLUT1 C-terminal dileucine-like motif sequence (fig.32) suggesting that the SVs are normally filled with glutamate. Instead, empty SVs from VGLUT1 KO neurons look

deformed and are much smaller (cf. fig.21B1 and 22A, B and C). The KO phenotype seems to be caused by the missing VGLUT1 function to fill SV with NT. Siksou et al., 2013 described flattening of SVs in VGLUT1 KO neurons as a result of a reduction in the osmotic pressure of the empty vesicles making them less resistant to the high tonicity of an aldehyde fixative.

However, both mutations, the FV510/511AA and the $S_{504}EEK_{507}$ deletion, exhibit an accumulation of enlarged vesicular structures (fig.33), that might be multivesicular bodies (MVBs) indicating an altered endocytic pathway or increased secretory pathway, which is known from cell degeneration processes (Cuenod et al., 1970; Diana, 2012; Hanson and Cashikar, 2012; Stahl and Barbieri, 2002). Further investigations, for example a proof by specific antibodies against MVB marker proteins, would be needed to confirm this possibility. In case of other synaptic proteins, which are important for SV endocytosis such as endophilin or dynamin, abnormal structures have been described as well. Elimination of the endophilin protein in neurons leads to an increased appearance of endocytic intermediates (Schuske, 2003; Verstreken et al., 2002). Dynamin 1 KO synapses also exhibit abnormally large vesicular structures (Ferguson et al., 2007), whereas the appearance of these enlarged structures are dependent on electrical stimulation (Hayashi et al., 2007). The EM data acquisition in the present study was without cell stimulation before fixating the neurons. Therefore, potential electrical stimulation-dependent effects of VGLUT1 C-terminus mutants on the SV morphology cannot be discussed. Mutations in synaptojanin, a protein involved in SV uncoating during endocytosis, also cause an increase in endosome-like structures, which may represent an effect of disrupted trafficking from the plasma membrane (Harris et al., 2000). As mentioned before, the VGLUT1 C-terminal dileucine-like motif sequence mutations also seems to affect the trafficking from the plasma membrane indicated by a higher VGLUT1 surface expression (fig.19B).

4.2 The C-terminus truncation VGLUT1Δ504-560 leads to decelerated VGLUT1 retrieval without affecting baseline synaptic transmission

The results of pHluorin-based experiments in combination with whole-cell patch clamp recordings demonstrate that the entire VGLUT1 C-terminal dileucine-like motif sequence $E_{505}EKCGFV_{511}$ is necessary for proper VGLUT recycling, but not for SV filling with glutamate and consequently also not for excitatory neurotransmission.

A remaining question is how important are the residual amino acids of the VGLUT1 C-terminus and its proper function?

A VGLUT1 specific endophilinA1 interaction at the second C-terminal PPR domain was suggested to regulate the release probability, which is lower in VGLUT1-expressing neurons compared to those expressing VGLUT2 or 3 (Weston et al., 2011). Furthermore, several putative VGLUT1 C-terminal serine phosphorylation sites are predicted with unknown functional relevance for VGLUT1. Therefore, these serine sites were also investigated in this study and in detail discussed in the following paragraph.

However, another question is, what are the functional consequences after a complete VGLUT1 C-terminus deletion?

To adress that question a VGLUT1 truncated version was created, where all the amino acids after the residue aa503 were removed („short truncation“: VGLUT1Δ504-560) including, among others, the dileucine-like motif sequence and its flanking putative serine phosphorylation site S504.

pHluorin-based imaging data show that the VGLUT1 recycling of VGLUT1Δ504-560 is drastically imapired (fig.19). The decay time of the fluorescence decline after electrical stimulation in the normalized 300AP-induced traces analyzed by using a single exponential fit is extremely slower in VGLUT1Δ504-560-pHluorin compared to the VGLUT1 WT rescue-pHluorin (fig.19A). For control, the VGLUT1 C-terminal FV510/511AA-pHluorin construct was used in this experiments knowing that the fluorescence decay time of this mutant construct is also significantly slower (Voglmaier et al., 2006; fig.19A). Furthermore, the pHluorin-based imaging experiments reveal that the rise time of the fluorescence change during electrical stimulation based on the release of VGLUT1-pHluorins is also affected of the C-terminus truncation VGLUT1Δ504-560 as well as the FV510/511AA construct (fig.19A). The rise time is slower in both mutants compared to the WT rescue (fig.19A). It can be argued that the significantly slower endocytic phase of the VGLUT1-pHluorin truncation version Δ504-560 and the FV510/511AA-pHluorin causes the delay in the exocytosis-based pHluorin fluorescence rising phase. This is presumably due to a hindered VGLUT1 trafficking to the SVs and can be also explained by the fact that endocytosis already occurs during ongoing electrical cell stimulation, which causes the AP-induced exocytosis. Evidence for a trafficking defect of VGLUT1Δ504-560 and FV510/511AA to SVs is the higher surface expression observed in the pHluorin experiments (fig.19B).

Interestingly, the NT release is not affected even though the VGLUT1 recycling is severely imapired (fig.19). EPSCs recorded before starting the pHluorin-based imaging protocol and the plot of the EPSCs during the 300AP stimulation of VGLUT1Δ504-560 reveal no significant differences compared to the WT rescue (fig.19D and F). Analyzing other electrophysiology parameters of VGLUT1Δ504-560 also reveal that the neurotransmission is not affected by that mutation. Here, besides EPSCs, mEPSCs and the RRP are not different compared to WT rescue levels as well (fig.16A, B and G). Likewise, the Pvr, PP ratio and 10 Hz train stimulation data of VGLUT1Δ504-560 show no changes (fig.16C, D and E). Even higher stimulation of 1,000AP at 20 Hz to deplete the SV pool and analysis of the subsequent recovery of the postsynaptic responses show no differences between the VGLUT1 truncation and the WT rescue (fig.20). Therefore, it can be concluded that SV filling with NT is not altered by a lack of the VGLUT1 C-terminus.

Against expectations from the electrophysiology results, the protein expression levels of VGLUT1Δ504-560 are substantially reduced (fig.37B, appendix), however without physiological consequences.

Equally unexpected, the overall SV recycling of VGLUT1Δ504-560-expressing neurons, tested by using additional synaptophysin-pHluorin, is not significantly altered. Synaptophysin is exclusively localized to SVs and therefore a common SV marker. Compared to the VGLUT1-pHluorin data, the synaptophysin-pHluorin data show no drastically slower SV recycling in the VGLUT1Δ504-560 construct compared to the WT rescue (fig.20). The surface expression of VGLUT1Δ504-560 in the synaptophysin-pHluorin experiments also shows no differences. These results illustrate that the VGLUT1 and synaptophysin recycling are independent from each other indicating that a decelerated VGLUT1 recycling does not affect the overall SV recycling.

To further investigate the importance of the VGLUT1 C-terminus another truncation construct with a deletion right after the last 12th transmembrane domain (VGLUT1Δ496-560) was tested in this study. Surprisingly, this „full“ truncation construct VGLUT1Δ496-560 does not restore postsynaptic responses to WT rescue levels (fig.12A). The EPSCs, but also the RRP of VGLUT1Δ496-560 are significantly reduced to almost VGLUT1 KO levels (fig.12A and B) indicating a loss of function of VGLUT1Δ496-560. The reason for the significantly reduced synaptic transmission of the truncation VGLUT1Δ496-560 seems to be incorrect protein localization evident in immunfluorescence data (fig.10). VGLUT1Δ496-560 accumulates more in extrasynaptic areas, such as the soma and dendrites, instead of being

predominantly expressed in the target synaptic locations, the SVs (fig.10B), which is usually reflected in a punctate expression pattern (fig.10A; Wojcik et al., 2004).

Another theory for the significantly reduced neurotransmission of VGLUT1Δ496-560 is impaired protein assembly or processing. Thereby, the protein structure might be altered to such an extent that correct VGLUT1 localization to SVs, which seems to be dependent on the interaction with adaptor proteins (Foss et al., 2013), or proper SV filling with NT is not possible. Further investigations, but also a VGLUT1 crystal structure might help to test this idea.

It could be also possible that the overall number of SVs is reduced in the C-terminus truncation VGLUT1Δ496-560 causing impaired NT release, but EM image quantifications could exclude this possibility. The SV density per synapse is not changed in any VGLUT1 C-terminus truncation constructs (fig.22D and E). However, the EM data also reveal a KO-like morphology of SVs from VGLUT1Δ496-560 (deformed and smaller; fig.21 and 22). Therefore, it can be concluded that VGLUT1Δ496-560-expressing neurons have no properly filled SVs, which confirms the loss of function of VGLUT1Δ496-560 observed in electrophysiology data. Furthermore, an accumulation of MVB and abnormal enlarged vesicular structures in VGLUT1 KO neurons as well as VGLUT1Δ496-560-expressing neurons were observed in EM images (fig.21B2, B3 and C). The occurrence of those vesicular structures might be a hint for an altered endocytic or secretory pathway similar to the observations in VGLUT1 C-terminal dileucine-like motif sequence mutants (cf. previous paragraph).

In contrast to the full C-terminus truncation VGLUT1Δ496-560, the shorter truncation VGLUT1Δ504-560 can rescue the morphological KO phenotype (fig.21 and 22) similar to the elctrophysiology data. The SV morphology is not different in VGLUT1Δ504-560 compared to the WT rescue (fig. 22A, B and E). Alike, VGLUT1Δ504-560-expressing neurons does not exhibit abnormal structures in EM images (fig.21D).

Because the shorter truncation VGLUT1Δ504-560 can rescue the KO-like phenotype of the full truncation version (VGLUT1Δ496-560) (fig.16) it can be concluded that the few additional amino acids after the last transmembrane domain including a conserved WAEPE motif sequence are crucial for proper VGLUT1 efficiency, supposedly for its trafficking to the target place, the SVs, to accomplish the basic function to fill them with glutamate.

For further investigations a VGLUT1 chimera construct was created using the full C-terminus truncation version VGLUT1Δ496-560 with a substitution of amino acids from the synaptophysin C-terminus (aa225-aa314). The idea was to test, whether the C-terminus of another vesicular protein with a similar sequence to the VGLUT1 WAEPE motif (for synaptophysin: WAAPF) is sufficient for normal VGLUT1 targeting to SVs to fill them with NT or, whether particularly the VGLUT1 C-terminus is necessary for that.

The chimera construct-expressing neurons show similar to those expressing the VGLUT1Δ496-560 construct significantly reduced NT release (fig.14) suggesting that specifically the VGLUT1 C-terminus is important for its correct trafficking and cannot be replaced by a C-terminus of another vesicular protein. It can be concluded that even similar structures of different proteins function differently.

Furthermore, investigating a full VGLUT2 C-terminus truncation construct until aa493 (VGLUT2Δ493-582) shows considerably impaired neurotransmission as well (fig.13) strengthen the idea that the amino acids directly after the last transmembrane domain including the conserved WE(X)PE motif sequence of all mammalian VGLUTs are essential to accomplish their function in baseline synaptic transmission.

4.3 The C-terminal VGLUT1 S504A mutation leads to higher neurotransmitter release

Another focus of this study was the investigation of potential roles of the putative VGLUT1 C-terminal serine phosphorylation sites S504, S519, S522 and S540 in glutamaterigic neurotransmission or SV/VGLUT1 cycling. Very recent data using radioactive labeled S519 and S522 provided first evidence that both sites are indeed VGLUT1 phosphorylation sites (Santos et al., 2014), but the study did not further investigate their functional relevance for VGLUT1.
Therefore, whether these C-terminal serine residues are important for VGLUT1 function was examined in this study as well.
Serine mutations by substitution with alanine or glutamic acid were created by site-directed mutagenesis and investigated by pHluorin-based imaging in combination with whole-cell voltage clamp recordings and EM.

Electrophysiological analyses of mutated VGLUT1 C-terminal S504, which flanks the dileucine-like motif sequence, shows significantly changes in comparison to the WT rescue towards a higher NT release apparent in EPSC and mEPSC frequency data (fig.23A and I). Accordingly, the calculated Pvr is significantly higher and the PP ratio lower by this single mutation (fig.23C and D).
This interesting finding of an increased NT release of VGLUT1 S504A is similar to results from mutated aspartic acid D38 to glycine G (D38G) of VGAT (Santos et al., 2014). D38 of VGAT is also located in front of a dileucine-like motif sequence. In case of VGAT, the change of the charge of D38 by G mutation increases the NT release as well, supposedly due to alterations in the distribution of the SV pools (Santos et al., 2013). Santos et al., 2013 suggest an increase of the RRP and the recycling pool, because for instance during stimulation the fluorescence intensity of VGAT D38G-pHluorin rises faster and reaches a higher peak than the WT control. This effect seems to be dependent on the adaptor protein 3 (Santos et al., 2013). VGLUT1 S504A-pHluorin does not exhibit such a faster rise time with higher peak fluorescence (fig.25A and B). The decay time analyzed by single exponential fit of the fluorescence decline after 300AP stimulation and the surface expression of S504A are also not altered compared to VGLUT1 WT rescue (fig.25A and C). However, the data from the electrophysiology experiments illustrate without any doubt a significantly higher NT release of S504A (fig.23A, B and I), which might be also due to an increased RRP or recycling pool. Supporting this idea, Voglmaier et al., 2006 showed that an adaptor protein 3

inhibition in VGLUT1 leads to an increased NT release as well, consistent with an increase in the recycling pool, but whether VGLUT1 S504 is indeed acting via the adaptor protein 3 on the recycling pool is not investigated yet. Experiments blocking the adaptor protein 3 pathway with brefeldin A (BFA) could help to point out this possibility.

The other two mammalian isoforms, VGLUT2 and 3, also exhibit a putative serine phosphorylation site preceding their C-terminal dileucine-like motif sequences (cf. fig.5), but a potential similar role for neurotransmission as S504 in VGLUT1 is unknown and needs to be further investigated.
Likewise, other vertebrates, such as the african frog *Xenopus laevis* or the zebrafish *Danio rerio* exhibit a serine site in front of their VGLUT dileucine-like motif sequences. Invertebrates such as *Drosophila melanogaster* also have a C-terminal VGLUT dileucine-like motif sequence, but no serine site in front of it (sequence alignment by www.uniprot.org). Therefore, it can be concluded that serine sites flanking the VGLUT dileucine-like motif sequence seems to play a functional role only for the neurotransmission in vertebrates.

In contrast, electrophysiological analyses to examine the NT release of the mutated putative phosphorylation sites S519A/522A and S540A show no significant differences in synaptic transmission (fig.23) in comparison with the WT rescue.
S519A/S522A exhibits a higher Pvr and lower PP ratio compared to WT rescue levels (fig.23C and D), which indicates a higher NT release, but no other expected changes, for example in EPSCs or mEPSC frequency (fig.23A and I). Therefore, the interpretation of the results of S519A/522A-expressing neurons must be taken with caution.
S540A also shows a higher Pvr and more depression in the 10 Hz train stimulation in comparison to the WT rescue (fig.23C and G), but no changes in other electrophysiological properties as well. Therefore, it can be concluded that those putative serine phosphorylation sites are not relevant for VGLUT1 physiology. So far, a role of phosphorylation of other vesicular NT transporter in NT release is not published.
However, several other studies showed that the phosphorylation state of NT transporters can play a role in other processes, such as protein trafficking or localization. For instance, in VAChT the serine site S480 equally close to the dileucine-like motif sequence as S504 in VGLUT1 regulates the protein sorting to dense core vesicles (Cho et al., 2000; Krantz et al., 2000). The localization of VMAT2 to large dense core vesicles (LDCVs) also requires phosphorylation of two serines by casein kinase 2 (Waites et al., 2001).

These data support the hypothesis of an important modulatory role of the VGLUT1 C-terminal S504 for its protein function, but kinases responsible for putative phosphorylation of VGLUTs are also not known so far and need to be further investigated.

Additional pHluorin-based imaging experiments of S519A/S522A and S540A to investigate the VGLUT1 cycling do not reveal any alterations compared to the WT rescue (fig.25). Consequently, all the tested putative VGLUT1 serine phosphorylation sites S504, S519, S522 and S540 in this study seem to play no essential role in VGLUT1 recycling.

Investigating the SV morphology and density of the putative VGLUT1 C-terminal serine phosphorylation sites by EM does not uncover differences compared to the WT rescue as well (fig.27). However, for the EM images non stimulated neurons were fixed, but physiological phosphorylation is usually a dynamic process and might be altered in response to various stimulation. Therefore, assumptions about potential morphological changes of the putative serine phosphorylation sites after AP-evoked NT release cannot be done. In addition, replacing a serine phosphorylation residue with alanine affects the local isoelectrical point (pI) of the protein with unknown outcome. So, whether the phosphodeficient mutants *in vitro* may really reflect the phosphorylation state similar to *in vivo* is unclear.

Another possibility to study protein phosphorylation is to create phosphomimetic mutants by replacing S with E. This was done only for the putative VGLUT1 phosphorylation site S504, because significant electrophysiological effects were seen by S504A mutation. Surprisingly, S504E does not show an opposite effect in NT release to S504A. The measured electrophysiological properties of S504E are not different to the WT rescue (fig.24) suggesting that only dephosphorylation of S504 seems to be relevant for VGLUT1 function.

5. Conclusions and outlook

The results of this thesis illustrate the great importance of the VGLUT1 C-terminus, in particular for its efficient recycling after SV fusion to fill newly formed vesicles with glutamate.

The absence of the VGLUT1 C-terminus (VGLUT1Δ504-560) leads to a substantially impaired VGLUT1 retrieval, but surprisingly the NT release remains unaffected. Therefore, it can be concluded that the SV filling with glutamate is not dependent on the VGLUT1 C-terminus. The data also suggests that the speed of VGLUT1 recycling is not a limiting factor for maintaining baseline synaptic transmission. Furthermore, the results of an experiment with synaptophysin-pHluorin show that the general SV recycling is not affected by slowed VGLUT1 retrieval indicating an independent VGLUT1 recycling mechanism.

Additional experiments with a further C-terminus truncation version VGLUT1Δ496-560 suggest that the VGLUT1 WAEPE motif sequence is necessary for its proper function in glutamatergic neurotransmission. Without that few more amino acids correct VGLUT1 targeting to SVs seems to be impaired. VGLUT1Δ496-560 does not show a synaptic immunfluorescence staining pattern, but extrasynaptic protein accumulations. Consequently, SVs are not adequately filled with glutamate resulting in a loss of function, which is apparent in a drastically reduced NT release and a VGLUT1 KO-like empty vesicle morphology of smaller and deformed SVs. However, no crystal structure of the VGLUT1 protein exists, which might help to solve the question, whether this VGLUT1 C-terminus deletion (Δ496-560) so close to the transmembrane domain might cause protein instability with subsequent protein degradation or maybe hinders proper glutamate filling.

Moreover, the results of this thesis illustrate the importance of the entire VGLUT1 C-terminal dileucine-like motif sequence for VGLUT1 trafficking. So far, only the FV motif was investigated. Here, the $S_{504}EEK_{507}$ residues were also examined and a deletion of them showed a slower VGLUT1 recycling similar to FV motif mutations. Further electrophysiological investigations of the VGLUT1 dileucine-like motif sequence mutations FV510/511AA and the $S_{504}EEK_{507}$ deletion show similar to the C-Terminus truncation data (VGLUT1Δ504-560) no effects on NT release.

Altogether, it can be hypothesized that for all mammalian VGLUT isoforms the C-terminus is crucial, because all VGLUTs exhibit the conserved WA(X)P(X) motif sequence and a

dileucine-like motif sequence, but further experiments are needed to explore in more detail how the VGLUT C-terminus affects its protein recycling. It can be speculated that missing interactions of the VGLUT1 C-terminus with other proteins, such as adaptor proteins, might be the reason for the impaired recycling. Whether this is true or other protein interactions may play a role for accurate VGLUT1 function, is not known and needs be further investigated.
A very recent study identified interactions *in vitro* with cytoskletal adaptor proteins, such as Nck, but also with the tyrosine kinase Lyn and ubiquitin ligases (Santos et al., 2014), but their relevance for VGLUT1 function, especially *in vivo*, was not tested.

In addition, a modulatory role could be shown for the putative VGLUT1 serine phosphorylation site S504 in regulating the NT release similar to D38 in VGAT. Both, D38G mutation in VGAT and S504A mutation in VGLUT, imitating permanent dephopshorylation, result in a higher NT release. Whether S504A acts in the same way as D38G by sorting VGLUT1 to the RRP or recycling pool via an adaptor protein-dependent pathway and thereby modulating the neurotransmission, needs to be further investigated as well.
The other putative VGLUT1 C-terminal serine phosphorylation site mutations S519A/S522A and S540A show no consistent changes in NT release. With these results it can be concluded that dephosphorylated S519/S522 and S540 are not relevant for VGLUT1 function, but whether other conditions, such as electrical cell stimulation or other combinations of mutations of putative VGLUT1 phosphorylation sites might play a role for VGLUT1 function should be also studied in future.
Another important future aim would be to confirm that the mutated C-terminal serine residues of VGLUT1 are in fact phosphorylation sites. Thus far, biochemical confirmation of all the tested putative VGLUT1 serine phosphorylation sites was not possible. Recent data only confirmed biochemically that VGLUT1 S519 and S522 play a role in VGLUT1 phosphorylation (Santos et al., 2014).
With the help of Dr. Sebastian Beck (group of professor Linscheid from Humboldt university, Berlin) and Dr. Stella Amrei (group of Dr. Shoichet from university medical center of the Charité, Berlin) mass spectrometry and a phos-tag-based phosphorylation detection assay were tried, but none of the assays gave sufficient results to confirm the other predicted VGLUT1 serine sites as phosphorylation sites. Otherwise, the changes in NT release by mutating VGLUT1 S504 with A are convincing and strengthen the software prediction that S504 is indeed a phosphorylation site.

Altogether, with this combination of molecular techniques paired with electrophysiology, live-cell imaging and EM new insights were gained of the VGLUT1 C-terminus and its role for VGLUT1 function.

Abstract

Vesicular glutamate transporters (VGLUTs) are essential for filling synaptic vesicles (SVs) with the neurotransmitter (NT) glutamate. After SV fusion and NT release, SVs are recycled to maintain a constant SV supply. In order for these SVs to participate again in neurotransmission, they must be refilled. Therefore, VGLUTs need to be efficiently and correctly targeted to SVs undergoing endocytosis.

Previous studies showed that the C-terminal VGLUT1 FV motif, which is part of the dileucine-like sequence, is a sorting signal for VGLUT1 trafficking to SVs. Mutations in the FV motif show slower VGLUT1 recycling (Foss et al., 2013; Voglmaier et al., 2006), but it is unknown, whether an impaired VGLUT1 retrieval consequently alters glutamatergic neurotransmission.

This issue was addressed by further studying mutant variants of this VGLUT1 C-terminal dileucine-like motif sequence. Another aim of the present study was to investigate software predicted putative VGLUT1 C-terminus serine phosphorylation sites to understand their potential role for the VGLUT1 physiology and SV cycling. Additionally, the functional consequences of an entire VGLUT1 C-terminus deletion were studied as well.

Therefore, VGLUT1 C-terminal mutants were expressed by lentivirus in autaptic hippocampal VGLUT1 knockout (KO) neurons and compared to a rescue of the KO neurons with expression of the VGLUT1 wildtype (WT) protein. Parameters of release and SV recycling were assessed using whole-cell voltage clamp recordings in combination with pHluorin-based imaging. With high resolution electron microscopy (EM) further information were obtained especially about SV morphology and SV number per synapse, which might be altered according to changes in vesicular release or recycling properties.

Thereby, it was found out that neurons expressing a full VGLUT1 C-terminus truncation construct (VGLUT1Δ496-560), where all amino acids immediately following the last 12th transmembrane domain are deleted, are not functional. Those neurons exhibit an electrophysiological and morphological VGLUT1 KO-like phenotype apparent in significantly reduced postsynaptic responses and deformed, smaller SVs compared to WT rescued neurons indicating that the SVs of VGLUT1Δ496-560 are not glutamate filled. A reason for the impairments of VGLUT1Δ496-560 may be protein mislocalization to vesicles. However, no crystal structure of the VGLUT1 protein exists and it is unclear,

whether this deletion may have been within or close enough to the transmembrane domain causing instability of the protein and subsequent degradation.

In contrast, neurons expressing a C-terminus truncation construct that was a few amino acids shorter (VGLUT1Δ504-560), including a WAEPE motif sequence, can rescue the VGLUT1 KO-like phenotype to WT rescue levels, suggesting that the main function of the transporter to fill SVs with NT is here not affected. Moreover, it could be also shown that the SV morphology is unaltered in the VGLUT1Δ504-560 mutant. However, the VGLUT1 recycling of VGLUT1Δ504-560 is substantially slower compared to WT rescue levels. Interestingly, additional experiments with synaptophysin-pHluorin show no significant changes in the general SV recycling when the shorter VGLUT1 C-terminus truncation mutant (VGLUT1Δ504-560) is present on vesicles. Furthermore, dileucine-like motif sequence mutants, which show also a slower VGLUT1 recycling, reveal no effects on neurotransmission as well. These results suggest that the entire VGLUT1 C-terminus, but in particular the dileucine-like motif sequence, are mainly essential for VGLUT1 recycling, but the speed of VGLUT1 recycling is not a limiting factor for maintaining baseline synaptic transmission.

Furthermore, it was discovered that a VGLUT1 mutant with one phosphodeficient mutation in a putative serine phosphorylation site, shows higher NT release, which might indicate a modulatory role in VGLUT1 function.

Zusammenfassung

Vesikuläre Glutamattransporter (VGLUTs) sind essenziell für die Befüllung synaptischer Vesikel (SV) mit dem Neurotransmitter (NT) Glutamat. Zur Aufrechterhaltung einer konstanten Vesikelbereitstellung nach ihrer Fusion mit der Plasmamambran und NT Freisetzung in den synaptischen Spalt werden die SV recycelt. Damit die SV erneut in der Neurotransmission mitwirken können, müssen sie wieder mit Glutamate befüllt werden. Dafür müssen VGLUTs während der Endozytose effizient und zielgerichtet zu den Vesikeln transportiert werden.

Frühere Studien haben gezeigt, dass das C-terminale VGLUT1 FV Motiv, welches Teil einer Di-Leucin-ähnlichen Sequenz ist, eine Signalsequenz für den Transport von VGLUT1 zu den SV darstellt und das Mutationen im FV Motiv zu einem verlangsamtem VGLUT1 Recycling führen (Foss et al., 2013; Voglmaier et al., 2006). Jedoch ist bislang nicht bekannt, ob in Folge eines beeinträchtigen VGLUT1 Recyclings die glutamaterge Neurotransmission verändert wird.

Ein Ziel der vorliegenden Arbeit war die Funktion des VGLUT1 C-terminalen Di-Leucin-ähnlichen Sequenzmotivs weiter zu charakterisieren. Hierfür wurden verschiedene durch zielgerichtete Mutagenese hergestellte Konstrukte des VGLUT1 C-Terminus untersucht. Ein weiteres Ziel dieser Arbeit war die Untersuchung Computersoftware-basierter vermeintlicher Serin Phosphorylierungsstellen des VGLUT1 C-Terminus zur Klärung ihrer potenziellen Rolle für die VGLUT1 Physiologie und den Vesikelzyklus. Darüber hinaus wurden auch die funktionellen Konsequenzen einer kompletten Deletierung des VGLUT1 C-Terminus untersucht.

Dabei wurde herausgefunden, dass Neurone die ein vollständig verkürztes VGLUT1 C-Terminus Konstrukt (VGLUT1Δ496-560) exprimieren, bei dem alle Aminsosäuren direkt nach der letzten 12ten Transmembrandomäne entfernt wurden, nicht funktionell sind. Diese Neurone weisen im Vergleich zu Wildtyp (WT) Neuronen einen VGLUT1 Knockout (KO)-ähnlichen Phänotyp mit signifikant reduzierten postsynaptischen Antworten und deformiert aussehenden, kleineren SV auf. Diese Ergebnisse deuten darauf hin, dass die Vesikel der VGLUT1Δ496-560 Mutante nicht mit Glutamat befüllt sind. Eine mögliche Ursache dieser Veränderungen der VGLUT1Δ496-560 Mutante könnte eine Misslokalisation des Proteins zu den SV sein. Allerdings gibt es bisher keine Kristallstruktur vom VGLUT1 Protein, welche belegen könnte ob diese Deletion in der Nähe der letzten

Transmembrandomäne der Grund für ein möglicherweise instabiles Protein und in Folge dessen einer Degradation darstellt.

Im Gegensatz dazu können Neurone, die ein weniger kurzes C-terminales Konstrukt (VGLUT1Δ504-560) exprimieren, welches eine WAEPE Motivsequenz einschließt, den KO-ähnlichen Pänotyp wieder auf WT-Niveau herstellen. Dieses Ergebnis zeigt, dass bei VGLUT1Δ504-560 Mutanten die Funktion des Transporters die SV mit NT zu füllen nicht beeinträchtigt ist. Dies spiegelt sich auch in der unveränderten Morphologie der Vesikel der VGLUT1Δ504-560 Mutante wieder. Allerdings ist das VGLUT1 Recycling in der VGLUT1Δ504-560 Mutante im Vergleich zum WT drastisch verlangsamt. Interessanterweise zeigen zusätzliche Experimente, dass der grundlegende Vesikelzyklus durch diese Mutation keine signifikanten Beeinträchtigungen aufweist. Mutationen in der Di-Leucin-ähnlichen Motivsequenz, welche genauso ein verzögertes VGLUT1 Recycling aufweisen, zeigen ebenfalls keine Effekte in der Neurotransmission.

Zusammengefasst zeigen die Ergebisse dieser Arbeit, dass der gesamte VGLUT1 C-Terminus, insbesondere das Di-Leucin-ähnliche Sequenzmotiv, hauptverantwortlich für das VGLUT1 Recycling ist. Dabei scheint die Geschwindigkeit des VGLUT1 Recyclings keinen limitierenden Faktor für die Erhaltung der grundlegenden synaptischen Transmission darzustellen.

Darüber hinaus kann in dieser Arbeit gezeigt werden, dass die Mutation einer putativen Serin-Phosphorylierungsstelle, welche eine permanent Dephosphorylierung mimt, die NT Freisetzung erhöht. Dieses Ergebnis weist darauf hin, dass Phosphorylierung von VGLUT1 dessen Funktion beeinflusst.

List of references

Publications:

Alabi A. and Tsien R. (2012) Synaptic Vesicle Pools and Dynamics. Cold Spring Harb Perspect Biol. 4(8):a013680

Amara S., (1998) Methods in enzymology, volume 296, Neurotransmitter transporters. Academic press

Amara S. and Fontana A. (2002) Excitatory amino acid transporters: keeping up with glutamate. Neurochem Int. 41(5):313-8

Anne C. and Gasnier B. (2014) Vesicular neurotransmitter transporters: mechanistic aspects. Curr Top Membr. 73:149-74

Bai L., Xu H., Collins J. and Grishan F. (2001) Molecular and functional analysis of a novel neuronal vesicular glutamate transporter. J Biol Chem. 276(39):36764-9

Bai J., Hu Z., Dittman J., Pym E., Kaplam J. (2010) Endophilin functions as a membrane-bending molecule and is delivered to endocytic zones by exocytosis. Cell. 143(3):430-41.

Baker P. and Knight D. (1986) Exocytosis: control by calcium and other factors. Br Med Bull. 42(4):399-404

Balschun D., Moechars D., Callaerts-Vegh Z., Vermaercke B., Van A., Andries L., D`Hooge R. (2009) Vesicular glutamate transporter VGLUT1 has a role in hippocampal long-term potentiation. and spatial reversal learning. Cereb Cortex. 20(3):684–693

Bedet C., Isambert M., Henry J., Gasnier B.(2000) Constitutive phosphorylation of the vesicular inhibitory amino acid transporter in rat central nervous system. J Neurochem. 75:1654–1663.

Bekkers J., Stevens C. (1991) Excitatory and inhibitory autaptic currents in isolated hippocampal neurons maintained in cell culture. Proc Natl Acad Sci. 88(17):7834-8.

Bellocchio E., Reimer R., Fremeau R. and Edwards R. (2000) Uptake of glutamate into synaptic vesicles by an inorganic phosphate transporter. Science. 289(5481):957–960

Betz W. and Angleson J. (1998) The synaptic vesicle cycle. Annu Rev Physiol. 60:347-63

Blagoveshchenskaya A., Hewitt E., Cutler D., (1999) Di-leucine signals mediate targeting of tyrosine and synaptotagmin to synaptic-like microvesicles within PC12 cells. Mol Biol Cell.10:3979-39990

Bonifacino and Traub (2003) Signals for sorting of transmembrane proteins to endosomes and lysosomes. Annu Rev Biochem. 72:395-447

Bjerggaard C., Fog J., Hastrup H., Madsen K., Loland C., Javitch J., Gether U. (2004) Surface targeting of the dopamine transporter involves discrete epitopes in the distal C terminus but does not require canonical PDZ domain interactions. J Neurosci. 24(31):7024-36

Brose N., Petrenko A., Südhof T. and Jahn R. (1992) Synaptotagmin: a calcium sensor on the synaptic vesicle surface. Science. 256(5059):1021-5

Bulland J., Qureshi T., Seal R., Rafiki A., Gundersen V., Bergersen L., Fremeau R., Edwards R., Storm-Mathisen J. and Chaudhry F. (2004) Expression of the vesicular glutamate transporters during development indicates the widespread corelease of multiple neurotransmitters. J Comp Neurol. 480(3):264-80

Carlsson M. and Carlsson A. (1990) Schizophrenia: a subcortical neurotransmitter imbalance syndrome? Schizophr Bull. 16(3):425-32

Cidon D. and Sihra T. (1989) Characterization of an H^+-ATPase in rat brain synaptic vesicles J Biol Chem. 264(14):8281-8288

Chapman E. (2002) Synaptotagmin: a Ca2+ sensor that triggers exocytosis? Nature. 3:498-508

Chaudhry F., Edwards R. and Phonon F. (2008) Vesicular neurotransmitter transporters as targets for endogenous and exogenous toxic substances. Annu Rev Pharmacy Toxicol. 48:277-301

Chavrier P., Parton R., Hauri H., Simons K. and Zerial M. (1990) Localization of low molecular weight GTP binding proteins to exocytic and endocytic compartments. Cell. 62(2):317-29

Chen K., Reese E., Kim H., Rapoport S. and Rao J. (2011) Disturbed neurotransmitter transporter expression in Alzheimer`s disease braim J Alzheimers Dis. 26(4):755-66

Cho G., Kim M. , Chai Y. , Gilmor M., Levey A., Hersh L. B. (2000) Phosphorylation of the rat vesicular acetylcholine transporter. J Biol Chem. 275:19942–19948

Clemens J. and Bekkers J. (1997) Detection of spontaneous synaptic events with an optimally scaled template. Biophys J. 73(1):220-9

Couteaux R. and Pecot-Dechavassine M. (1970) Synaptic vesicles and pouches at the level of "active zones" of the neuromuscular junction. C R Acad Sci Hebd Seances Acad Sci. 271:2346-2349

Cuenod M., Sandri C. and Akert K (1970) Enlarged synaptic vesicles as an early sign of secondary degeneration in the optic nerve terminals of the pigeon. J Cell. 6:605-613

Dahl R. and Staehelin L. (1989) High-pressure freezing for the preservation of biological structures: theory and practise. J Electrin Microsc Tech. 13(3):165-74

Daniels R., Miller B., Diantonio A. (2011) Increased vesicular glutamate transporter expression causes excitotoxic neurodegeneration. Neurobiol. Disease. 41(2): 415--420

Darna M., Schmutz I., Richter K., Yelamanchili S., Pendyala G., Höltje M., Albrecht U. and Ahnert-Hilger G. (2009) Time of day-dependent sorting of the vesicular glutamate transporter to the plasma membrane. J Biol Chem. 284(7):4300-7

DeGois S, Jeanclos E, Morris M, Grewal S, Varoqui H, Erickson JD (2006) Identification of endophilins 1 and 3 as selective binding partners for VGLUT1 and their co-localization in neocortical glutamatergic synapses: implications for vesicular glutamate transporter trafficking and excitatory vesicle formation. Cell Mol Neurobiol 26(4-6):679-93

DeRobertis E. and Bennett H. (1955) Some features of the submicroscopic morphology of synapses in frog and eathworm. J. Biophys and Biochem. 1(1):47-58

DeVries K., Geijtenbeek A., Brian E., DeGraan P., Ghijsen W. and Verhage M. Dynamics of munc18-1 phosphorylation/dephosphorylation in rat brain nerve terminals. Eur J Neurosci. 12(1):385-90

Diana A. (2012) Autophagosomes and multivesicular bodies in neuronal development and degeneration. Translat neurosci. 3(4).384-387

Dobrunz L. (2002) Release probability is regulated by the size of the readily releasable vesicle pool at excitatory synapses in hippocampus. Int J Dev Neurosci. 20(3-5):225-36

Doherty G. and McMohan H. (2009) Mechanism of endocytosis. Annu rev Biochem. 78:857-902

Dreosti E. and Lagnado L. (2010) Optical reporters of synaptic activity in neural circuits. Exp Physio. 96:4-12

Dresbach T., Qualmann B., Kessels M., Garner C. and Gundelfinger E. (2001) The presynaptic cytomatrix of brain synapses. Cell Mol Life Sci. 58(1):94-116

Eastwood S., Harrison P. (2005) Decreased expression of vesicular glutamate transporter 1 and complexin II mRNAs in schizophrenia: further evidence for a synaptic pathology affecting glutamate neurons. Schizophr Res. 73(2-3):159–172

Erickson J., Varoqui H., Schäfer M., Modi W., Diebler M., Weihe E., Rand J., Eiden L., Bonner T. and Usdin T. (1994) Functional identification of a vesicular acetylcholine transporter and its expression from a“ cholinergic“ gene locus. J Boil Chem. 269:21929-21932

Fairman W., Vandenberg R., Arise J., Kavanaugh M. and Amara S. (1995) An excitatory amino-acid transporter with properties of a ligand-gated chloride channel. Nature. 375(6532):599-603

Fei H., Grygoruk A., Brooks E., Chen A. and Krantz D. (2008) Trafficking of Vesicular Neurotransmitter Transporters. Traffic. 9(9):1425-1436

Ferguson S., Brasnjo G., Hayashi M., Wölfel M., Collesi C., Giovedi S., Raimondi A., Gong L., Ariel P., Paradise S., O`Toole E., Flavell R., Cremona O., Miesenböck G., Ryan T. and DeCamilli P. (2007) A Selective Activity-Dependent Requirement for Dynamin 1 in Synaptic Vesicle Endocytosis. Science. 316(5824):570-4

Fire A., Xu S., Montgomery M., Kostas S., Driver S. and Mello O. (1998) Potent and specific genetic interference by double-stranded RNA in Caenorhabditis elegans. Nature. 391(6669):806-11

Foss S., Li H., Santos M., Edwards R., Voglmaier S. (2013) Multiple Dileucine-like Motifs Direct VGLUT1 Trafficking. J Neurosci. 33(26):10647-60

Fremeau R., Troyer M., Pahner I., Nygaard G., Tran C., Reimer R., Bellocchio E., Fortin D., Storm-Mathiesen J., Edwards R. (2001) The expression of vesicular glutamate transporters defines two classes of excitatory synapse. Neuron. 31:247-260

Fremeau R., Kam K., Qureshi T., Johnson J., Copenhagen D., Storm-Mathisen J., Chaudgry F., Nicoll R., Edwards R. (2004) Vesicular glutamate transporters 1 and 2 target to functionally distinct synaptic release sites. Science. 304(5678):1815–1819

Gargiulo P. and Landa De Gargiulo A. (2014) Glutamate and modeling of schizophrenia symptoms: Review of our Findings: 1990-2014. Pharmacol Rep. 66(3):343-352

Garcia-Alloza M., Gil-Bea F., Diez-Ariza M., Chen C., Francis P. Lasheras B. and Ramirez M. (2005) Cholinergic-seritonergic imbalance contributes to cognitive and behavioral symptoms in Alzheimer`s disease. Neuropsychologia. 43(3):442-9

Granseth B., Odermatt B., Royle S. and Lagnado L. (2006) Clathrin-Mediated Endocytosis Is the Dominant Mechanism of Vesicle Retrieval at Hippocampal Synapses. Neuron. 51(6): 773-786

Gras C., Herzog E., Blench G., Bernard V., Ravassard P., Pohl M., Gasnier B., Giros B. and El Mestikawy S. (2002) A third vesicular glutamate transporter expressed by cholinergic and seritonergic neurons. J Neurosci. 22:5442-5451

Gras C., Vinatier J., Amilhon B., Guerci A., Christov C., Ravassard P., Giros B. and Mestikawy S. (2005) Developmentally regulated expression of VGLUT3 during early post-natal life. Neuropharmacology. 49(6):901-11

Hanson P. and Cashikar A. (2012) Multivesicular body morphogenesis. Annu Rev Cell Dev Biol. 28:337-62

Harata N., Choi S., Pyle J., Aravanis A. and Tsien R. (2005) Frequency-Dependent Kinetics and Prevalence of Kiss-and-Run and Reuse at Hippocampal Synapses Studied with Novel Quenching Methods. Neuron. 49(2):243-56

Harris T., Hartwig E., Horvitz R. and Jorgensen E. (2000) Mutations in Synaptojanin Disrupt Synaptic Vesicle Recycling. J Cell Biol. 150(3):589-600

Hayashi M., Otsuka M., Morimoto R., Hirota S., Yatsushiro S., Takeda J., Yamamoto A. and Miriam Y. (2001) Differentiation-associated Na+-dependent inorganic cotransporter (DNPI) is a vesicular glutamate transporter in endocrine glutamatergic systems. J Biol Chem. 276:43400-43406

Hayashi M., Raimondi A., O`Toole E., Paradise S., Collesi C., Cremona O., Ferguson S. and DiCamilli P. (2007) Cell- and stimulus-dependent heterogeneity of synaptic vesicle endocytic recycling mechanisms revealed by studies of dynamin 1-null neurons. Proc Natl Acad Sci USA. 105(6): 2175-2180

Hilfiker S., Pieribine V., Nordstedt C., Greengard P. and Czernik A. (2001) Regulation of synaptotagmin I phosphorylation by multiple protein kinases. J Neurochem. 73(3):921-32

Hnasko T. and Edwards R. (2012) Neurotransmitter corelease: mechanism and physiological role. Annu Rev Physiol. 74:225-43

Jarousse N. and Kelly R. (2001) Endocytosis mechanisms in synapses. Curr Opin Cell Biol. 13(4):461-9

Jahn R., (2010) VGLUTs-potential targets for the treatment of seizures? Neuron. 68(1):6-8

Juge N., Yoshida Y., Yatsushiro S., Omote H., Moriyama Y. (2006) Vesicular glutamate transporter contains thwo independent transport machineries. J Biol Chem. 281(51):39499-506

Juge N., Gray J., Omote H., Miyaji T., Inoue T., Hara C., Uneyama H., Edwards R., Nicoll R., Moriyama Y. (2010) Metabolic control of vesicular glutamate transport and release. Neuron. 68: 99-112

Kanai Y and Hedgier M (1992) Primary structure and functional characterization of a high-affinity glutamate transporter. Nature. 360(6403):467-71

Kandel E., Schwartz J., Jessell T. (2000) Principles of neuroscience New York: McGraw-Hill, USA

Kashani A., Lepicard E., Poirel O., Videau C., Daid J., Fallet-Bianco C., Simon a., Delacourte A., Giros B., Epelbaum J., Beatncur C., El Mestikawy (2008) Loss of VGLUT1 and VGLUT2 in the prefrontal cortex is correlated with cognitive decline in Alzheimer disease. Neurobiol Aging. 29(11):1619-30

Kjaerulff O., Brodin L. and Jung A. (2011) The structure and function of endophilin proteins. Cell Biochem Biophys. 60(3): 137-54

Kononenko N., Puchkov D., Classen G., Walter A., Pechstein A., Sawade L., Kaempf N., Trimbuch T., Lorentz D., Rosenmund C., Maritzen T. and Haucke V. (2014) Clathrin/AP-2

mediate synaptic vesicle reformation from endosome-like vacuoles but are not essential for membrane retrieval at central synapses. Neuron. 82:981-988

Kim J., Lee S., Li L., Park H., Park J., Lee K., Kim M., Shin B. and Choi S. (2011) High cleavage efficiency of a 2A peptide derived from porcine teschovirus-1 in human cell lines, zebrafish and mice. Plos One. 6(4):e18556

Kirchhausen T., Macia E, Pelish H. (2008) Use of dynasore, the small molecule inhibitor of dynamin, in the regulation of endocytosis. Methods Enzymol. 438:77-93

Krantz D., Peter D., Liu Y. and Edwards R. (1997) Phosphorylation of a Vesicular Monoamine Transporter by Casein Kinase II. J Biol Chem. 272(10):6752-9

Krantz D., Waites C., Oorschot V., Liu Y., Wilson R., Tan P., Klumperman J., Edwards R. (2000) A phosphorylation site regulates sorting of the vesicular acetylcholine transporter to dense core vesicles. J Cell Biol. 149(2):379-96

Kwon S. and Chapman E. (2011) Synaptophysin regulates the kinetics of synaptic vesicle endocytosis in central neurons. Neuron. 70(5):847-54

Lanari A., Amenta F., Silvestrelli G., Tomasoni D. and Parnetti L. (2006) Neurotransmitter deficits in behavioural and psychological symptoms of Alzheimer`s disease. Mech Ageing Dev. 127(2):158-65

Larsen W. (1977) Structural diversity of gap junctions. A review. Tissue Cell. 9(3):373-94

Lyshevski S. (2007) Nano and Molecular Electronics Handbook. CRC Press

Li H., Waites C., Staal R., Dobryy Y., Park J., Sulzer D. and Edwards R. (2005) Sorting of vesicular monoamine transporter 2 to the regulated secretory pathway confers the somatodendritic exocytosis of monoamines. Neuron. 48(4):619-33

Lieferringe J., Massie A., Portelli J., DiGiovanni G. and Smolders I. (2013) Are vesicular neurotransmitter transporters potential treatment targets for temporal lobe epilepsy? Front Cell Neurosci. 7:139

Liraz O., Boehm-Cagan A., Michaelson D. (2013) ApoE4 induces Aβ42, tau, and neuronal pathology in the hippocampus of young targeted replacement apoE4 mice. Mol Neurodegener.17;8:16

Liu H., Dean C., Arthur C., Dong M. and Chapman E. (2009) Autapses and networks of hippocampal neurons exhibit distinct synaptic transmission phenotypes in the absence of synaptotagmin I. J Neurosci. 29(23):7395-7403

Lois C., Hong E., Pease S., Brown E. and Baltimore D. (2002) Germline transmission and tissue-specific expression of transgenes delivered by lentiviral vectors. Science. 295(5556):868-72

Masson J., Sang C., Hamon M. and El Mestikawy S. (1999) Neurotransmitter Transporters in the Central Nervous System. Pharmacol Rev. 51:439–464

Marks M., Woodruff L., Ohno H. and Bonifacino J. (1996) Protein targeting by tyrosine- and di-leucine-based signals: evidence for distinct saturable components. J Cell Biol. 135(2):341-54

Mellman I. (1996) Endocytosis and molecular sorting. Annu Rev Cell Dev Biol.575-625

Miesenbock G., De Angelis D., Rothman J. (1998) Visualizing secretion and synaptic transmission with pH-sensitive green fluorescent proteins. Nature. 394:192–195.

Milosovic I., Giovedi S., Lou X., Raimoni A., Collesi C., Shen H., Paradise S., O`Toole E., Ferguson S., Cremona O. and DeCamilli P. (2011) Recruitment of endophilin to clathrin-coated pit necks is required for efficient vesicle uncoating after fission. Neuron. 72(4):587-601

Moechars D., Weston M., Leo S., Callaerts-Vegh Z., Goris I., Daneels G. Buist A., Cik M., van der Spek P., Kass S., Meert T., D`Hooge R., Rosenmund C., Hampson R. (2006) Vesicular glutamate transporter VGLUT2 expression levels control quantal size and neuropathic pain. J Neurosci 6(46):12055–12066

Mu F., Callaghan J., Steele-Mortimer O., Stenmark H., Parton R., Campbell P., Mc Cluskey J., Yeo J., Tock E. and Toh B. (1995) EEA1, an early endosome-associated protein. EEA1 is a conserved alpha-helical peripheral membrane protein flanked by cysteine "fingers" and contains a calmodulin-binding IQ motif. J Biol Chem. 270(22):13503-11

Naito S and Ueda T. (1985) Characterization of glutamate uptake into synaptic vesicles. J Neurochem. 44(1):99-109

Nelson and Cox (2005) Lehinger Biochemie. Springer publisher. 3rd edition

Newton A., Kirchhausen T., Murthy V. (2006) Inhibition of dynamin completely blocks compensatory synaptic vesicle endocytosis. PNAS. 103(47):17955-60

Nicholson-Tomishima K. and Ryan T. (2004) Kinetic efficiency of endocytosis at mammalian CNS synapses requires synaptotagmin I. Proc Natl Acad Sci USA. 101(47):16648-52

Nikiti T. and Augustine G. (2004) Synaptotagmin I synchronizes transmitter release in mouse hippocampal neurons. J. Neurosci. 24(27): 6127-6132

Numberger and Draghun (1996) Labor im Fokus `Patch-clamp Technik´ Spektrum akademischer Verlag

Oni-Orisan A., Kristiansen L., Haroutunian V., Meador-Woodruff J., McCullumsmit R. (2008) Altered vesicular glutamate transporter expression in the anterior cingulate cortex in schizophrenia. Biol Psychiatry. 63(8):766-75

Palay S., and Palade G. (1954) The fine structure of neurons. J. Biophys and biochem. Vol.1, N°1

Purves D., Augustine G., Fitzpatrick D., Katz L., LaMantia A., McNamara J., Williams S. (2001) Neuroscience, 2nd edition. Sunderland Sinauer Associates

Poskanzer K., Fetter R. and Davis G. (2006) Discrete residues in the C_2B domain of Synaptotagmin I independently specify endocytic rate and synaptic vesicle size. Neuron. 50:49-62

Pyott S. and Rosenmund C. (2002) The effects of temperature on vesicular supply and release in autaptic cultures of rat and mouse hippocampal neurons. J Physiol. 539(Pt2):523-35

Raimondi A., Ferguson S., Lou X., Armbruster M., Paradise S., Giovedi S., Messa M., Kono N., Takasaki J., Cappello V., O`Toole E., Ryan T. and DeCamilli P. (2011) Overlapping Role of Dynamin Isoforms in Synaptic Vesicle Endocytosis. Neuron. 70(6):1100-14

Ramamoorthy S., Shippenberg T. and Jayanthi L. (2011) Regulation of monoamine transporters: Role of transporter phosphorylation. Pharmacol Ther. 129(2):220-38

Reichert H. (1990) Neurobiologie, Thieme Verlag, Germany

Reichert H. (2000) Neurobiologie. Thieme publishing company. 2nd edition

Rizzoli S. and Betz W. (2005) Synaptic vesicle pools. Nat Rev Nerosci. 6:57-69

Rogers S., Wells R. and Rechsteiner M. (1986) Amino acid sequences common to rapidly degraded proteins: the PEST hypothesis. Science. 234(4774):364-8
Rosenmund C. and Stevens C. (1996) Definition of the readily releasable pool of vesicles at hippocampal synapses. Nature. 16(6):1197-207

Rosenmund C., Clements J. and Westbrook G. (1993) Nonuniform probability of glutamate release at a hippocampal synapse. Science.262(5134):754-7

Royle S., Granseth B., Odermatt B., Derevier A. Lagnado L. (2008) Imaging phluorin-based probes at hippocampal synapses. Methods Mol Biol. 457:293-303

Ryan K. (1992) Cryofixation of tissues for electron microscopy: a review of plunge cooling methods. Scanning Microsc., 6:715-743

Santos M., Barbosa J., Veloso g., Ribeiro F., Kushmerick C., Gomez M., Ferguson S., Prado V., Prado M. (2001) trafficking of green fluorescent protein tagged-vesicular acetycholine transporter to varicosities in a cholinergic cell line. J Neurochem. 78:1104-1113

Santos M., Park C., Foss S., Li H., Voglmaier S. (2013) Sorting of the vesicular GABA transporter to functional vesicle pools by an atypical dileucine-like motif. J Neurosci. 33(26):10634-46

Santos M., Foss S., Park K. and Voglmaier S. (2014) Protein interactions of the vesicular glutamate transporter VGLUT1. Plos One. 9(10):e109824

Schallier A., Massie A., Loyens E., Moechars D., Drinkenburg W., Michotte Y., Smolders I. (2009)
VGLUT2 heterozygous mice show more susceptibility to clonic seizures induced by pentylenetetrazol. Neurochem Int. 55(1-3):41-4

Schuske K., Richmond j., Matthiws D., Davis W., Runz S., Rube D., van der Bliek A., Jorgensen E. (2003) Endophilin is required for synaptic vesicle endocytosis by localizing synaptojanin. Neuron. 40(4):749-62

Seal R. and Amara S. (1999) EXCITATORY AMINO ACID TRANSPORTERS: A Family in Flux. Annu Rev Pharmacy Toxicol. 39:431-56

Shumway S., Maki M. and Miyamoto S. (1999) The PEST domain of IkappaBalpha is necessary and sufficient for in vitro degradation by mu-calpain. J Boil Chem. 274(43):30874-81

Smear M., Tao H., Staub W., Orger M., Gosse N., Liu Y., Takahashi K., Poo M., Baier H. (2007)Vesicular glutamate transport at a central synapse limits the acuity of visual perception in zebrafish. Neuron. 53(1):65-77

Snyder D., Kelly M. and Woodbury D. (2006) SNARE complex regulation by phosphorylation. Cell Biochem Biophys. 45(1):111-23
Stahl P. and Barbieri A. (2002) Multivesicular bodies and multivesicular endosomes: the "in and outs" of endosomal traffic. Sci. STKE. 141: (32)

Schäfer M., Varoqui H., Defamie N., Weihe E. and Erickson J. (2002) Molecular cloning and functional identification of mouse vesicular glutamate transporter 3 and its expression in subsets of novel excitatory neurons. J Biol Chem. 277(52):50734-48

Schneggenburger R., Sakaba T. and Neher E. (2002) Vesicle pools and short-term synaptic depression: lessons from a large synapse. Trends Neurosci. 25(4):206-12

Schneider S. (2001) Kiss and run mechanism in exocytosis. J Memb Biol. 181(2):67-76

Schuske K., Richmond J., Matthies D., Davis W., Runz S., Rube D., van der Bliek A. and Jorgenson E. (2003) Endophilin Is Required for Synaptic Vesicle Endocytosis by Localizing Synaptojanin. Neuron. 40(4):749-62

Shigeri Y., Seal R. and Shimamoto K. (2004) Molecular pharmacology of glutamate transporters, EAATs and VGLUTs. Brain Res Brain Res Rev. 45(3):250-65

Siksou L., Slim K., Biesemann C., Nehring R., Wojcik S., Triller A., Mestikawy S., Marty S. and herzog E. (2013) A role for vesicular glutamate transporter 1 in synaptic vesicle clustering and mobility. Eur J Neurosci. 37(10):1631-42

Sreedharan S., Shaik J., Olszewski P., Levine A., Schiöth H. and Fredriksson R. (2010) Glutamate, aspartate and nucleotide transporters in the SLC17 family form four main phylogenetic clusters: evolution and tissue expression. BMC Genomics. 11:17

Stensrud M., Chaudhry F., Leergaard T., Bjaalie J. and Gundersen V. (2013) Vesicular glutamate transporter-3 in the rodent brain: vesicular colocalization with gamma-aminobutyric acid transporter. J Comp Neurol. 52(13):3042-56

Südhof T. (1995) The synaptic vesicle cycle: a cascade of protein-protein interactions. Nature. 375(6533):645-53

Südhof T. (2004) The synaptic vesicle cycle. Annu Rev Neurosci. 27:509-47

Südhof T. and Jahn R. (1991) Proteins of synaptic vesicle involved in exocytosis and membrane recycling. Neuron. 6:665-677

Südhof T. and Rizo J. (2011) Synaptic vesicle exocytosis. Cold Spring Harb Perstect Biol. 3(12)

Sundborger A., Soderblom C., Vorontsova O., Evergren E., Hinshaw J., Shupliakov O. (2010) An endophilin-dynamin complex promotes budding of clathrin-coated vesicles during synaptic vesicle recycling. Journal of cell science. 124(Pt 1):133-43

Takamori S., Rhee J., Rosenmund R. and Jahn R. (2000) Identification of a vesicular glutamate transporter that defines a glutamatergic phenotype in neurons. Nature. 407:189–194

Takamori S., Malherbe P., Borger C. and Jahn R. (2002) Molecular cloning and functional characterization of human vesicular glutamate transporter 3 EMBO. 3:798-803

Takamori S., Holt M., Stenius K., Lemke E., Gronborg M., Riedel D., Urlaub H., Schenk S., Brügger B., Ringler P., Müller S., Rammner B., Gräter F., Hub J., DeGroot B., Mieskes G., Moriyama Y., Klingauf J., Grubmüller H., Heuser J., Wieland F. and Jah R. (2006) Molecular anatomy of a trafficking organelle. Cell. 127(4):831-46

Takamori S. (2006) VGLUT: 'exciting' times for glutamatergic research? Neurosci. Res. 55:343-51

Tan P., Waites C., Liu Y., Krantz D., Edwards R. (1998) A leucine-based motif mediates the endocytosis of vesicular monoamine and acetylcholine transporters. J Biol Chem. 273:17351-17360

Tan P., Waites C., Liu Y., Krantz D. and Edwards R. (1998) A leucine-based motif mediates the endocytosis of vesicular monoamine and acetylcholine transporters. J Biol Chem.28:17351–17360

Tordera R., Totterdell S., Wojcik S., Brose N., Elizalde N., Lashera B., Del Rio J. (2007) Enhanced anxiety, depressive-like behaviour and impaired recognition memory in mice with reduced expression of the vesicular glutamate transporter 1 (VGLUT1). Eur J Neurosci. 25(1): 281-290

Uezato R., Meador-Woodruff J., McCullumsmith R. (2009) Vesicular glutamate transporter mRNA expression in the medial temporal lobe in major depressive disorder, bipolar disorder, and schizophrenia. Bipolar Disord. 11(7):711–725

Valtorta F., Meldolesi J. and Fesce R. Synaptic vesicles: is kissing a matter of competence? Trends Cell Biol. 11:324-328

Verona M., Zanotti S., Schäfer T., Racagni G. and Popoli M. (2000) Changes of synaptotagmin interaction with t-SNARE proteins in vitro after calcium/calmodulin-dependent phosphorylation. J Neurochem. 74(1):209-21

Verstreken P., Kjaerulff O., Lloyd T., Atkinson R., Zhou Y., Meinertzhagen I. and Bellen H. (2002) Endophilin mutations block clathrin-mediated endocytosis but not neurotransmitter release. Cell.109(1):101-112

Vinatier J., Herzog E., Plamont M., Wojcik S., Schmidt A., Brose N., Daviet L., Mestikway S. and Giros B. (2006) Interaction between the vesicular glutamate transporter type 1 and endophilin A1, a protein essential for endocytosis. J Neurochem. 97(4):1111-25

Voglmaier S., Kam K., Yang H., Fortin D.,Hua Z., Nicoll R., Edwards R. (2006) Distinct Endocytic Pathways Control the Rate and Extent of Synaptic Vesicle Protein Recycling. Neuron. 51:71-84

Wallén-Mackenzie Å., Wootz H. and England H. (2010) Genetic inactivation of the vesicular glutamate transporter 2 (VGLUT2) in the mouse: What have we learnt about functional glutamatergic neurotransmission? Ups J Med Sci. 115(1):11-20

Watanabe S., Rost B., Camacho-Pérez M., Davis M., Söhl-Kielczynski B., Rosenmund C. and Jorgensen E. (2013) Ultrafast endocytosis at mouse hippocampal synapses. Nature. 504(7479):242-7

Watanabe S., Trimbuch T., Camacho-Pérez M., Rost B., Brokowski B., Söhl-Kielczynski B., Felies A., Davis M., Rosenmund C. and Jorgensen E. (2014) Clathrin regenerates synaptic vesicles from endosomes. Nature.

Watson M. (1958) Staining of tissue sections for electron microscopy with heavy metals. J Biophys Biochem Cytol. 25;4(4):475-8

Weinberger A. and Gerst J. (2004) Regulation of SNARE assembly by protein phosphorylation. Current Genetics. 10:145-170

Weston M., Nehring R., Wojcik S., Rosenmund C. (2011) Interplay between VGLUT isoforms and endophilin A1 regulates neurotransmitter release and short-term plasticity. Neuron. 69(6):1147-59

Wojcik S., Rhee J., Herzog e., Sigler Al., Jahn R., Takamori S., Brose N. and Rosenmund C. (2004) An essential role for vesicular glutamate transporter 1 (VGLUT1) in postnatal development and control of quantal size. Proc Natl Acad USA. 101(18):7158-63

Yao J., Kwin S., Gaffaney J., Dunning M. and Chapman E. (2012) Uncoupling the roles of Synaptotagmin I during endo- and exocytosis of synaptic vesicles. Nature neurosci. 15:243-249

Zhai R. and Bellen H. (2004) The architecture of the active zone in the presynaptuc nerve terminal. Physiology. 19:262-270

Zhao Z., Scott M., Chiechio S., Wang J., Renner K., Gereau R., Johnson R., Deneris E., Chen Z. (2006) Lmx1b is required for maintenance of central serotonergic neurons and mice lacking central serotonergic system exhibit normal locomotor activity. J Neurosci. 26:12781–12788.

Zhu Y., Xu J. and Heinemann S. (2009) Two pathways of synaptic vesicle retrieval revealed by single-vesicle imaging. Neuron. 61:397–411

Zhou L., McInnes J. and Verstreken P. (2014) Ultrafast synaptic endocytosis cycles to the center stage. Dev Cell. 28(1):5-6

Zimmermann H., Volknandt W., Henkel A., Bonzelius F., Janetzko A., Kanaseki T. (1989) The synaptic vesicle membrane: origin, axonal distribution, protein components, exocytosis and recycling. Cell Biol Int Rep. 13(12):993-1006

Webpages:

www.ebi.ac.uk/Tools/msa/clustalw2/

www.uniprot.org

www.kinasephos2.mbc.nctu.edu.tw/

www.cbs.dtu.dk/services/NetPhos/

Appendix

A1 Immunocytochemical and electrophysiological quantifications of the VGLUT2 knockdown

To quantify the effect of the VGLUT2 knockdown (KD) by short hairpin ribonucleic acid (sRhNA) immuncytochemistry (ICC) and ratiometric imaging analyses were performed to investigate the fluorescence intensities, reflecting protein expression levels. Therefore, neurons were lentiviral infected to express either one shRNA version, N° 1 or 2 (sequences see paragraph 2.4 „RNA interference by shRNA for protein knockdown“) or as control, a a scrambled shRNA, which has no target in the VGLUT2 genome.

For this, hippocampal VGLUT1 KO neurons or striatal VGLUT2 WT cells were lentiviral infected to express VGLUT2 (fig.34). The idea was to express VGLUT2 in VGLUT1 KO neurons to make it easier to clearly detect changes in the fluorescence intensities of virus infected cells to quantify the VGLUT2 KD efficiency. Usually only about 12% of the hippocampal neurons express VGLUT2 (Wojcik et al., 2004). VGLUT1 KO neurons were also directly lentiviral infected to express the shRNAs (N°1 or 2) or the scrambled shRNA without VGLUT2 overexpression (fig.34). The sRhNAs were lentiviral expressed in endogenous VGLUT2 WT-expressing cells as well (fig.35). For this, thalamic neurons were used, because they mainly express VGLUT2 (cf. fig.3).

To quantify the VGLUT2 KD effect by ratiometric imaging anti-VGLUT2 and anti-synaptophysin 1 antibody stainings were performed (fig.34 and 35).

In all experiments, the KD has a clear effect, which is very similar for both shRNA constructs, N° 1 and 2 (3.56a.u. ± 0.25 in VGLUT2+scramble, 0.66a.u.± 0.05 in VGLUT2+KD N°1, 0.75a.u.± 0.08 in VGLUT2+ KD N°2, 0.14a.u.± 0.01 in KO+ KD N°1, 0.13a.u.± 0.01 in KO+ KD N°2, 0.21a.u.± 0.02 in KO+ scramble, fig.34 and 1.0a.u.± in WT, 0.44a.u.± 0.08 in WT+ KD N°1, 0.97± 0.19 in WT+ scramble, fig.35). Therefore, the shRNA construct N° 1 was used for all KD experiments and further physiological characterization.

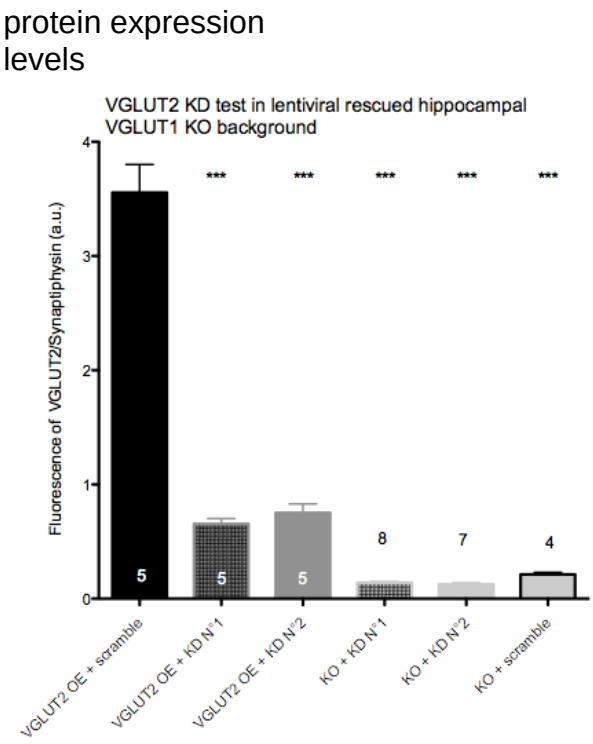

Fig. 34: **ICC quantification of VGLUT2 KD in hippocampal neurons:** hipppocampal VGLUT1 KO neurons were lentiviral infected to overexpress VGLUT2 (OE) together with one of two different shRNAs, N°1 and 2, to achieve VGLUT2 KD. For control, cells expressed a scrambled unspecific shRNA (black). To quantifiy the KD effect ICC and ratiometric imaging was performed using an anti-VGLUT2 and anti-synaptophysin 1 antibody. Both shRNA constructs (dark grey, N° 1 in addition with small boxes) could reduce the VGLUT2 expression more than 2/3 of the VGLUT2 OE level. Pure VGLUT1 KO neurons (light grey) were also lentiviral infected to directly express the VGLUT2 shRNAs or scramble shRNA (black border) without VGLUT2 OE. Thereby, the KD effect of both tested shRNAs could be confirmed (n numbers correspond to 1cell culture, bars indicate mean±SEM, statistics to test significance: One way ANOVA with tukey`s multiple comparison test: ***p<0.0001).

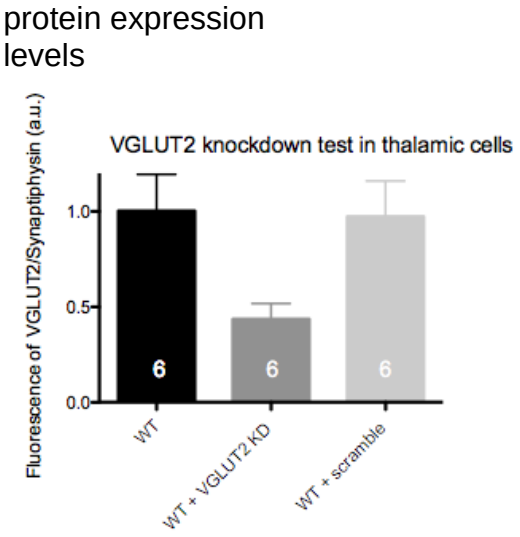

Fig. 35: **ICC quantification of VGLUT2 KD in thalamic neurons:** thalamic neurons mostly express VGLUT2 (cf. fig.3). To quantifiy the VGLUT2 KD effect, WT thalamic neurons (black) were lentiviral infected to express the VGLUT2 shRNA virus N°1 (dark grey). VGLUT2 WT control cells expressed a scrambled unspecific shRNA (light grey) or were not virus infected at all (WT, black). ICC and ratiometric imaging were performed using an anti-VGLUT2 and anti-synaptophysin 1 antibody. The VGLUT2 expression could be reduced by the KD (dark grey) more than half of the WT level or respectively the WT level plus scramble (n numbers correspond to 1cell culture, bars indicate mean±SEM, statistics to test significance: One way ANOVA with tukey`s multiple comparison test).

The VGLUT2 KD was also quantified by investigating the electrophysiology of lentivirus infected neurons, which expressed the different shRNAs (fig.36). For this, the shRNA N° 1 was expressed in hippocampal VGLUT1 WT or VGLUT1 KO neurons. The KO neurons were also lentiviral infected to express a scrambled shRNA as control.

The EPSC amplitudes are significantly reduced in VGLUT2 shRNA expressing KO neurons compared to the scramble-expressing KO control group and VGLUT2 sRhNA-expressing VGLUT2 WT neurons (5.17nA± 1.1 in WT plus shRNA, 0.02nA± 0.01 in KO plus shRNA,

0.23nA± 0.08 in KO plus scramble, fig.36A). Equally, the RRP size and mean mEPSC frequency are decreased in VGLUT2 shRNA expressing KO cells (RRP: 683.7pC± 97.1 in WT plus shRNA, 44.7pC± 14 in KO plus shRNA, 79pC± 14.9 in KO plus scramble; mEPSC frequency: 6.4Hz± 1.1 in WT plus shRNA, 0.5Hz± 0.2 in KO plus shRNA, 1.6Hz± 0.7 in KO plus scramble, fig.36B and E). Only the mEPSC amplitudes of the shRNA infected WT neurons show no significant differences to control (fig.36D). To calculate the Pvr not enough cells with a descent response in VGLUT2 shRNA or scramble-expressing KO neurons could be recorded. 10 Hz train stimulation data also exhibited much error. Therefore, the 10 Hz data are not shown. However, the results verify that the KD of the target protein VGLUT2 is functioning.

A: Evoked postsynaptic responses

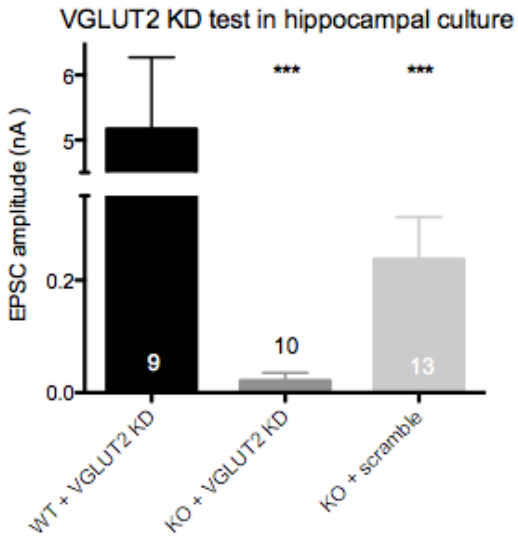

B: Readily releasable pool

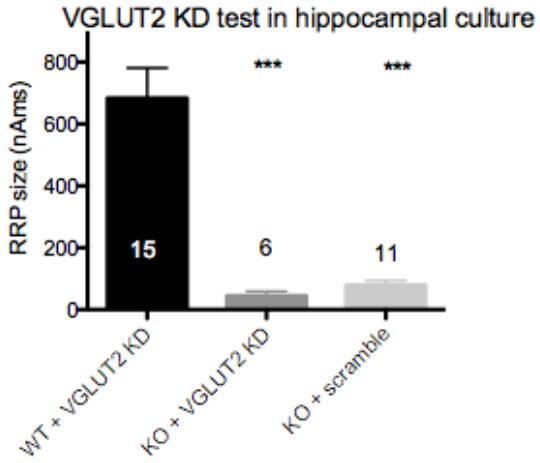

C: Paired pulse ratio

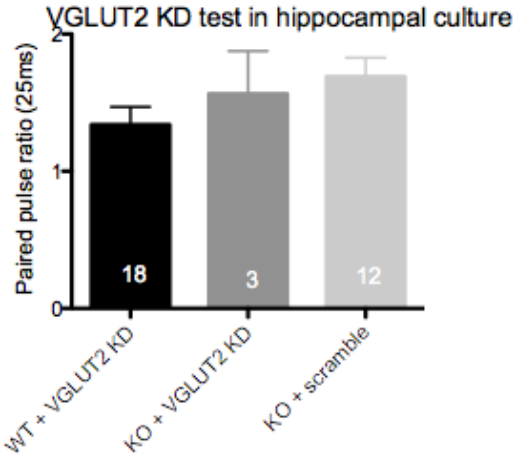

D: spontaneous activity (mEPSC amplitude)

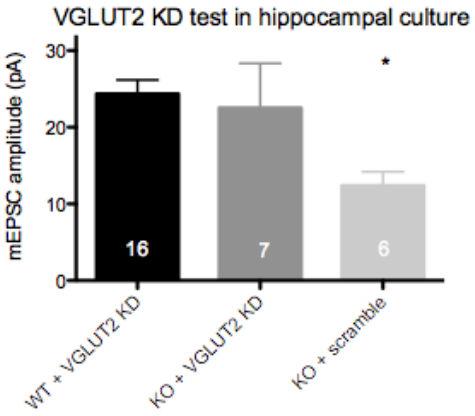

E: spontaneous activity (mEPSC frequency)

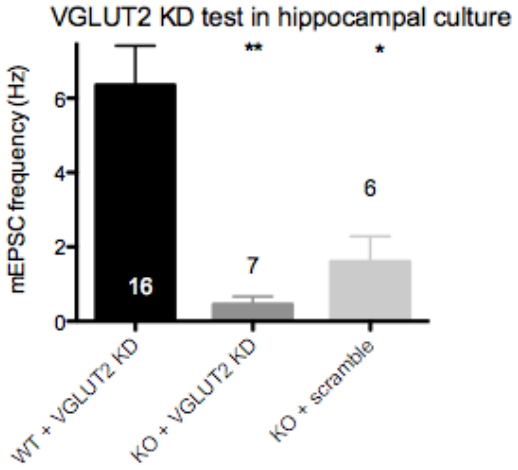

Fig. 36 (A-E): **Electrophysiological quantification of VGLUT2 KD:** hippocampal VGLUT1 WT (black) or KO (dark grey) neurons were lentiviral infected to express shRNA virus N°1 to KD VGLUT2. KO control cells were also lentiviral infected to express a scrambled, unspecific shRNA (light grey). EPSCs (A) and RRP size (B) are significantly reduced by the VGLUT2 shRNA compared to scramble-expressing cells. The PP ratio (C) and mean mEPSC amplitude (D) of the KO neurons expressing the VGLUT2 sh RNA are not changed, but the mean mEPSC frequency (E) is also reduced by VGLUT2 shRNA compared to scrambled sRhNA-expressing cells (data of 1 cell culture, mean±SEM,One way ANOVA with tukey`s multiple comparison test: *p<0.05, **p<0.001, ***p<0.0001).

A2 Immunocytochemical quantifications of different VGLUT1 constructs

The protein expression levels were determined for all main experiments and mentioned and interpreted in the results and discussion chapters.

A: protein expression levels

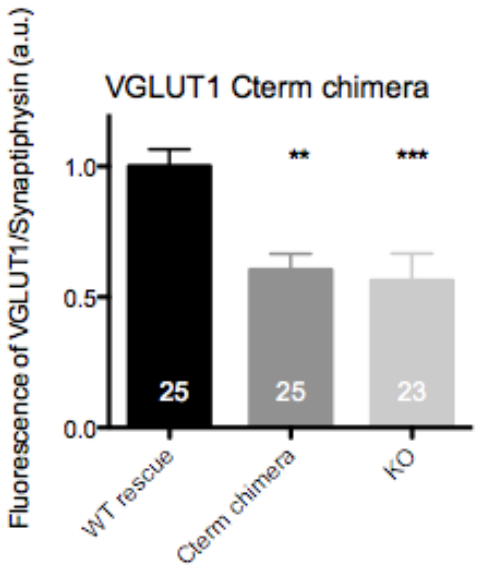

B: protein expression levels

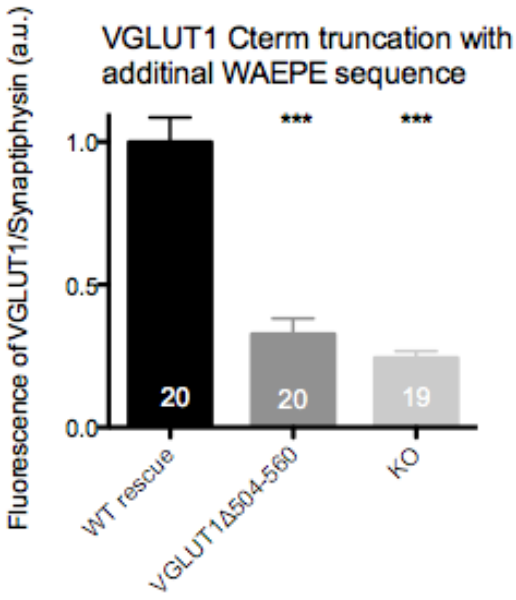

C: protein expression levels

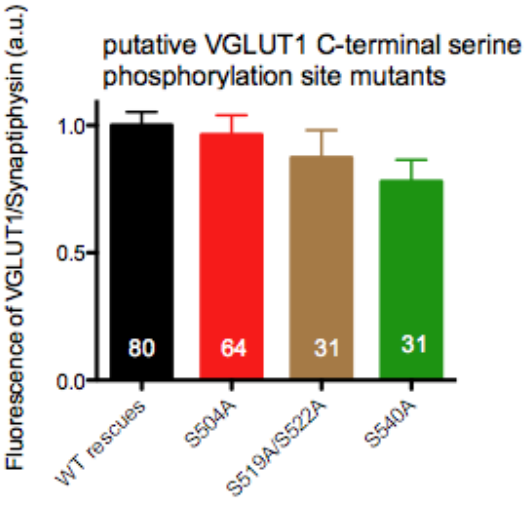

D: protein expression levels

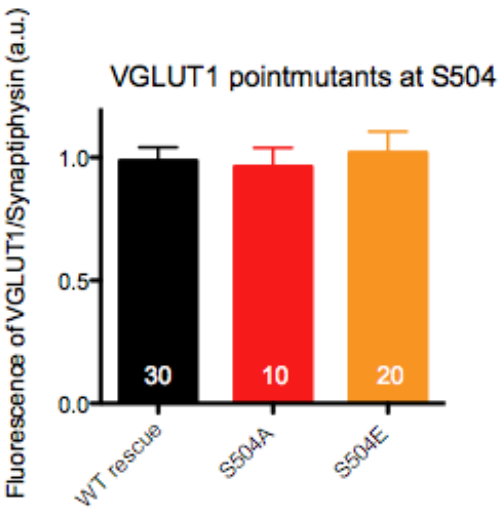

E: protein expression levels

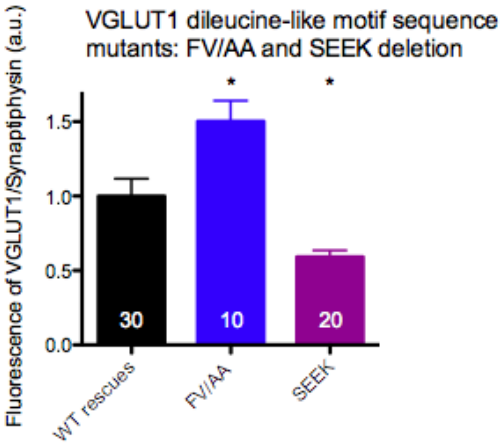

F: protein expression levels

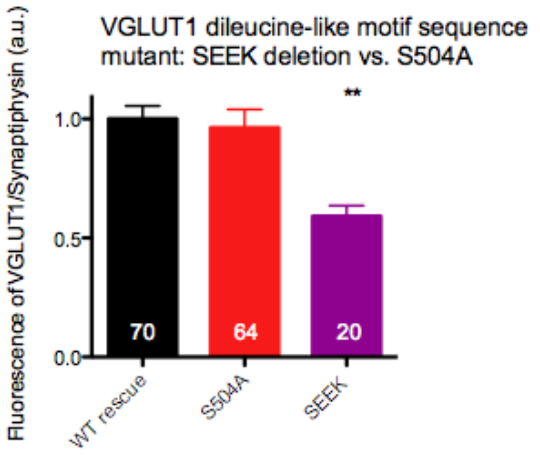

Fig. 37 (A-F): **ICC quantifications of different VGLUT1 constructs:** hippocampal VGLUT1 KO neurons were lentiviral infected to express different VGLUT1 C-terminal rescue constructs in comparison with WT rescue (black) and in some experiments with VGLUT1 KO cells (light grey). For the VGLUT1 chimera construct (dark grey) the C-terminus was substituted with the C-terminal end of synaptophysin (aa225-aa314), a common vesicle marker protein. The chimera protein expression level is significantly reduced compared to the WT rescue (A). The shorter VGLUT1 truncation VGLUT1Δ504-560 (dark grey) also shows a significantly reduced protein expression (B). The different mutated VGLUT1 serine phosphorylation sites S504A (red), S519A/S522A (brown) and S540A (green) have similar protein expression levels as the WT rescue (C). Alike, the comparison of the protein expression levels between the pointmutants S504A and S504E (orange) with the WT rescue show no differences (D). The dileucine-like motif sequence mutants FV510/511AA (blue) and the $S_{504}EEK_{507}$ deletion (purple) show both differences in their protein expression levels compared to WT rescue or respectively S504A (E and F). The protein expression of FV510/511AA is increased (E). The protein expression of the $S_{504}EEK_{507}$ deletion is significantly reduced (F) (n numbers correspond to 3 cell cultures, bars indicate mean±SEM, statistics to test significance: One way ANOVA with tukey`s multiple comparison test: *p<0.05, **p<0.001, ***p<0.0001).

Statement of contributions

All experimental executions were done by myself. Technical support for the preparation of an astrocytic feeder layer for neuronal cultures was given by the technician Annegret Felies. The animal preparation of the VGLUT1 hippocampal or VGLUT2 thalamic neuron cultures were done independently. The experimental design and production of lentiviral constructs for different VGLUT1 or 2 variants and VGLUT2 shRNA for protein KD was organized and instructed by Dr. Thorsten Trimbuch. Technical support was given by Katja Pötschke, Bettina Brokowski and Carola Schweinoch. The quantification of the VGLUT2 KD effect by ICC and electrophysiology was done together with Melissa Herman, PhD. The EM image aquisition and EM sample preparation was done by Dr. Frauke Ackermann and Berit Söhl-Kielczynski. For ICC Berit Söhl-Kielczynski also helped. The mentioned contributors are all from Rosenmund`s laboratory (Charité), with exception of Frauke Ackermann. She works in the Greg Garner laboratory (Charité).

Der Lebenslauf ist in der Online-Version aus Gründen des Datenschutzes nicht enthalten.